EXCITON SATURATION DYNAMICS AND SPIN GRATINGS IN MULTIPLE QUANTUM WELL SEMICONDUCTORS

Alasdair R. Cameron

A Thesis Submitted for the Degree of PhD
at the
University of St Andrews

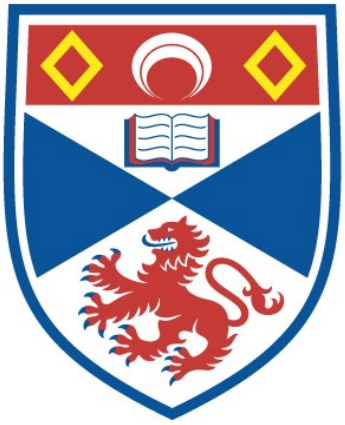

1997

Exciton saturation dynamics and spin gratings in multiple quantum well semiconductors

Alasdair R. Cameron, B.Sc.

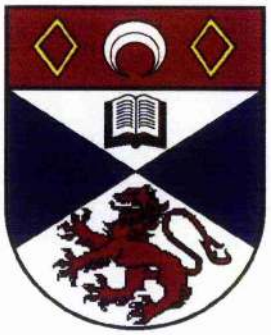

J. F. Allen Physics Research Laboratories
Department of Physics and Astronomy
University of St Andrews
Fife, Scotland

A thesis submitted to the University of St Andrews
in application for the degree of Doctor of Philosophy,

August 1996

TL C106

I, Alasdair Ross Cameron, hereby certify that this thesis, which is approximately 25,000 words in length, has been written by me, that it is the record of work carried out by me and that it has not been submitted in any previous application for a higher degree.

Date 12/10/96. Signature of candidat

I was admitted as a research student in September 1993 and as a candidate for the degree of PhD; the higher study for which this is a record was carried out in the University of St. Andrews between 1993 and 1996.

Date 12/10/96. Signature of candidat

I hereby certify that the candidate has fulfilled the conditions of the Resolution and Regulations appropriate for the degree of Doctor of Philosophy in the University of St. Andrews and that the candidate is qualified to submit this thesis in application for that degree.

Date 12/10/96 Signature of supervisor ...

In submitting this thesis to the University of St. Andrews I understand that I am giving permission for it to be made available for use in accordance with the regulations of the University Library for the time being in force, subject to any copyright vested in the work not being affected thereby. I also understand that the title and abstract will be published, and that a copy of the work may be made and supplied to any bona fide library or research worker.

Date 12/10/96 Signature of candidate

You can't expect an arse like me to tell a story competently. It's all I can bloody do to work this foul machine. I've counted up the words processed, a thing I do every hour, and, if technology can be trusted, it looks as if you're in for 94,536 of them. Good luck to you. You asked for it, you paid me for it, you've got to sit through it. As the man said, I've suffered for my art, now it's your turn.

"The Hippopotamus" Stephen Fry

Abstract

The dynamics of exciton saturation in GaAs/AlGaAs multiple quantum wells are investigated using picosecond optical pulses.

The main contributions to exciton saturation have been shown to be phase space filling, Coulomb screening and exciton lineshape broadening. The spin dependent nature of the phase space filling nonlinearity has allowed its separation from the effects due to Coulomb screening and broadening. The effect of lineshape broadening on exciton saturation has been investigated through its density dependence for a number of quantum well widths. The results show that the effects due to broadening are important in narrow wells of high quality.

An investigation into electron spin relaxation at room temperature has been carried out as a function of the well width. The observed decrease in the electron spin relaxation time with decreasing well width is in good agreement with previously reported results and suggests the D'Yakonov-Perel mechanism is the dominant spin-flip mechanism for electrons in quantum wells at room temperature.

The first demonstration of an electron spin grating in a quantum well semiconductor is reported by utilising the optical selection rules for quantum wells and optical polarisation gratings. Time resolved studies of the grating decay have allowed the first optical measurement of the in-plane electron diffusion coefficient in a quantum well semiconductor.

Contents

1

Introduction

The ability to form a junction between two differing semiconductors has been fundamental in the growth of the semiconductor industry. From the very early junction diodes [1.1] to the most recent quantum cascade lasers [1.2], the ability to form a junction has been of critical importance. With the advent of molecular beam epitaxy in the early 1970s the science of junction technology took on a whole new meaning.

Molecular beam epitaxy allows the growth of semiconductor layers on a truly atomic scale. The grower can now choose the composition and thickness of semiconductor layers to a precision previously unheard of. This control has allowed the production of semiconductor layered structures where the layer thickness is comparable to the deBroglie wavelength of the electron and has so lead to the explosion in the field of low-dimension semiconductor structures.

The most basic low-dimension structure that can be manufactured is that of the single quantum well. This consists of an ultrathin layer of semiconductor sandwiched between two layers of a larger band-gap semiconductor, see Figure 1.1. These structures were initially used to verify some of the postulates of quantum theory most notably the quantisation of the electron and hole energy levels due to their confinement in the quantum well [1.3] and the tunnelling of an electron across a potential barrier [1.4].

If single quantum wells are sandwiched together (with many layers of ultrathin semiconductor separated from each other by thin layers of the larger bandgap semiconductor) then what is know as a multiple quantum well is formed. The advantage of the multiple quantum well over the single quantum well is most

apparent in optical studies. The multiple quantum well will ideally have the same properties as the single quantum well but the optical density experienced by light passing through the structure parallel to the growth direction will be increased by a factor N, where N is the number of quantum well periods. It is the optical properties of this structure that will be investigated in this thesis.

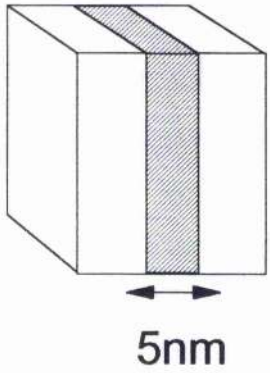

Figure 1.1 *Schematic of a single quantum well.*

Quantum wells and multiple quantum wells have received a great deal of attention over the last twenty years. The quantum effects that occur in these structures modify their optical properties in very distinct ways. In the past, effects such as those due to excitons (bound electron-hole pairs) have only been observable in bulk semiconductors at very low temperatures. In quantum wells, these effects remain clearly visible even at room temperature [1.5]. This shows how quantum wells can lead to the enhancement of bulk effects.

Quantum wells also show a number of new properties when compared to bulk. One such feature is the quantum confined Stark effect [1.6], which produces a red shift in the absorption edge when an electric field is applied across the quantum well layers. The discovery of this effect has lead to the realisation of electroabsorption devices, such as the SEED (self electro optic effect device) [1.7]. Other applications of quantum wells include quantum well heterostructure lasers [1.8], optical switches [1.9] and modulators [1.10].

The construction of lasers with the ability to produce ultrashort pulses with widths on the order of picoseconds and below has lead to intense investigation into the dynamics of the electronic processes which occur within quantum wells.

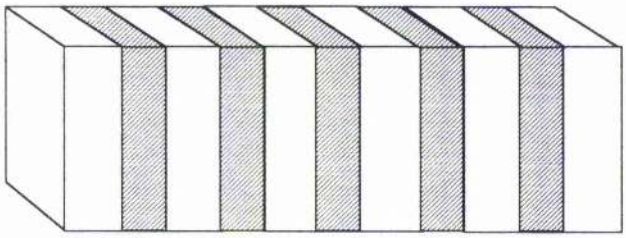

Figure 1.2 *Schematic of a multiple quantum well.*

In this thesis an attempt is made to optically measure a number of important parameters pertaining to quantum wells. In chapters two and three the basic physics of quantum wells and their optical properties are introduced. In chapter four the factors relating to the motion of carriers within the quantum wells are considered. The experimental techniques employed and the samples under investigation are described in chapters five and six. In chapter seven the contributions of screening, broadening and phase space filling to exciton saturation in multiple quantum wells are investigated. Chapter eight address the interesting field of spin relaxation which has seen a resurgence in interest. Optical measurements of the combined motion of electrons and holes in quantum wells are presented in chapter nine, and in chapter ten a new technique is introduced to directly measure the motion of the electrons alone. In chapter eleven the concept of carrier mobility is discussed in light of the results from the previous two chapters. Finally chapter twelve draws the results together in conclusion.

1.1 References

1.1 W. Shockley, "The theory of p-n junctions in semiconductors and p-n junction transistors", Bell Syst. Tech. J., **28**, 435, , (1949).

1.2 J. Faisl, F. Capasso, D.L. Sivco, C. Sirtori, A.l. Hutchinson and A.Y. Cho, "Quantum cascade laser", Science, **264**, 5158, 553-556, (1994).

1.3 R. Dingle, W. Wiegmann and C.H. Henry, "Quantum states of confined carriers in very thin Al(x)Ga(1-x)As GaAs Al(x)Ga(1-x)As heterostructures", Phys. Rev. Letts., **33**, 14, 827-830, (1974).

1.4 L.L. Chang, L. Esaki and R. Tsu, "Resonant tunnelling in semiconductor double barriers", Appl. Phys. Lett. , **24**, 12, 593-595, (1974).

1.5 D.S. Chemla, D.A.B. Miller, P.W. Smith, A.C. Gossard and W. Wiegmann, "Room temperature excitonic nonlinear absorption and refraction in GaAs/AlGaAs multiple quantum well structures", IEEE J. Quant. Electron., **20**, 3, 265-275, (1984).

1.6 D.A.B. Miller, "Quantum-well self-electro-optic effect devices", Opt. Quant. Electrons., **22**, s61-s98, (1990).

1.7 D.A.B. Miller, D.S. Chemla, T.C. Damen, A.C. Gossard, W. Wiegmann, T.H. Wood and C.A. Burrus, "Band-edge electroabsorption in quantum well structures: the quantum-confined Stark effect", Phys. Rev. Letts., **53**, 22, 2173-2176, (1984).

1.8 P.S. Zory, *Quantum well lasers*, (Academic Press Inc. 1993).

1.9 P. LiKamWa, A. Miller, M. Ogawa and R.M. Park, "All-optical bistable switching in an active InGaAs quantum-well waveguide", IEEE Phot. Tech. Lett., **3**, 6, 507-509, (1991).

1.10 K. Wakita, I. Kotaka, O. Mitomi, H. Asai, Y. Kawamura and M. Naganuma, "High-speed InGaAlAs/InAlAs multiple quantum well optical modulators", J. Light. Tech., **8**, 7, 1027-1031, (1990).

2

Quantum well basics

2.1 Summary

This chapter describes some of the basic properties relating to structures exhibiting quantum confinement. The concept of energy level quantisation and its corresponding effect on the density of states are discussed. Excitonic molecules are introduced and their influence on the optical properties of quantum wells are explored. The semiconductor alloy, GaAs/AlGaAs will form the basis for this thesis and so the concepts above are illustrated with examples relating to this compound.

2.2 Bulk GaAs

For the results presented in the following chapters the semiconductor of interest is GaAs and so the properties relating to it in its bulk form will be introduced before the effects of quantum confinement are considered. GaAs is a III-V semiconductor with a band structure which is shown in Figure 2.1. The area of interest is the Γ point which lies at the centre of the Brillouin zone. The conduction band is denoted by Γ_6 and is two-fold degenerate. The valence bands are labelled Γ_7 and Γ_8. The Γ_7 band is split from the Γ_8 band due to the effects of spin-orbit coupling by 0.34 eV. The Γ_8 band is four-fold degenerate at the zone centre but this degeneracy is partly removed away from the zone centre where the band is resolved into the light and heavy hole valence bands which are each

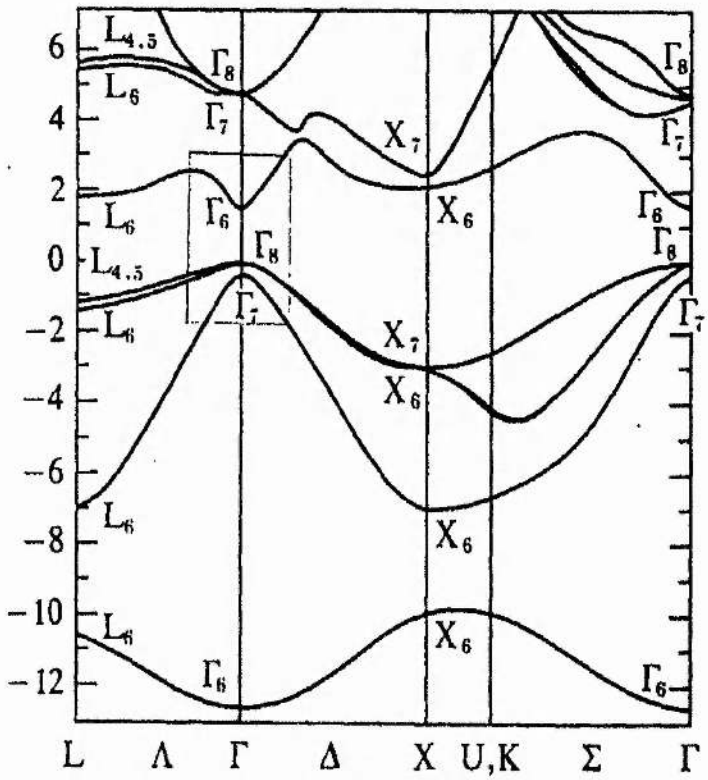

Figure 2.1 *Extended band structure for GaAs.*

two-fold degenerate. In GaAs the bandgap is the difference in energy between the Γ_6 and Γ_8 bands at the zone centre and has the value of 1.42 eV at room temperature.

2.3 GaAs/AlGaAs multiple quantum wells

The quantum wells discussed in this thesis relate to the so called type-I heterostructure. In this structure the electron and hole are confined in the same semiconductor material. These are distinct from type-II heterostructures where the electron and hole are confined within different materials. The type-I heterostructure is exemplified by the GaAs/$Al_xGa_{1-x}As$ combination.

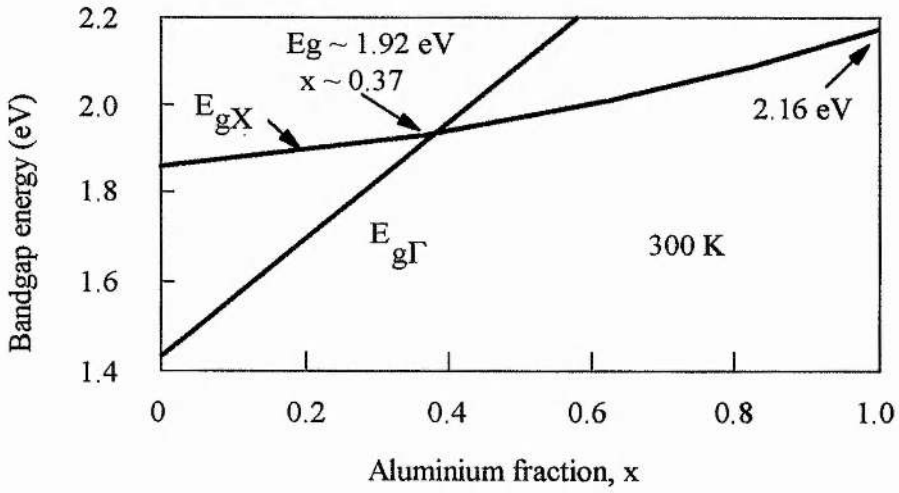

Figure 2.2 *Variation in the band gap energy of AlGaAs with increasing Al concentration.*

The band gap of GaAs is 1.42 eV as was stated previously. The band gap of $Al_xGa_{1-x}As$ is dependent on the molar fraction, x, of Al present. The variation in the bandgap of $Al_xGa_{1-x}As$ is shown in Figure 2.2. As the aluminium concentration is

increased so the bandgap of the material increases. The increase in the bandgap can be described by the formula

$$E_g = 1.4247 + 1.247x \quad \text{for } x < \sim 0.4 \qquad 2.1$$

Above an aluminium concentration of ~0.4 the bandgap becomes indirect in nature.

Figure 2.3 shows a schematic band diagram for a type-I heterostructure. The difference in band gaps of the two semiconductor materials determines the band offset ratio a:b, where $\Delta E_c = a\Delta E_g$ and $\Delta E_v = b\Delta E_g$. This ratio is essentially determined empirically from fits to experimental data. The ratio used in the following work will be that proposed by Miller et al [2.1]. He suggested a ratio of 57:43 with accompanying effective masses of $m_e^* = 0.0665m_0$ for the electron, $m_{hh}^* = 0.34m_0$ for the heavy hole and $m_{lh}^* = 0.094m_0$ for the light hole.

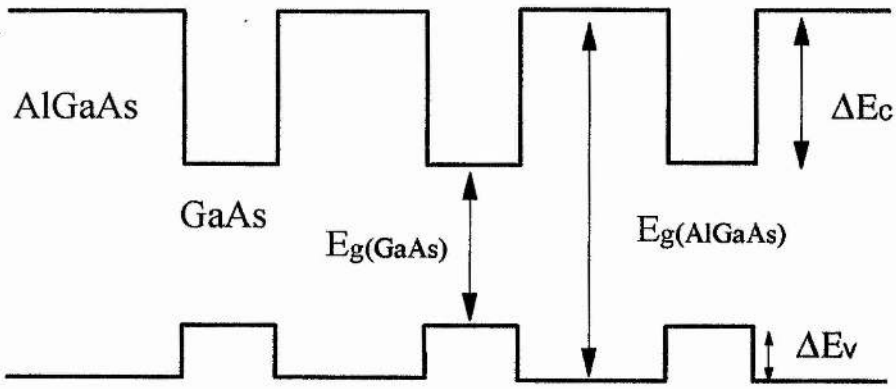

***Figure 2.3** Band structure for a GaAs/AlGaAs multiple quantum well.*

2.4 Quantisation of energy levels

The main effect that confinement has on the properties of electrons and holes is to quantise the energy levels available to them [2.2]. The energy levels for an infinite square well potential, of width L_z, are calculated by solving the Schrödinger equation

$$\left(\frac{-\hbar^2}{2m^*}\right)\frac{\partial^2}{\partial z^2}\Psi_n(z)+V_c(z)\Psi_n(z)=E_n\Psi_n(z) \qquad 2.2$$

which has solution

$$E_n=\frac{\hbar^2}{2m}\left(\frac{n\pi}{L_z}\right)^2 \qquad 2.3$$

For a finite potential well, of height V_0, which is the case for a quantum well formed between semiconductors, the solutions are obtained by again solving the Schrödinger equation. Applying continuity constraints to the wavefunction and its first derivative at the boundary regions the following transcendental equations are obtained

$$\frac{k}{m_a^*}\tan\left(\frac{kL_z}{2}\right)=\frac{\kappa}{m_b^*} \qquad 2.4$$

$$\frac{k}{m_a^*}\cot\left(\frac{kL_z}{2}\right)=-\frac{\kappa}{m_b^*} \qquad 2.5$$

where m_a^* and m_b^* are the effective masses of the electron in the well and barrier regions and

$$k^2 = \frac{2m_a^*}{\hbar^2}(E - V_0) \qquad 2.6$$

$$\kappa^2 = \frac{2m_a^*}{\hbar^2}E \qquad 2.7$$

Only the energy levels in the growth direction are quantised as the other two dimensions (x and y) are essentially unaffected by any confinement and can be thought of as essentially bulk semiconductor with their energy states given, approximately, by the parabolic relation

$$E_{xy} = \frac{\hbar^2\left(k_x^2 + k_y^2\right)}{2m_a^*} \qquad 2.8$$

The hole energy levels in the quantum well are also quantised in the growth direction. The equations are identical to those above with the effective electron masses m^* replaced by either the light hole or heavy hole effective masses. The band diagram for the holes in the other two dimensions (xy) however cannot be accurately described using a parabolic relationship.

In bulk GaAs the highest energy valence bands have J=3/2 symmetry, where J is the angular momentum. The bands are four-fold degenerate at the zone centre. For the case of a quantum well the confinement in the growth direction, z, lifts the degeneracy between $J_z = \pm 3/2\hbar$ and $J_z = \pm 1/2\hbar$ near k=0 and leads to each band having a distinct energy.

The dispersion of the hole subbands near k=0 can be described by solutions of the Luttinger Hamiltonian [2.3]. For the case of a bulk semiconductor and taking k_z in the direction [100], the energies of the holes are given by

$$E = \frac{\hbar^2 k_z^2}{2\left[m_0/(\gamma_1 - 2\gamma_2)\right]} \qquad 2.9$$

for $J_z = \pm 3/2\hbar$ and

$$E = \frac{\hbar^2 k_z^2}{2\left[m_0/(\gamma_1 + 2\gamma_2)\right]} \qquad 2.10$$

for $J_z = \pm 1/2\hbar$. The heavy and light hole masses are given by $m_0/(\gamma_1-2\gamma_2)$ and $m_0/(\gamma_1+2\gamma_2)$. γ_1 and γ_2 are the Luttinger parameters of the valence band.

In a quantum well, in the direction perpendicular to the growth direction, the above dispersion relationships become

$$E = \frac{\hbar^2 k_\perp^2}{2\left[m_0/(\gamma_1 + \gamma_2)\right]} \qquad 2.11$$

for $J_z = \pm 3/2\hbar$ and

$$E = \frac{\hbar^2 k_\perp^2}{2\left[m_0/(\gamma_1 - \gamma_2)\right]} \qquad 2.12$$

for $J_z = \pm 1/2\hbar$.

From Eqn 2.11 and Eqn 2.12 it can be seen that the $J_z = \pm 3/2\hbar$ heavy hole band now has a light effective mass ($m_0/(\gamma_1 + \gamma_2)$), and the $J_z = \pm 1/2\hbar$ light hole band has a heavy effective mass ($m_0/(\gamma_1 - \gamma_2)$). Due to the higher lying nature of the heavy hole band it might be expected that band crossing will be observed (see Figure 2.5). This situation is avoided by the inclusion of high order **k.p** perturbation terms which lead to an anti-crossing behaviour (see Figure 2.6).

It should be noted that the non-parabolicity of the valence bands should dramatically influence the valence band density of states (to be described in the following chapter) from an exact step-like shape to more complicated structures. The subband dispersion in the plane perpendicular to the quantum well growth direction is invaluable in determining the density of states and the transport properties.

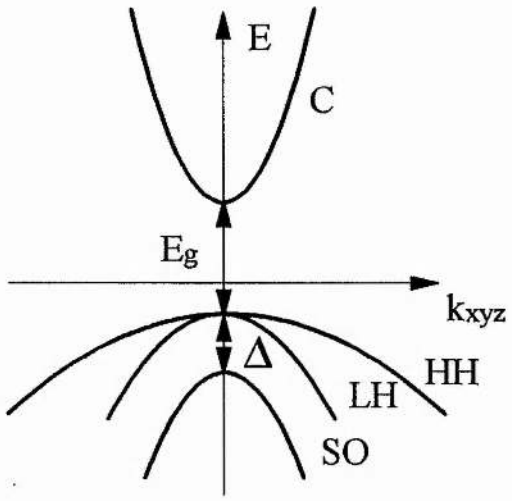

Figure 2.4 *The conduction and valence bands in bulk, showing the light hole (LH), heavy hole (HH), and split-off (SO) bands.*

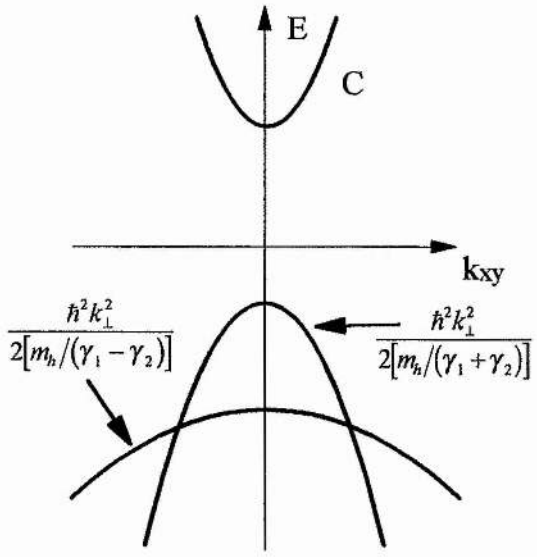

Figure 2.5 *The band crossing predicted by the solutions to the Luttinger Hamiltonian in a quantum well.*

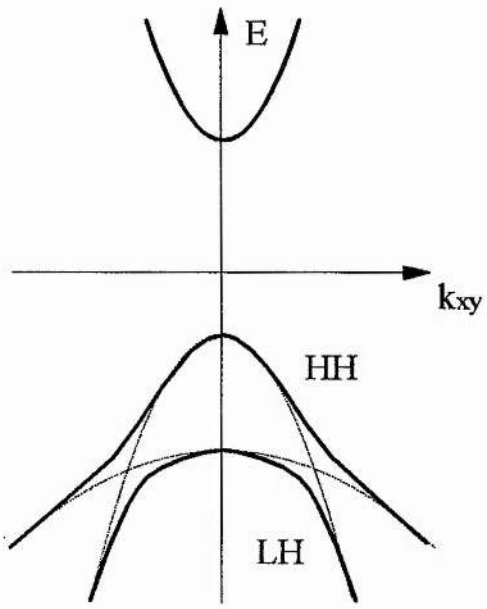

Figure 2.6 *The anticrossing produced by higher order perturbation terms.*

2.5 Excitons

Within semiconductors the electrons and holes can form excitons. Excitons are bound electron hole pairs where the attraction between the pair can be described simply as a Coulomb interaction. The attractive potential can be quantified by

$$V(r) = -\frac{e^2}{\varepsilon r} \qquad 2.13$$

where r denoted the separation between the electron and hole, e is the electronic charge and ε is the dielectric constant.

In three dimensions the excitonic energy levels can be obtained using the methods of the hydrogen atom. This leads to the production of a series of discrete hydrogenic states given by

$$E_n^{3D} = E_g - \frac{R_0}{n^2} \qquad 2.14$$

where the 3D Rydberg is given by

$$Ry^* = \frac{\mu^* e^4}{2(4\pi\varepsilon\hbar)^2} \qquad 2.15$$

μ^* is the reduced effective mass of the exciton which is given by

$$\frac{1}{\mu} = \frac{1}{m_e^*} + \frac{1}{m_h^*} \qquad 2.16$$

The effective Bohr radius for the exciton, which describes its spatial extent is given in 3D by

$$a_B^* = \frac{4\pi\varepsilon\hbar^2}{\mu^* e^2} \qquad 2.17$$

Excitons are classified into two types depending on their spatial extent. In solids with large effective electron and hole masses the exciton will only extend to a few lattice spacings. These are known as Frenkel excitons and are most commonly found in ionic solids where they are tightly bound and localised. In bulk GaAs the exciton has a Bohr radius which corresponds to around 40 lattice spacings. This type of exciton is denoted as a Wannier exciton. The Wannier exciton is weakly bound and non-localised.

Considering the exciton placed in an ideal 2D system, the solutions using the hydrogenic method are

$$E_n^{2D} = E_g - \frac{R_0}{\left(n-\frac{1}{2}\right)^2} \qquad 2.18$$

The ground state Bohr radius is also reduced by a factor of two due to the confinement. This leads to the electron and hole orbiting closer together and increases the ground state binding energy by a factor of four compared to its bulk value. The oscillator strength of the exciton in 2D is also increased compared to that of bulk.

In GaAs quantum wells the expected value of the exciton binding energy is around 16 meV, assuming the ideal 2D case. In reality, due to the quasi-2D nature of the quantum wells, the binding energy is reduced to around 9 meV.

2.6 References

2.1 R.C. Miller, D.A. Kleinman and A.C. Gossard, "Energy-gap discontinuities and effective masses for GaAs-Al(x)Ga(1-x)As quantum wells", Phys. Rev. B., **29**, 12, 7085-7087, (1984).

2.2 R. Dingle, W. Wiegmann and C.H. Henry, "Quantum states of confined carriers in very thin Al(x)Ga(1-x)As-GaAs-Al(x)Ga(1-x)As heterostructures", Phys. Rev. Letts., **33**, 14, 827-830, (1974).

2.3 Luttinger, "Quantum theory of cyclotron resonance in semiconductors: general theory", Phys. Rev. , **102**, 4, 1030-1041, (1956).

3

Optical properties of multiple quantum wells

3.1 Summary

In this chapter the optical properties of semiconductors will be discussed. The effects of quantum confinement on the density of state function are described. Excitons dominate the optical absorption spectra and are rapidly ionised at room temperature in quantum wells. Their increased effects in quantum wells and their ionisation mechanisms are discussed. Optical selection rules play an important role in the experiments described in future chapters and so their relevance is introduced. Bandgap resonant nonlinearities, optical orientation and spin relaxation are also discussed.

3.2 Density of states

In 3D semiconductors, assuming parabolic bands, the density of states is given by the following

$$D_{3D}(E) = \frac{1}{2\pi^2}\left(\frac{2m^*}{\hbar^2}\right)^{\frac{3}{2}} E^{\frac{1}{2}} \qquad 3.1$$

where E is the energy and m^* is the carrier effective mass. In a quantum well the energy levels are quantised and the density of states is modified as follows

$$D_{2D} = \frac{nm^*}{\pi\hbar^2} \qquad 3.2$$

where n is the quantum number n= 1,2,3,... The 2D density of states now has a "step-like" appearance and remains finite even for low energies. The 3D and 2D density of states are shown graphically in Figure 3.1. The optical absorption in a semiconductor is proportional to the density of states function. A typical room temperature absorption spectrum for a GaAs multiple quantum well is shown in Figure 3.2. The "step-like" nature of the density of states can be clearly seen along with sharp resonance features which correspond to excitons.

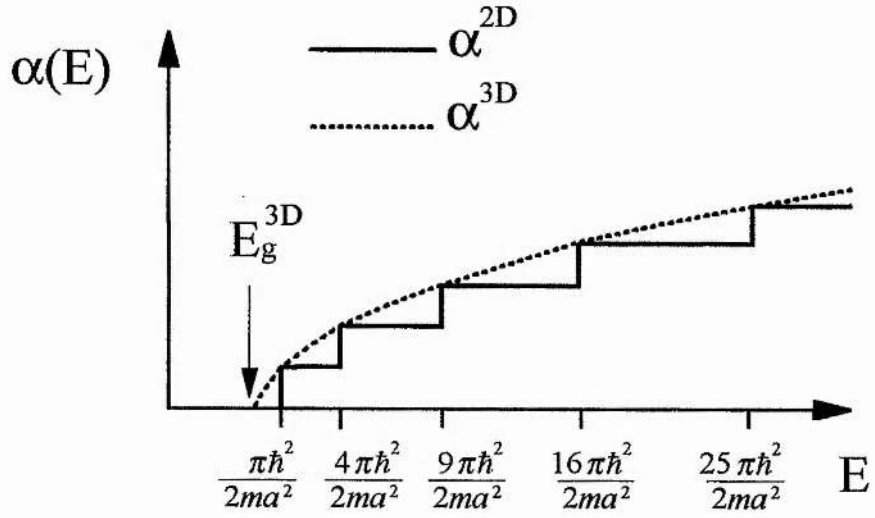

Figure 3.1 *Comparison of the 2D and 3D density of states functions.*

3.3 Excitons

In bulk semiconductors and multiple quantum wells, excitons are rapidly ionised at room temperature by LO-phonon collisions. To enable the observation of excitonic effects in bulk semiconductors, the material must therefore be cooled to low temperatures, to freeze out the LO-phonons. In quantum wells the exciton binding energy is increased and so the excitons are still observable up to room temperature. The presence of excitons is evident from the increase in the absorption at each of the "steps". The lifting of the degeneracy between the light and heavy hole can be seen in the double peaks at the n=1 resonance in Figure 3.2.

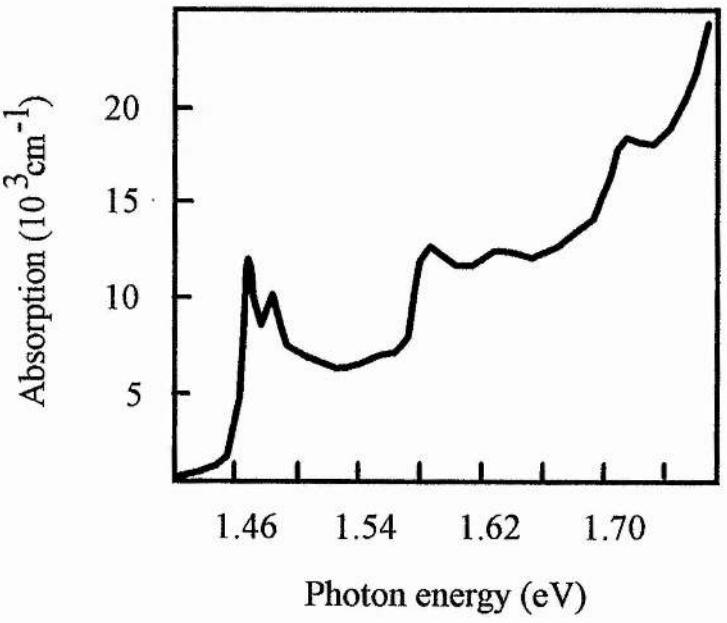

Figure 3.2 *The linear absorption spectrum of a GaAs/AlGaAs multiple quantum well.*

3.4 Optical excitation

In semiconductors illumination with a suitable energy of photon will result in the promotion of a electron into the conduction band and the formation of a hole in the valence band. The selection rules which govern these transitions are obtained by calculating the dipole matrix elements for the interband transitions. For a 3D semiconductor the selection rules are shown below.

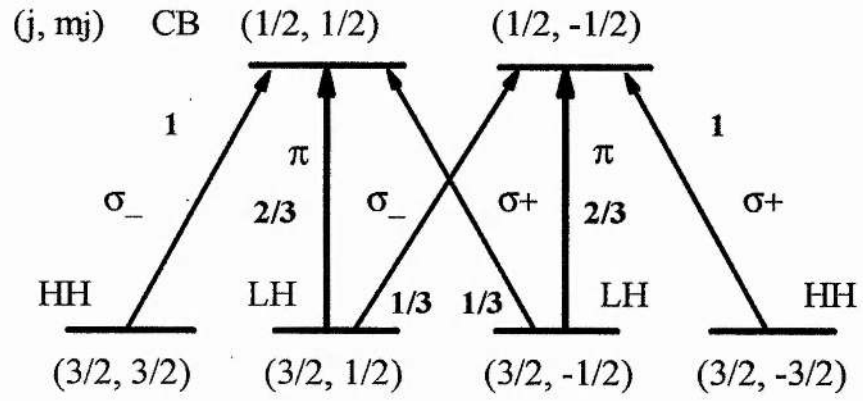

Figure 3.3 Selection rules in bulk GaAs.

In a quantum well the lifting of the degeneracy between the light and heavy holes modifies the transition levels as shown in Figure 3.4. The various allowed transitions can be summarised as follows:

$\Delta J = \pm 1$

$\Delta J_z = -(+)\hbar$ for right (left)-hand circularly polarised light, labelled $\sigma^-(\sigma^+)$,

$\Delta J_z = 0$ for linear light, labelled π.

The probabilities for the transitions [3.1] are also shown in the figures.

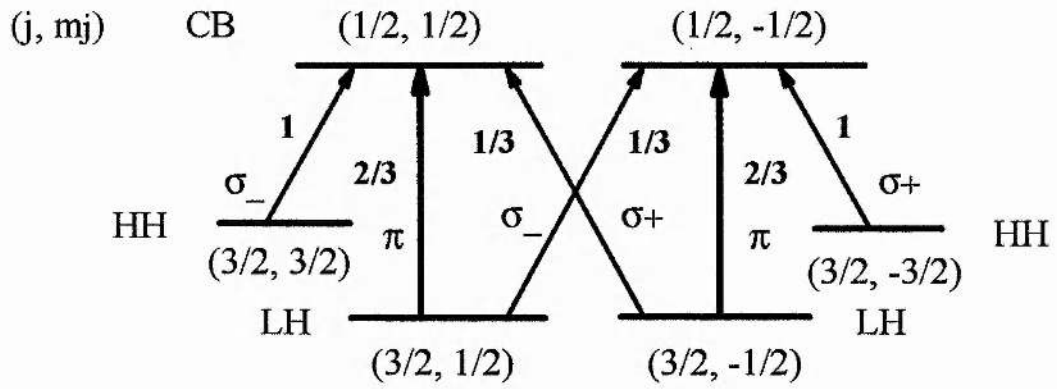

Figure 3.4 *Selection rules in GaAs multiple quantum wells.*

On excitation of a bulk semiconductor with left or right handed circular light populations of both $J_z = +\frac{1}{2}\hbar$ and $J_z = -\frac{1}{2}\hbar$ electrons are generated along with correspondingly polarised holes. The electrons are generated in the ratio 3:1 which limits the polarisation of the electrons to only 50%. The polarisation is defined as

$$P = \frac{N_\uparrow - N_\downarrow}{N_\uparrow + N_\downarrow} \qquad 3.3$$

where $N_\uparrow$ is the number of spin-up carriers and $N_\downarrow$ the number of spin-down.

In a quantum well due to the lifting of the degeneracy between the light and heavy holes valence bands it is now possible to generate electrons with 100% spin polarisation using circularly polarised light resonant with the heavy hole (or associated exciton) transition.

3.5 Bandgap resonant nonlinearities

The optical generation of carriers within a semiconductor can produce a number of nonlinear effects such as Coulomb screening, band filling, phase space filling, bandgap renormalisation and lineshape broadening.

3.5.1 Coulomb screening

The generation of an electron-hole plasma will lead to a screening of the Coulomb potential between charges. After excitation, electrons and holes occupy states within the conduction and valence bands respectively. These carriers will screen the Coulomb interaction between carriers of the same band and also that between carriers in different bands. The term screening is used to signify the decrease in the Coulomb potential of a charge when other charges are present. If a plasma consisting solely of electrons is considered, the addition of a test charge will result in a redistribution of the plasma as a result of the repulsive Coulomb interaction. The redistribution of the system acts to reduce the overall energy of the system and can be thought of as the effect of decreasing the effective energy of the test charge. This screening will reduces the attractive force between the electron and hole that form the exciton and in so doing reduces the exciton binding energy.

The effects of Coulomb screening can be divided into contributions due to a long and short range term and an exchange contribution, these are discussed in more detail in Chapter 7.

3.5.2 Band and phase space filling

Electrons and holes are Fermions and so due to the Pauli exclusion principle can occupy each quantum state only once. For each k-state that exists in a semiconductor band there are two possible states available. These correspond to either a spin-up or a spin-down carrier. A filled state is no longer available as a final state in an absorption process and so the corresponding transition is bleached. The principle of energy minimisation dictates that carriers in quasi-equilibrium occupy the lowest available states. This results in the filling of the states near the bottom of the conduction band by electrons and the top of the valence band by holes. Bandfilling arises from the consideration that for a valence to conduction band transition to occur, the valence band state has to be filled by an electron and the conduction band state has to be empty. So if the lowest lying states are already occupied by electrons and holes then their presence effectively blocks further transitions involving these

states and the absorption is bleached. This results in a shift of the absorption edge to higher energies.

The presence of excited electrons and holes also prevent the formation of excitons derived from the states that they occupy. This mechanism is denoted phase space filling. It is therefore common to refer to band filling when discussing electrons and holes and to phase space filling when referring to excitons. At low temperatures or for short periods after the generation at room temperature, exciton states are occupied and a similar process to band filling for electrons and holes occurs. This "real-space-filling" [3.2] considers the excitons as hard spheres which occupy a volume in real space. Once the available volume is filled, no further excitons can be contained and so the excitonic absorption is reduced.

3.5.3 Bandgap renormalisation

When considering the free electron and hole plasmas, Coulomb screening reduces the single particle energies due to many body effects and leads to a red shift in the band edge. This energy reduction results due to the exchange effect for particles with equal spin, and the Coulomb correlation effects for all particles. The exchange effect arises due to the Pauli exclusion principle. The probability that two Fermions with identical quantum numbers are at the same point in real space is zero. Hence the Pauli exclusion effect leads to a reduction of the probability that equally charge particles come close together, and so reduces the repulsive contribution. This situation with particles of equal spins is often described by the presence of an exchange hole, where each Fermion is surrounded by a region where the probability for the existence of another identical Fermion is very small. Correspondingly, equally charged Fermions with different quantum numbers, e.g. electrons with different spins, avoid each other because of the coulomb repulsion. As in the case of the exchange-hole this coulomb hole also leads to a decrease of the overall energy.

The combined effects of the exchange-hole and the Coulomb hole is termed bandgap renormalisation.

3.5.4 Lineshape broadening

At low temperatures the linewidth of an exciton can be attribute to a number of broadening mechanisms. These include interaction with impurities and acoustic phonons. These mechanisms result solely in homogeneous broadening of the exciton resonance. In a quantum well scattering of the excitons from well width [3.3] and alloy concentration fluctuation will result in either homogeneous or inhomogeneous broadening of the exciton resonance depending on the size of the irregularities (average diameter X). Well width or alloy fluctuations with X greater than twice the exciton Bohr radius will cause inhomogeneous broadening whereas fluctuation with X less then twice the exciton Bohr radius will result in homogeneous broadening.

As the temperature is raised the exciton linewidth increases due to thermal broadening. This results from the increased probability of collision with an LO-phonon. This contribution from thermal broadening to the exciton linewidth can be written as

$$\Gamma(T) = \Gamma(0) + \frac{\Gamma_{ph}}{\left[\exp\left(\frac{-\hbar\Omega_{LO}}{kT}\right) - 1\right]} \qquad 3.4$$

where $\Gamma(0)$ is the temperature independent linewidth. Γ_{ph} is a parameter which describes the effect of LO-phonons. $\hbar\Omega_{LO}$ is the phonon energy and T is the temperature [3.4]. Due to the large LO-phonon energy, when compared to the exciton binding energy, any collision with an exciton will result in its complete ionisation. At room temperature the exciton ionisation time has been measured to be 300 fs by Knox et al. [3.5].

The homogeneous linewidth of the exciton is also influenced by the effects of collisions with excitons or free-carriers. At room temperature collisional broadening results predominantly from exciton collisions with free-carriers. The presence of free carriers, created by optical excitation, increases the exciton linewidth. The density dependence of the exciton linewidth can, in the low density regime, be described by

$$\Gamma(N) = \Gamma(0) + \gamma a_B^{\,2} E_B N \qquad 3.5$$

where $\Gamma(0)$ is the density independent linewidth, γ is a dimensionless parameter which gives a measure of the collision efficiency of the exciton-free carrier interaction, a_B is the exciton Bohr radius, E_B is the exciton binding energy and N is the density of free-carriers [3.6].

3.6 Optical orientation

As previously discussed the absorption of circularly polarised light can selectively generate spin polarised electron and holes. The effect that light has on the spin angular momentum of the carriers which it interacts with is described as optical orientation.

In bulk GaAs the light and heavy hole transitions are degenerate at k=0. This along with unequal transition probabilities (see Figure 3.3) results in a maximum induced polarisation of 50%. For the case of GaAs multiple quantum wells the degeneracy between the heavy and light hole states is lifted (see Figure 3.4) and so it becomes possible to obtain 100% polarisation of the excited carriers.

After generation an initially spin polarised population of carriers will, over time, relax due to various scattering mechanisms to produce equal numbers of carriers in both of the spin states. Spin relaxation occurs on timescales ranging from femtoseconds up to 100s of picoseconds. The mechanisms that cause the spin to relax will now be discussed first for bulk GaAs and then for the case of quantum wells.

3.6.1 Spin relaxation in bulk GaAs

In bulk GaAs the hole spins are expected to randomise on very short timescales due to the degeneracy of the light and heavy hole valence bands at k=0. This time is essentially the same as the hole momentum relaxation time.

There have been a number of mechanisms proposed to describe the spin relaxation of electrons in bulk semiconductors. The most notable are the D'yakonov-Perel (DP), the Elliott-Yafet (EY) and the Bir-Aharonov-Pikus (BAP) mechanisms.

The EY and DP mechanisms for spin relaxation are derived from band structure effects near the Γ-point of the conduction band. It should be noted that although the number of electrons excited by optical pumping is small, they are not all located at the Γ-point, due to thermalisation which produces a spread in k-space.

The mechanism proposed by Elliott and Yafet [3.7,3.8] results from mixing of valence band wavefunctions into the conduction band states away from k=0. This mixing allows the electrons to flip spin due to momentum scattering from optical and acoustical phonons as well as impurities. It has been suggested [3.9] that the EY mechanism will contribute to electron spin relaxation at high temperatures and/or low hole concentrations. The effect is expected to be reduced when compared to the DP mechanism due to the strong temperature dependence of the electron spin relaxation time for temperatures above 50 K.

The DP mechanism involves spin flipping during collisions [3.10,3.11]. This mechanism arises due to the spin splitting of the conduction band in semiconductors without a centre of inversion (such as GaAs). In zinc blende crystals, this splitting is proportional to the cube of the momentum and the contribution to the spin relaxation time from the DP mechanism rapidly increases with increasing electron energy [3.12].

The spin splitting of the conduction band is equivalent to the existence of a magnetic field acting on the electron spins. The magnitude and direction of this pseudo-field depends on the magnitude and direction of the momentum. In the absence of collisions this would result in an increase in the electron spin relaxation time.

Between collisions the spin of each electron precesses about the direction of the effective magnetic field which defines the direction of the quasi-momentum. During collisions the changes in momentum lead to the rotation of the precession axis which allows the spin to flip. If the time between collisions is less than the precession period, then the electron spin is unable to follow the frequent rotations of the precession axis. This reduces the effect of the spin splitting and slows the spin relaxation process. The DP mechanism has been shown experimentally to be dominant for low acceptor impurity concentrations and/or at high temperatures [3.13, 3.14] through the temperature dependence of the electron spin relaxation time.

The BAP mechanism is important when the excited electrons are surrounded by a high concentration of holes. The increased probability of electron and hole collisions allows the electron and hole spins to interact via the exchange interaction and so flip the electron spins [3.15]. The spin relaxation time is inversely proportional to the hole momentum scattering time, if the holes are strongly scattered by impurities or phonons. This mechanism has been shown to be dominant in heavily p-doped semiconductors and at low temperatures [3.16, 3.17] again through the temperature dependence of the electron spin relaxation time.

A number of investigations [3.18, 3.19] have characterised the transition from DP to BAP in GaAs and shown them to be the dominant mechanisms for electron spin relaxation in bulk GaAs.

A further mechanism based on the virtual recombination of colliding electron hole pairs, to produce a virtual photon which on subsequent virtual absorption could produce a new electron-hole pair with flipped spins was suggested by Kleinman and Miller [3.20]. This mechanism was needed to explain results obtained with degenerate hole distributions at low temperature.

3.6.2 Spin relaxation in GaAs multiple quantum wells

The spin dynamics of electrons and holes in quantum wells are still not well understood. The main difficulty seems to arise from sample dependent mechanisms which make quantitative comparisons between samples unreliable.

In a quantum well the degeneracy between the heavy hole and light hole valence bands is lifted at k=0. Since the spin-flip of holes arises solely from the admixture of the heavy and light hole band states, it has been suggested that this mechanism will lead to a reduced spin relaxation rate in quantum wells. A number of papers have presented theoretical models relating to hole spin relaxation where a number of scattering mechanisms are considered [3.21-24]. Ferreira et al [3.24] predicted a slow hole spin relaxation from alloy and impurity scattering. A much faster hole spin relaxation mechanism was proposed by Uenoyama [3.23] which arose due to scattering from phonons. Since the excited hole energy is generally small compared to the optical phonon energy, scattering from optical phonons is not considered to be important for hole spin relaxation. The most important mechanism seems to be the scattering of hole from acoustic phonons through the deformation potential and piezo-electric coupling. The hole spin relaxation has been measured at low temperature to be 4 ps [3.25,3.26] and it is now established that the hole spin relaxation time is the order of the momentum relaxation time. Comparison of the experimental results with the theoretical prediction has proved difficult because of the different scattering processes that contribute to hole relaxation. A number of authors [3.25-27] have reported large variations in the hole spin relaxation time between samples. Kohl et al [3.27] reported that for samples with non-optimised growth conditions widely differing results were obtained. This suggests that interface scattering processes in quantum well samples play an important role.

Electron spin relaxation in quantum wells is also poorly understood. Damen et al [3.25] measured a low temperature electron spin relaxation time of 150 ps in a p-doped GaAs quantum well. This time is 4x shorter than the value obtained for bulk. They suggest that the increased electron-hole exchange interaction that exists in quantum wells is responsible for this and proposed that the BAP mechanism is the dominant mechanism in p-doped quantum wells at low temperature.

At room temperature the DP mechanisms has been proposed as in the case of bulk electron spin relaxation [3.28]. The decrease in the electron spin relaxation time has been investigate theoretically by D'yakonov and Kachorovskii [3.29]. In the two-dimensional case the projection of the electron momentum q, along the normal to the layer plane is much greater than the two-dimensional momentum k, in this plane. This

leads to an increase in the spin splitting compared to the bulk case. It follows that the effective magnetic field in the two-dimensional case is considerably greater than the three-dimensional one and therefore the spin relaxation rate is increased.

The spin relaxation of excitons in quantum wells has received a great deal of interest [3.30-3.37]. The situation is more complex than when considering spin relaxation solely due to electrons or holes and has to be considered for experiments performed at low temperatures. The exciton can relax its spin either through electron and hole exchange interaction which can result in the mutual spin flipping of the electron and hole, or by independent spin relaxation of the electron and hole. Experiments have shown that the BAP mechanism should be dominant.

The inspiration for this thesis comes from the low temperature work of Snelling et al [3.38] on spin relaxation in quantum wells. The room temperature spin dynamics of optically excited carriers were investigated by Snelling et al [3.39]. Circularly polarised light was used to separate the phase space filling and Coulomb screening contributions to exciton saturation and observe density dependent broadening of the exciton resonance. In this thesis the effects due of density dependent broadening of the exciton resonance are further investigated through its well width dependence.

The initial work carried out by Perozzo [3.40] on the well width dependence of the electron spin relaxation time at room temperature is expanded to include new results. This has enables a clearer understanding of the mechanisms involved and allowed tentative suggestions to be made as to the dominant mechanism at room temperature.

Finally the spin relaxation of electrons at room temperature is combined with the production of polarisation gratings in GaAs quantum wells. This has allowed the production of electron spin gratings and the first direct all optical measurement of the in-plane electron mobility at room temperature.

3.7 References

3.1 C. Weisbuch and B. Vinter, *Quantum semiconductor structures*, (Academic Press Inc. 1991).

3.2 S. Schmitt-Rink, D.S. Chemla and D.A.B. Miller, "Theory of transient excitonic optical nonlinearities in semiconductor quantum-well structures", Phys. Rev. B., **32**, 10, 6601-6609, (1985).

3.3 C. Weisbuch, R. Dingle, A.C. Gossard and W. Wiegmann, "Optical characterisation of interface disorder in GaAs-Ga(1-x)Al(x)As multi-quantum well structures", Solid. State. Comms., **38**, , 709-712, (1981).

3.4 D.S. Chemla and D.A.B. Miller, "Room-temperature excitonic nonlinear-optical effects in semiconductor quantum-well structures", J. Opt. Soc. Am. B, **2**, 7, 1155-1173, (1985).

3.5 W.H. Knox, R.L. Fork, M.C. Downer, D.A.B. Miller, D.S. Chemla, C.V. Shank, A.C. Gossard and W. Wiegmann, "Femtosecond dynamics of resonantly excited excitons in room-temperature GaAs quantum wells", Phys. Rev. Letts., **54**, 12, 1306-1309, (1985).

3.6 A. Honold, L. Schultheis, J. Kuhl and C.W. Tu, "Collisional broadening of two-dimensional excitons in a GaAs single quantum well", Phys. Rev. B., **40**, 9, 6442-6445, (1989).

3.7 R.J. Elliott, "Theory of effect of spin-orbit coupling on magnetic resonance in some semiconductors", Phys. Rev., **96**, 2, 266-279, (1954).

3.8 Y. Yafet, "g factors and spin-lattice relaxation of conduction electrons", Solid. State. Phys., **14**, 1-98, (1963).

3.9 A.H. Clark, R.D. Burnham, D.J. Chadi and R.M. White, "Spin relaxation of conduction electrons in GaAs", Solid. State. Comms., **20**, 385-387, (1976).

3.10 M.I. D'yakonov, and V.I. Perel', "Spin orientation of electrons associated with the interband absorption of light in semiconductors", Sov. Phys. JETP, **33**, 5, 1053-1059, (1971).

3.11 M.I. D'yakonov, and V.I. Perel', "Spin relaxation of conduction electrons in noncentrosymmetric semiconductors", Sov. Phys. Solid State, **13**, 12, 3023-3026, (1972).

3.12 R.J. Seymour, M.R. Junnarkar and R.R. Alfano, "Spin relaxation of photogenerated degenerate electron distributions in GaAs", Phys. Rev. B., **24**, 6, 3623-3625, (1981).

3.13 Clark, R.D. Burnham, D.J. Chadi and R.M. White, "Spin relaxation of conduction electrons in Al(x)Ga(1-x)As", Phys. Rev. B., **12**, 12, 5758-5765, (1975).

3.14 V.L. Berkovits, A.I. Ekimov and V.I. Safarov, "Optical orientation in a system of electrons and lattice nuclei in semiconductors. Experiment", Sov. Phys. JETP, **38**, 1, 169-176, (1974).

3.15 G.L. Bir, A.G. Aronov and G.E. Pikus, "Spin relaxation of electrons due to scattering by holes", Sov. Phys. JETP, **42**, 4, 705-712, (1976).

3.16 G. Fishman, and G. Lampel, "Spin relaxation of photoelectrons in p-type gallium arsenide", Phys. Rev. B., **16**, 2, 820-831, (1977).

3.17 R.J. Seymour, and R.R. Alfano, "Time-resolved measurement of the electron-spin relaxation kinetics in GaAs", Appl. Phys. Letts., **37**, 2, 231-233, (1980).

3.18 A.G. Aronov, G.E. Pikus and A.N. Titkov, "Spin relaxation of conduction electrons in p-type III-V compounds", Sov. Phys. JETP, **57**, 3, 680-687, (1983).

3.19 K. Zerrouati, F. Fabre, G. Bacquet, J. Bandet, J. Frandon, G. Lampel and D. Paget, "Spin-lattice relaxation in p-type gallium arsenide single crystals", Phys. Rev. B., **37**, 3, 1334-1341, (1988).

3.20 D.A. Kleinman, and R.C. Miller, "Relaxation of optically pumped electron spins through a virtual photon: Experimental evidence in heavily Zn-doped GaAs", Phys. Rev. Letts., **46**, 1, 68-71, (1981).

3.21 A. Twardowski, and C. Hermann, "Variational calculation of polarisation of quantum-well photoluminescence", Phys. Rev. B., **35**, 15, 8144-8153, (1987).

3.22 T. Uenoyama, and L.J. Sham, "Carrier relaxation and luminescence polarisation in quantum wells", Phys. Rev. B., **42**, 11, 7114-7123, (1990).

3.23 T. Uenoyama, and L.J. Sham, "Hole relaxation and luminescence polarisation in doped and undoped quantum wells", Phys. Rev. Letts., **64**, 25, 3070-3073, (1990).

3.24 R. Ferreira, and G. Bastard, ""Spin"-flip scattering of holes in semiconductor quantum wells", Phys. Rev. B., **43**, 12, 9687-9691, (1991).

3.25 T.C. Damen, L. Vina, J.E. Cunningham and J. Shah, "Subpicosecond spin relaxation dynamics of excitons and free carriers in GaAs quantum wells", Phys. Rev. Letts., **67**, 24, 3432-3435, (1991).

3.26 S. Bar-Ad, and I. Bar-Joseph, "Exciton spin dynamics in GaAs heterostructures", Phys. Rev. Letts., **68**, 3, 349-352, (1992).

3.27 M. Kohl, M.R. Freeman, D.D. Awschalom and J.M. Hong, "Femtosecond spectroscopy of carrier-spin relaxation in GaAs-Al(x)Ga(1-x)As quantum wells.", Phys. Rev. B., **44**, 11, 5923-5926, (1991).

3.28 R.C. Miller, D.A. Kleinman, W.A. Nordland and A.C. Gossard, "Luminescence studies of optically pumped quantum wells in GaAs-Al(x)Ga(1-x)As multilayer structures", Phys. Rev. B., **22**, 2, 863-871, (1980).

3.29 M.I. D'yakonov, and V.Y. Kachorovskii, "Spin relaxation of two-dimensional electrons in noncentrosymmetric semiconductors", Sov. Phys. Semicond., **20**, 1, 110-112, (1986).

3.30 S. Adachi, S. Takeyama, Y. Takagi, A. Tackeuchi and S. Muto, "Ultrafast optical sampling pump-probe measurement of exciton spin relaxation in GaAs/AlGaAs quantum wells", Appl. Phys. Letts., **68**, , 964, (1996).

3.31 L.J. Sham, "Theory of spin dynamics of excitons and free carriers in quantum wells" in *Optical phenomena in semiconductors* Ed. D.J. Lockwood, Kluwer, (1993).

3.32 B. Baylac, T. Amand, M. Brousseau, X. Marie, B. Dareys, G. Bacquet, J. Barrau and R. Planel, "Exciton spin relaxation in the 2D dense excitonic phase: the role of exchange interaction", Semicond. Sci. Technol., **10**, 295-301, (1995).

3.33 A. Vinattieri, J. Shah, T.C. Damen, K.W. Gossen, L.N. Pfeiffer, M.Z. Maialle and L.J. Sham, "Electric field dependence of exciton spin relaxation in GaAs/AlGaAs quantum wells", Appl. Phys. Letts., **63**, 23, 3164-3166, (1993).

3.34 Y. Takagi, S. Adachi, S. Takeyama, A. Tackeuchi, s. Muto and J.J. Dubowski, "Ultrafast exciton spin relaxation in GaAs/AlGaAs and CdMnTe multiple quantum wells", J. Lumin., **58**, 202-205, (1994).

3.35 A. Frommer, A. Ron, E. Cohen, J.A. Kash and L.N. Pfeiffer, "Dynamics and spin relaxation of excitons in GaAs/Al(x)Ga(1-x)As quantum wells", Phys. Rev. B., **50**, 16, 11833-118, (1994).

3.36 T. Amand, B. Dareys, B. Baylac, X. Marie, J. Barrau, M. Brousseau, D.J. Dunstan and R. Planel, "Exciton formation and hole-spin relaxation in intrinsic quantum wells", Phys. Rev. B., **50**, 16, 11624-116, (1994).

3.37 M.Z. Maialle, A.E. de Andrada e Silva and L.J. Sham, "Exciton spin dynamics in quantum wells", Phys. Rev. B., **47**, 23, 15776-157, (1993).

3.38 M.J. Snelling, A.S. Plaut, G.P. Flinn, A.C. Tropper, R.T. Harley and T.M. Kerr, "Spin relaxation in optically excited quantum wells", J. Lumin., **45**, 208-210, (1990).

3.39 M.J. Snelling, P. Perozzo, D.C. Hutchings, I. Galbraith and A. Miller, "Investigation of excitonic saturation by time resolved circular dichroism in GaAs-AlGaAs multiple quantum wells", Phys. Rev. B, **49**, 24, 17160-171, (1994).

3.40 P. Perozzo, PhD thesis, *University of Central Florida*, (1995).

4

Carrier transport phenomena

4.1 Summary

This chapter will discuss a number of carrier transport phenomena that have important implications for some of the experiments described in the following chapters. The two basic transport mechanisms that will be discussed are those of drift (the movement of charge due to an electric field) and diffusion (the flow of charge due to a density gradient). The drift velocity of a carrier is related to the electric field by a parameter called the mobility. The concept of carrier drift and mobility will be introduced and the differences between Hall and drift mobilities are discussed. The scattering mechanisms in bulk and quantum well semiconductors and how they influence the mobilities of the carriers are given. The combined motion of electrons and holes, termed ambipolar, is also introduced.

4.2 Carrier drift, conductivity and the Hall effect

An electric field applied to a semiconductor will cause electrons and holes to move. This movement, due to the presence of the electric field, is called drift. In a uniform electric field the accelerating charged particles undergo collisions and scattering events which alter the velocity of the particle. The particle will appear over a period of time to be travelling with an average velocity v_{av} which can be written as

$$v_{av} = \mu E \tag{4.1}$$

where E is the electric field and μ is the proportionality constant called the mobility. The mobility describes how well the charged carrier moves in an electric field. The drift of both electrons and holes in an electric field will give rise to a combined drift current density which is given by

$$J_{drift} = e(\mu_n n + \mu_p p)E \tag{4.2}$$

where μ_n and μ_p are the mobilities corresponding to the electron (n) and hole (p) concentrations.

The conductivity, σ, of a semiconductor is defined

$$\sigma = (\mu_n n + \mu_p p) \tag{4.3}$$

and is a function of the electron and hole concentrations as well as their corresponding mobilities. In extrinsic semiconductors the conductivity is primarily a function of the majority carrier parameters.

The Hall effect results from the forces that a moving charge experiences from electric and magnetic fields. The Hall coefficient can be written as

$$R = -\frac{1}{ne} \tag{4.4}$$

when the charge carriers are electrons and

$$R = \frac{1}{pe} \tag{4.5}$$

when the charge carriers are holes. The Hall effect provides a practical way of determining whether a semiconductor is n-type or p-type and determining the

concentration of carriers. When combined with a measurement of the conductivity, the Hall effect can also be used to determine the mobility of the charge carriers. The Hall mobility, μ_H, is defined as the product of the Hall coefficient and the conductivity.

$$\mu_H = |R\sigma| \tag{4.6}$$

The Hall mobilities are obtained from quantities that are easily measured and have the same dimensions as the drift mobilities.

4.3 Comparison of Hall and drift mobilities

The Hall mobilities for electrons and holes can be converted into the true drift mobilities using the following equations

$$\mu_p = \mu_{Hp}\left(\overline{(\tau_p)^2} \Big/ \overline{\tau_p^2}\right) \tag{4.7}$$

for the hole mobility and

$$\mu_n = \mu_{Hn}\left(\overline{(\tau_n)^2} \Big/ \overline{\tau_n^2}\right) \tag{4.8}$$

for the electron mobility. The quantity τ is the mean free time between carrier collisions. The quantity $\overline{(\tau_n)^2} \Big/ \overline{\tau_n^2}$ is dependent on the dominant scattering mechanism that exists in the semiconductor. This does not usually deviate far from unity and so the Hall mobility will give a rough indication of the true mobility. In the following chapters, where experimental measurements of carrier mobilities are made, the mobility measured will always be the true drift mobility.

4.4 Scattering mechanisms

It has previously been stated that the mobility relates how well a charge carrier moves within an electric field. The movement of the charge carrier will obviously be affected by collisions or scattering mechanisms. The mobility can also be written in the form

$$\mu = \frac{e\tau}{m^*} \qquad 4.9$$

In semiconductors the most important scattering processes involve the interaction of electrons or holes with lattice vibrations and with impurity atoms. At high temperatures or in high purity samples the scattering due to lattice vibrations dominates. In impure samples or at low temperatures the effects due to impurity scattering becomes more important. The scattering mechanisms will now be discussed with reference to GaAs. The cases of bulk, heterostructure and quantum well samples are considered.

4.4.1 Scattering in bulk samples

There are two mechanisms that dominate the scattering of electrons and holes in bulk GaAs [4.1] samples: phonon or lattice scattering and ionised impurity scattering.

At low temperatures the thermal energy available to excite optical-mode lattice vibrations is low and so most lattice scattering will occur due to acoustic-mode lattice vibrations. The scattering effects due to acoustic phonon scattering contribute only 10% to the total lattice scattering at room temperature where the effects of optical-mode scattering are more pronounced.

Lattice vibrations cause the atoms that make up the crystal to vibrate about their normal lattice positions. These vibrations disrupt the perfect periodic potential present in solids. This leads to interaction between the electrons or holes with the vibrating lattice atoms. The lattice scattering is related to the thermal motion of the

atoms and so is a function of temperature. The mobility due to lattice scattering can be written as

$$\mu \propto \frac{1}{T^{\frac{3}{2}}} \qquad 4.10$$

The mobility due to lattice scattering will increase as the temperature decreases.

The second scattering mechanism of importance in bulk GaAs is that due to the presence of ionised impurity atoms [4.2]. These scattering effects dominate the mobility at low temperatures and also reduce the mobility at high temperatures (see Figure 4.1).

The scattering occurs due to the Coulomb interaction that exists between charge carriers. This interaction will alter the velocity characteristics of the charge carriers through collisions or scattering events. The mobility due solely to ionised impurity scattering can be written as

$$\mu \propto \frac{T^{\frac{3}{2}}}{N_I} \qquad 4.11$$

where N_I is the total ionised impurity concentration. As the temperature increases so the thermal motion of the carriers increases, reducing the time that a charge carrier spends interacting with any ionised impurity. The less time spent interacting, the smaller is the expected scattering effect and so a larger mobility is expected. If the ionised impurity concentration is increased then there is a higher probability that the charge carrier will encounter an impurity atom and so the mobility is expected to be reduced.

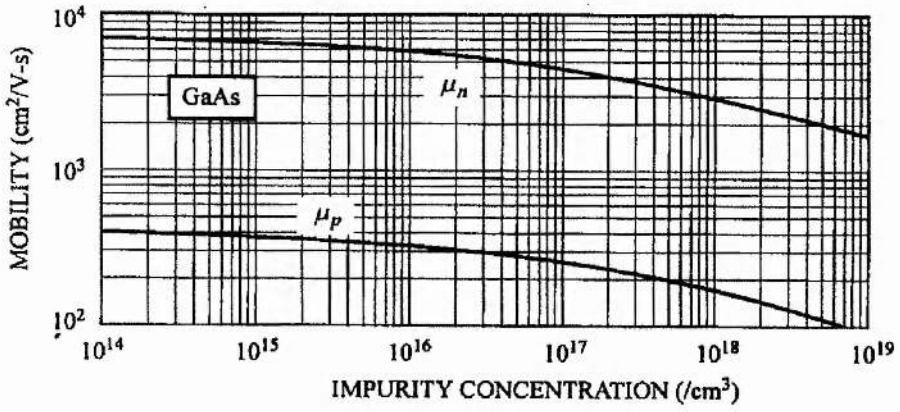

Figure 4.1 *Drift mobility for GaAs at 300K as a function of impurity concentration (after Sze [4.2]).*

If these two scattering mechanisms can be considered to be independent then it is possible to sum the mobilities due to each scattering mechanism as follows

$$\frac{1}{\mu} = \sum_n \frac{1}{\mu_n} \qquad 4.12$$

The additional scattering processes that are present in heterostructures and quantum wells will now be considered.

4.4.2 Scattering in heterostructures

There has been a number of reports on the electron mobilities in modulation-doped materials. This doping technique separates the mobile carriers from their ionised parents and creates a two-dimensional electron layer within the semiconductor host. The confinement occurs in a triangular potential well with dimensions ~ 10-20 nm. The separation of the electrons from the ionised impurity atoms has allowed very high electron mobilities to be obtained at low temperatures [4.3]. There have been fewer studies on the corresponding hole mobilities [4.4]. The

investigations have shown that the mobilities for 2D electrons and holes follow the mobilities obtained in high quality bulk materials down to low temperatures. The main scattering mechanisms are the same as those in bulk semiconductors.

4.4.3 Scattering in quantum wells

There are a number of additional scattering mechanisms in quantum well semiconductors that are not evident in bulk or heterostructure samples. When quantum wells are compared to heterostructures it is obvious that the confinement is more pronounce in the quantum well case. For well-widths below ~7 nm scattering mechanisms due to the interface become important.

Microscopic fluctuations in the quantum well well-width will lead to fluctuations in the quantisation energy. These fluctuations become more important as the well-width is reduced [4.5] and lead to what is termed as interface roughness scattering. The mobility due to this mechanism has been found theoretically and experimentally to be strongly dependent on the well width [4.6].

When the quantum well is surrounded by a ternary or quaternary barrier material, as is the case for GaAs/AlGaAs quantum wells, barrier-alloy-disorder scattering occurs [4.5,4.7]. This mechanism is related to the penetration of the carrier wavefunction into the barrier material and depends on the barrier height and the well width. Atoms from the alloy are randomly distributed in the barrier and this leads to a fluctuating potential and causes a scattering process in the barrier itself. This mechanism is very small in heterostructure but becomes more important as the confinement increases.

The two scattering mechanisms described above for the case of quantum well semiconductors will limit the mobility at low temperatures and reduce it at high temperatures. They are both due to localised perturbations near the interface. This will lead to a stronger effect on "s-type" wavefunctions such as electrons than on the "p-type" wavefunctions of holes [4.5]. A further consequence of this will be band tailing in the energy spectrum.

The scattering of charge carriers from ionised impurities in 2D has been shown to be larger than that in 3D [4.8]. This arises from the increased overlap of the

charge carriers wavefunctions with the impurities and that the screening of impurities is weaker when compared to bulk semiconductors.

4.5 Carrier diffusion

There is a second mechanism which will lead to the movement of carriers within a semiconductor known as diffusion. Diffusion is the process where particle flow from a region of high concentration toward a region of low concentration. This motion of charge carriers results in a diffusion current density which is related to the spatial gradient of the charge concentration by the following relationship

$$J_{diff} = (-)eD_{e(h)}\frac{dn(p)}{dx} \qquad 4.13$$

where n and p refer to electrons and holes and x denotes the direction of the concentration gradient. $D_{e(h)}$ is the electron (hole) diffusion coefficient which relates how well the electrons (holes) move due to a density gradient.

The diffusion coefficient can be related to the mobility, within the Boltzman approximation, using the Einstein relation

$$\frac{D_e}{\mu_e} = \frac{D_h}{\mu_h} = \frac{kT}{e} \qquad 4.14$$

The mobilities have been shown to be strongly dependent on scattering processes and so therefore are the diffusion coefficients.

4.6 Ambipolar transport

When excess electrons and holes are generated in a semiconductor by a process such as optical excitation the electrons and holes do not move independently

of each other. They will diffuse and drift with the same effective diffusion coefficient and drift mobility. This phenomena is called ambipolar transport.

When an excess population of electrons and holes are generated at a certain point within a semiconductor they will diffuse to cancel any gradient in the carrier concentration. Due to the higher mobility of the electrons when compared to the holes, the electrons would be expected to diffuse faster leaving the holes behind. Since the motion involves charge carriers any separation of the electrons and holes will lead to the formation of an electric field. This field will tend to slow the motion of the electrons and increase the motion of the holes. The electron and hole distributions will therefore diffuse together with a single effective diffusion coefficient. This diffusion coefficient is called the ambipolar diffusion coefficient and is given as

$$D_a = \frac{D_e D_h (n+p)}{D_e n + D_h p} \qquad 4.15$$

In GaAs $D_e >> D_h$ and the ambipolar diffusion coefficient is dominated by the slower hole diffusion. The ambipolar diffusion coefficient can be approximated to twice the hole diffusion coefficient (with n = p) as shown below.

$$D_a \rightarrow \frac{D_e D_h 2n}{D_e n} = 2D_h \qquad 4.16$$

4.7 References

4.1 J.S. Blakemore, "Semiconducting and other major properties of gallium arsenide", J. Appl. Phys., **53**, 10, R123-R181, (1982).

4.2 S.M. Sze, *Physics of semiconductor devices*, (Wiley & Sons Inc.,1981).

4.3 B.J.F. Lin, D.C. Tsui, M.A. Paalanen and A.C. Gossard, "Mobility of two-dimensional electron gas in GaAs-Al(x)Ga(1-x)As heterostructures", Appl. Phys. Letts., **45**, 6, 695-697, (1984).

4.4 H.L. Stormer, A.C. Gossard, W. Wiegmann, R. Blondel and K. Baldwin, "Temperature dependence of the mobility of two-dimensional hole systems in modulation-doped GaAs-(AlGa)As", Appl. Phys. Letts., **44**, 1, 139-141, (1984).

4.5 G. Bastard, *Wave mechanics applied to semiconductor heterostructurers*, (les editions de physique, 1988).

4.6 H. Sakaki, T. Noda, K. Hirakawa, M. Tanka and T. Matsusue, "Interface roughness scattering in GaAs/AlAs quantum wells", Appl. Phys. Letts., **51**, 23, 1934-1936, (1987).

4.7 H. Hillmer, A. Forchel, S. Hansmann, M. Morohashi, E. Lopez, H.P. Meier and K. Ploog, "Optical investigations on the mobility of two-dimensional excitons in GaAs/Ga(1-x)Al(x)As quantum wells", Phys. Rev. B., **39**, 9, 10901-109, (1989).

4.8 W.T. Masselink, "Ionized-impurity scattering of quasi-two-dimensional quantum-confined carriers", Phys. Rev. Letts., **66**, 11, 1513-1516, (1991).

5

Experimental techniques

5.1 Summary

In the following chapter the basic experimental techniques used to study the optical properties of multiple quantum wells are introduced.

5.2 Introduction

The optical properties of multiple quantum wells provide important information on fundamental physical properties as well as allowing their use in a number of optical devices. In a multiple quantum well or indeed any semiconductor the creation of free electrons and holes can occur via the absorption of radiation with a photon energy above the band gap energy. The radiation can take the form of a standard white light source or that emitted from a laser. The principle experiments of interest are ones that allow the measurement of linear absorption spectra, these provide important information on the position of exciton resonances and band structure, and those that allow the dynamical behaviour of initially excited carriers to be monitored. In the following sections the experimental techniques utilised to make these measurements will be discussed.

5.3 Linear absorption measurements

The measurement of the linear absorption of a semiconductor sample can be carried out in a number of ways. The basic technique involves measuring the absorption of light passing through the multiple quantum well sample while scanning the wavelength of the incident light. The light source can be a laser, in this case the laser wavelength is scanned, or a standard white light source, where the wavelength selection is made via a monochromator. Care must be taken to ensure that the incident light does not induce any saturation as this will clearly not allow the measurement of the linear absorption. (The technique using the laser can be used to look at saturation effects as the power can usually be varied above the linear regime). It is also important that the obtained data is calibrated for any spectral variation in the power of the light source as the wavelength is scanned.

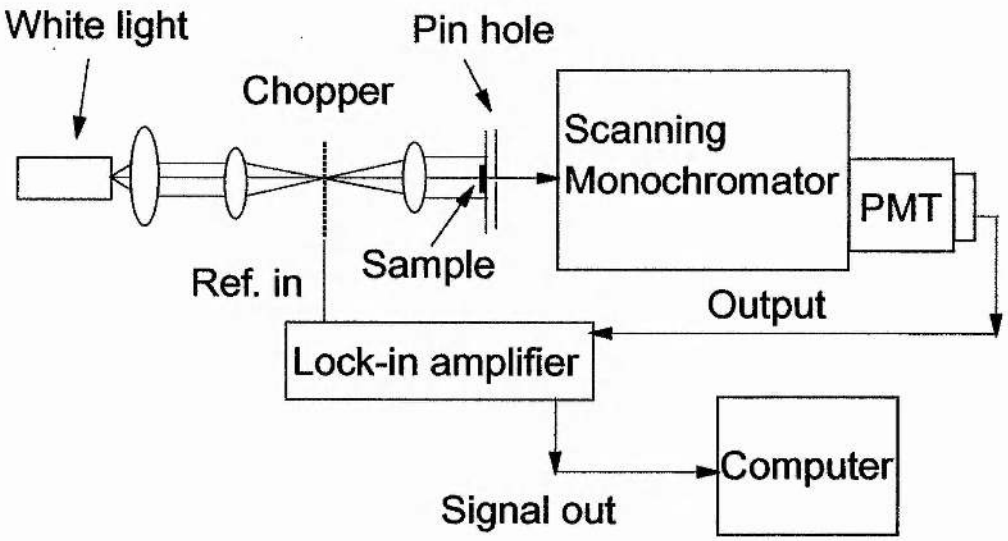

Figure 5.1 *Experimental set-up for the measurement of the linear absorption using a white light source.*

The experimental arrangement for the measurement of the linear absorption using a white light source is shown above.

The light from the source, usually a high power (100 W) tungsten bulb is collimated and then focused on the blade of a chopper using a series of lenses. The chopper is used to allow phase sensitive detection via the lock-in amplifier. After the chopper the light is again collimated and made incident on the sample which is positioned directly in front of an aperture. A scanning monochromator in conjunction with a photomultiplier and lock-in amplifier are then used to measure the absorption as the wavelength is scanned. The data is recorded at incremental steps of the wavelength scan, by the computer. If necessary the experiment can be repeated a number of times to allow averaging. Once the experiment is completed the data is corrected for the spectral response of the lamp using a control run which is carried out with no sample present.

The measurement of the linear absorption using a laser is essentially the same as the method described above. The spectral purity of the laser light negates the need for the monochromator, although the danger of inducing saturation is much more of a problem. This can be resolved by measuring the absorption at a number of power levels to ensure the experiment is being carried out within the linear regime. The experimental set-up is shown below.

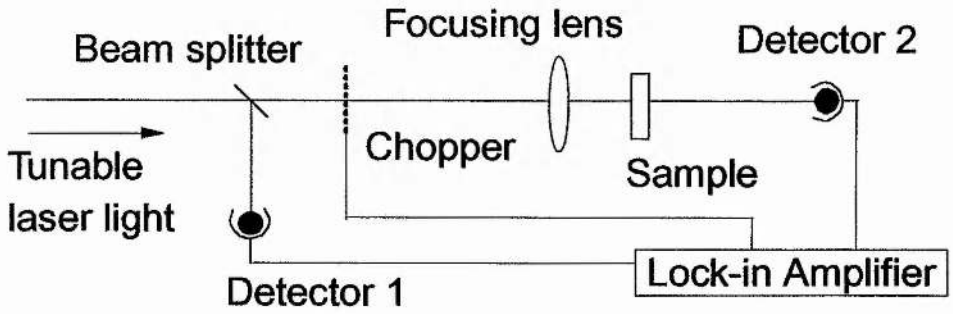

Figure 5.2 *Experimental set-up for the measurement of the linear absorption using a laser.*

Phase sensitive detection, via the chopper and a lock-in amplifier, is again used to increase the signal to noise ratio. The detector measuring the intensity of the light reflected from the beam splitter is used to normalise the signal and in so doing correct the data in real time for any power variation in the laser light. The data is again recorded using a computer. To obtain the full wavelength sweep of the linear absorption the laser must be tuneable over that range. These measurements can provide no detail on the temporal dynamics of the processes that occur within quantum wells. For these measurements the technique know as degenerate time-resolved pump-probe is used.

5.4 Degenerate time-resolved pump-probe

To time resolve the optical properties of quantum wells the most commonly used technique is that of degenerate time-resolved pump-probe. This technique measures the changes in transmission of a sample as the relative delay between a strong pump pulse and a weaker probe pulse is varied. By detecting the probe transmission as the delay is scanned it is possible to time resolve a number of mechanisms. The source used in these experiments is a self-mode locked Titanium:sapphire laser.

5.4.1 Self-mode locked Titanium:sapphire laser

The self-modelocked titanium:sapphire used in the following experiments is a Spectra Physics Tsunami. The Tsunami is pumped by a Spectra Physics 2060 Beamlock argon ion laser typically producing 7 W (multiline). The Tsunami can produce femtosecond or picosecond pulses which can be tuned over the range 720-1080nm (770-920 nm with current mirror set). The laser operates in a pulsed mode with a repetition frequency of 82 MHz. For the purpose of the experiments described in this thesis the laser was operated solely in the picosecond regime. The pulses are measured using autocorrelator techniques and observed to have durations of ~1 ps (FWHM).

5.4.2 Autocorrelation measurements

With picosecond pulses the temporal duration of the pulses are measured using autocorrelation techniques. This method uses the non-linear process of second harmonic generation in a crystal to obtain a spatial autocorrelation trace of the optical intensity rather than the actual pulse shape. The principle of operation relies on the instantaneous electronic mechanism underlying second harmonic generation together with the ability to accurately measure length. The autocorrelator is based on a Michelson interferometer with a scanning arm. The arrangement can be seen in Figure 5.3.

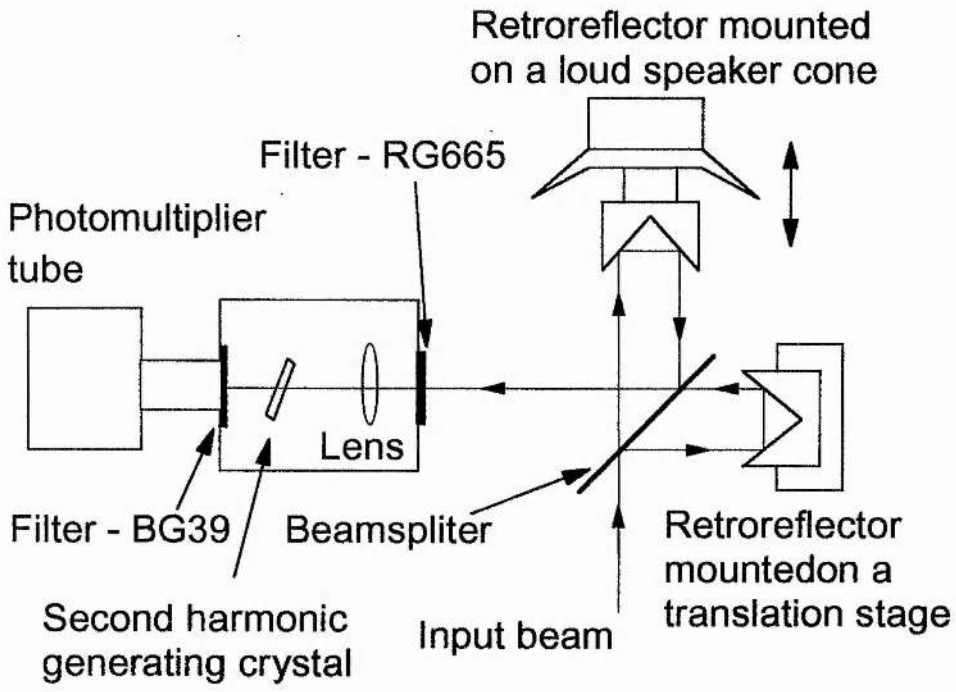

Figure 5.3 *Autocorrelator set-up for measuring picosecond pulses.*

The incoming pulses pass through the interferometer and are then focused into the second harmonic crystal and the second harmonic generated light is then detected with photomultiplier tube.

One arm of the autocorrelator contains a stationary mirror and the other has the end mirror mounted on an audio speaker to provide a varying delay between the arms. The width of the detected second harmonic signal gives the laser pulse width (assuming $sech^2$ pulse shapes an autocorrelation factor of 1.54 is used in converting the measured autocorrelation pulse width to the actual laser pulse widths). An example of an intensity autocorrelation for a 1.5 ps pulse (FWHM) is given in Figure 5.4.

5.4.3 Pump-probe experimental setup

The basic experimental setup is shown in Figure 5.5. The output from the laser is steered into the pump-probe set-up and divided in two by the beamsplitter (50:50 BBS-650.0-1100-2025-45). The pump pulses pass straight through the beamsplitter and are focused onto the sample by a 10cm lens. The probe pulses are delay in an optical delay line to afford the temporal variation in the time between the pump pulse being incident on the sample and the probe pulse arriving.

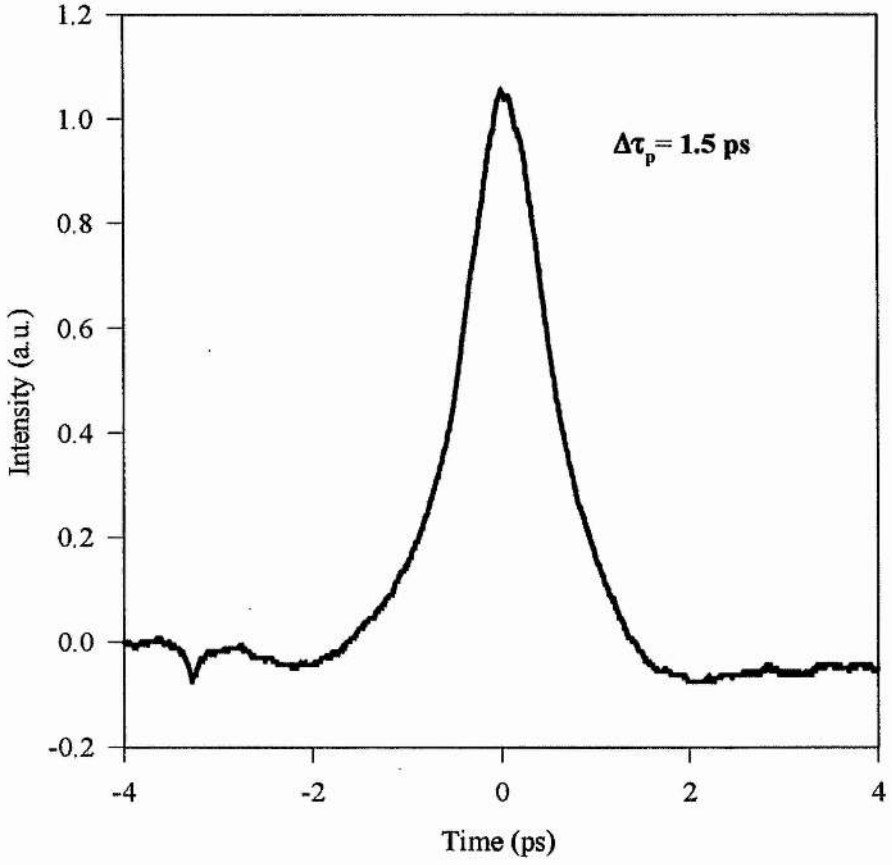

Figure 5.4 *Intensity autocorrelation of a 1.5 ps pulse (FWHM).*

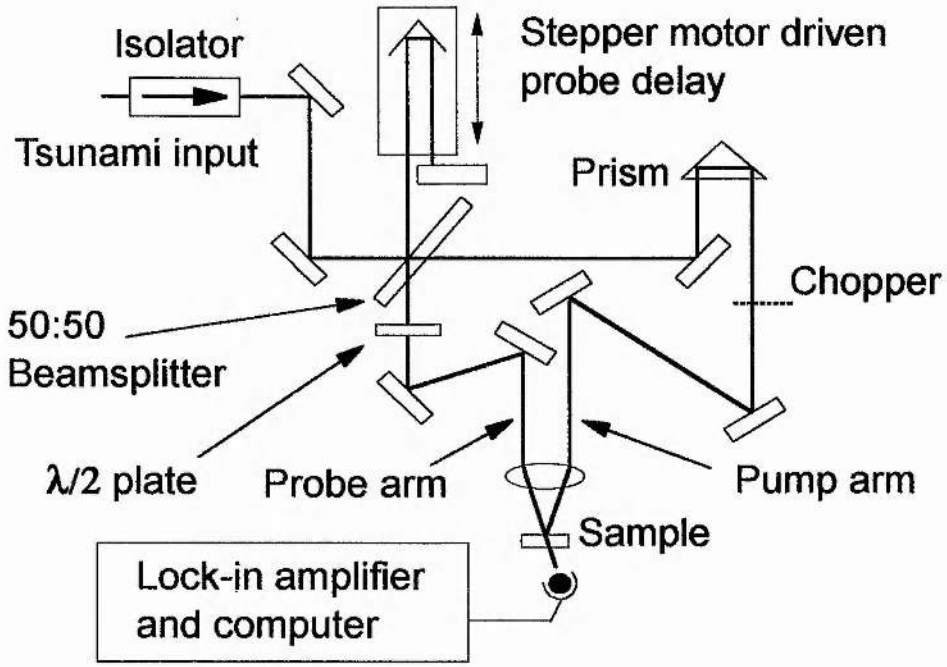

Figure 5.5 *Experimental set-up for degenerate time resolved pump-probe measurements.*

The optical delay line consists of a aluminium retroreflector mounted on a stepper motor driven translation stage. The stage is computer controlled via an IEEE interface. The pulses are bounced off the retroreflector and then onto a plane mirror. The probe pulses are reflected back along their original path by the mirror. The use of the plane mirror eliminates variation in the pointing direction of the probe beam as the delay line is scanned. Due to the four reflections of the probe beam in the delay line the pulses see 4cm of path change for every 1cm that the stage is scanned. The probe pulses are then focused through the same lens used for the pump pulses onto the sample under investigation. The probe is typically made much weaker than the pump pulse (1: 20) using neutral density filters. The total path seen by the pump pulses is matched to that seen by the probe pulses to give the zero delay point. All the mirrors used in the experimental setup were dielectric with a broadband infra-red coating (BB1-R2)

The pump pulses were chopped using an optical chopper to allow phase sensitive detection. The modulation of the pump beam is transferred to the probe beam which is measured using an amplified silicon detector (DET1-SI/M) and a lock-in amplifier (SR810). If the probe was chopped the resulting signal would be a measure of the sum of the transmission change (dT) and the transmission (T). Since the signal of interest is the transmission change (dT), which is usually much smaller than the transmission T, the pump was chopped to allow the direct detection of dT. A $\lambda/2$ plate (QWPO-830-05-2) was used to enable polarisation selection of the probe pulses and rejection of the strong pump pulses. The motion of the stage and the collection of the readings from the lock-in amplifier were under computer control. A typical result obtained using the pump probe technique is shown in Figure 5.6.

The trace obtained from the pump probe experiment shows an initial dramatic rise in the transmission for the probe pulses followed by a very long recovery. The initial change in the transmission occurs due to saturation of an optical transition by the passage of the pump pulse through the sample. The pump pulse generates free electrons and holes which occupy the lowest lying levels in the valence and conduction bands. These optically generated carriers block further generation into these levels and so the delayed probe pulses experience a reduced absorption. This effect is heightened if the transition corresponds to that of an exciton resonance. (The excitons are thermalised on sub-picosecond timescales at room temperature, into free electrons and holes by LO-phonon collisions.)

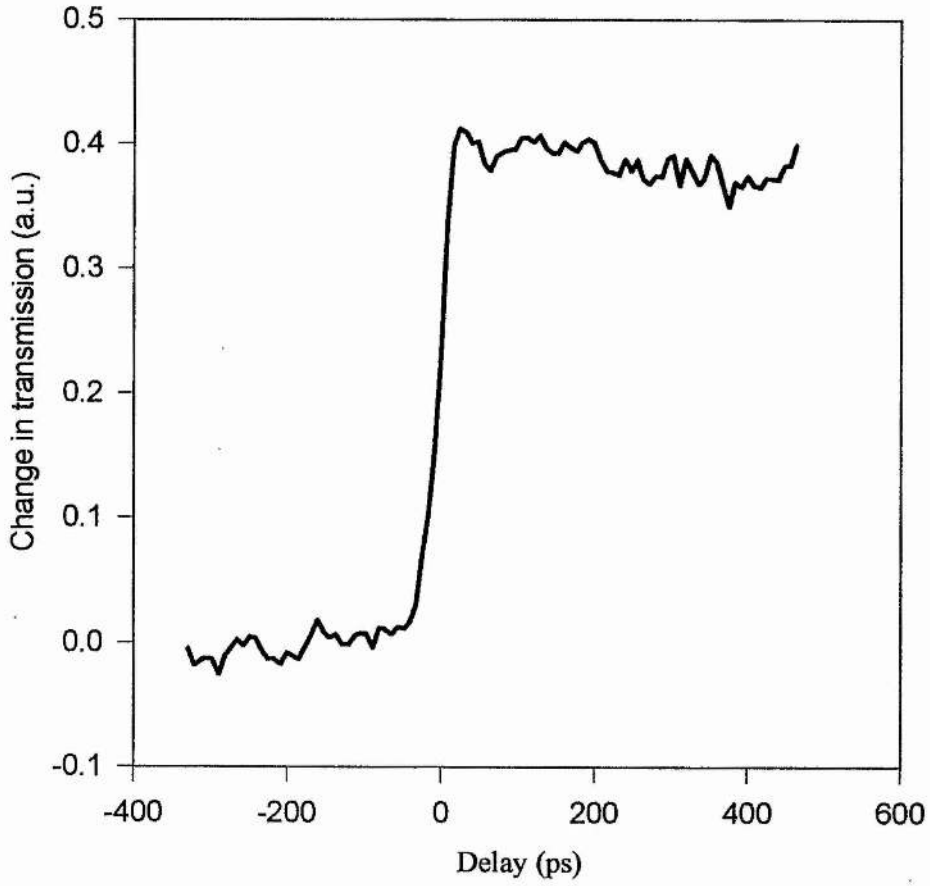

Figure 5.6 *Time-resolved change in transmission for sample S51 at a wavelength of 811 nm.*

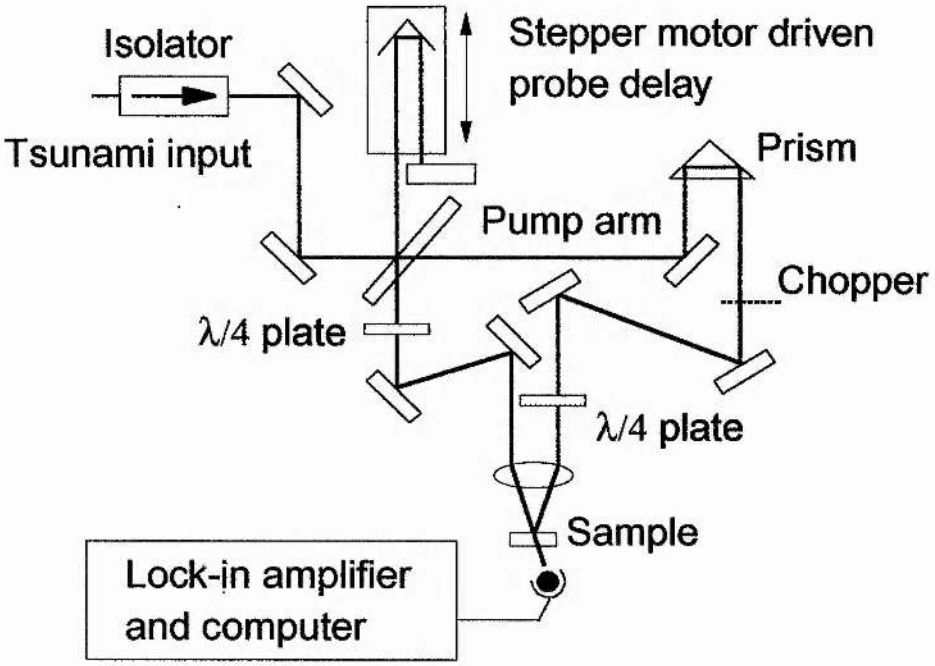

Figure 5.7 *Experimental set-up for spin relaxation studies.*

The probe pulses are scanned temporally and map out the recovery of the transmission to the level experienced before the pump pulse was incident on the sample. The recovery occurs due to the recombination of the generated free carriers. This can correspond to timescales of 1ns or longer.

Further modifications to the standard pump-probe set-up can be made to allow the measurement of a number of additional time constant. These include spin relaxation and transient grating studies.

5.4.4 Spin relaxation studies

The experimental setup for the investigation of spin relaxation is essentially the same as that previously described for degenerate pump-probe studies. The only difference is the addition of λ/4 plates (IOQM20HM-15) in the pump and probe arms to produce circularly polarised light (see figure 5.7). Circularly polarised light is confirmed by placing an analyser after the λ/4 plate and checking that the emerging

signal is of equal intensity when the analyser is orientated parallel and perpendicular to the initially linear polarised laser light.

5.5 Transient grating studies

Transient gratings within semiconductors can be used to measure a number of nonlinear optical properties. Monitoring the grating decay allows the spatial dynamics of optically excited carriers to be investigated.

The experimental setup used in the production and subsequent monitoring of the gratings are shown in Figure 5.8.

The two excite pulses are made incident at an angle of θ to the normal at the sample surface. The pulses are overlapped both temporally and spatially, allowing interference to occur and the production of a concentration grating. A third time delayed pulse is then used to probe the grating and monitor its decay.

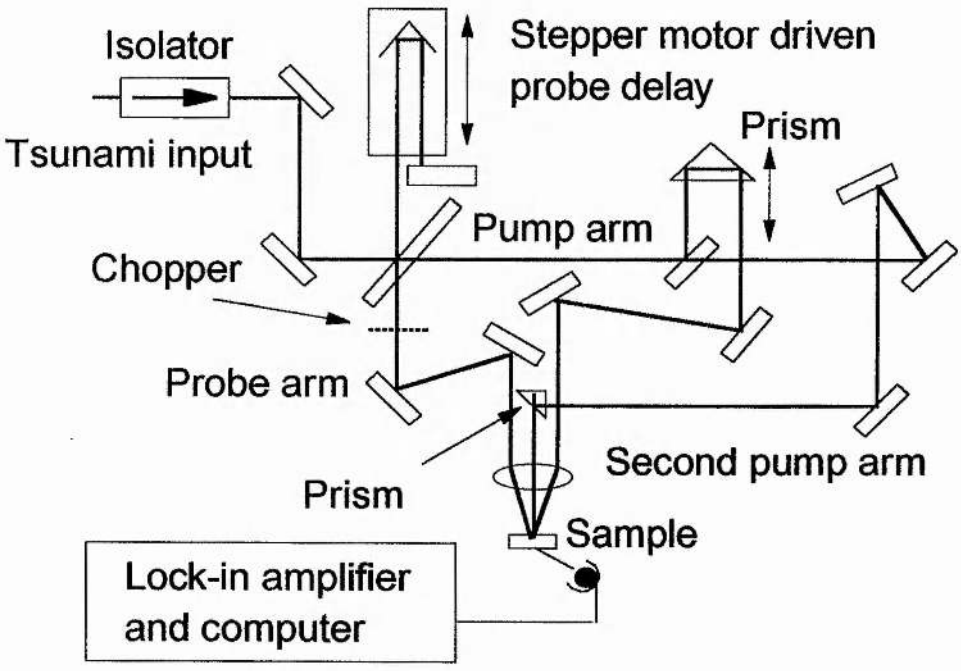

Figure 5.8 *Experimental set-up for concentration grating studies in multiple quantum wells.*

The pulses are overlapped spatially and checked using an IR-camera. Their temporal overlap is achieved by carrying out pump-probe measurements with the probe and each of the excite beams in turn. This allows the "zero delay point", which corresponds to temporal overlap, to be ascertained for each of the excite beams. One of the excite beams is then translated in time relative to the other and so ensures overlap between the two excite pulses. The photodiode placed at the diffraction angle to measure the grating decay, also allows the signal to be further maximised by small changes in the spatial and temporal overlap. The two excite beams are coplanar but the probe beam is made to approach on a different plane. This allows better signal to noise on detection as the diffracted probe beam direction is distinct from any of the other beams.

The beams are focused using a single lens onto the sample. This allows the grating period to be changed by simply moving the two excite beams closer together or further apart to increase or decrease the spacing respectively.

6

Sample description and optical properties

6.1 Summary

This chapter introduces the samples that will be used in the following chapters and introduces their basic optical properties.

6.2 Introduction

In this chapter the samples under investigation will be described. To begin with the structure of each sample is outlined from the point of view of composition, quantum well width and doping levels. The linear absorption curves for the samples are given and the positions of the exciton resonances are noted. The saturation of optical transitions is then studied using wavelength scans of the initial transmission change induced in pump probe measurements. For two of the samples a simple single beam measurement is also carried out to look at intensity dependent saturation of the exciton resonance.

The results obtained from the above experiments are compared to theoretical prediction of the optical properties using simple models. The carrier densities are calculated for the power levels used in these and the following experiments. The samples are described in order of decreasing quantum well width beginning with FK141 (well width 9.0nm), G1273 (well width 8.0nm), KLB (well width 6.5nm) and finally S51 (well width 4.4nm).

6.3 Sample FK141

Sample FK141 was grown by T. Brennan and G. Hammons of the USAF Phillips Laboratory. The sample was grown by molecular beam epitaxy. The structure consists of a 20Å GaAs cap grown on a 700Å $Al_{0.2}Ga_{0.8}As$ barrier followed by 15 periods of 90Å GaAs wells and 100Å $Al_{0.2}Ga_{0.8}As$ barriers, a 700Å layer of AlAs etch stop, a 3961Å GaAs buffer and a 500μm GaAs (100) substrate. The wells are unintentionally doped with p-type dopant levels under $2x10^{14}cm^{-3}$. The sample was anti-reflection coated with two layers of Ta_2O_5 and SiO_2.

The linear absorption curve for FK141 is shown in Figure 6.1(a). The positions of the heavy hole exciton resonance is clearly resolved around 846nm. The position is more apparent in the differential transmission spectra given in Figure 6.1(b). This curve was obtained using the previously described pump-probe technique with the probe pulses set to arrive at a fixed positive delay with respect to the pump pulses. The change in transmission of the probe pulses was then measured as a function of the laser wavelength. Figure 6.1(b) shows a small contribution due to broadening evidenced by the negative transmission change in the wings of the exciton resonance.

The energy levels in the quantum wells of FK141 were calculated using graphical solutions to the equations for a finite potential well (Chapter 2). The first two levels for the electron, E_e, the heavy hole, E_{hh}, and the light hole, E_{lh}, are given in the table below. These give the position of the band edge to be at approximately 847 nm and the heavy hole exciton resonance at 852 (assuming an exciton binding energy of ~ 8 meV). These are in reasonable agreement with the features of the linear absorption spectrum and can be seen as confirmation of the stated well width.

Table 6.1 *Energy levels in sample FK141.*

	E_e (eV)	E_{hh} (eV)	E_{lh} (eV)
1st	0.0332	0.0068	0.0241
2nd	0.1188	0.0267	0.0843

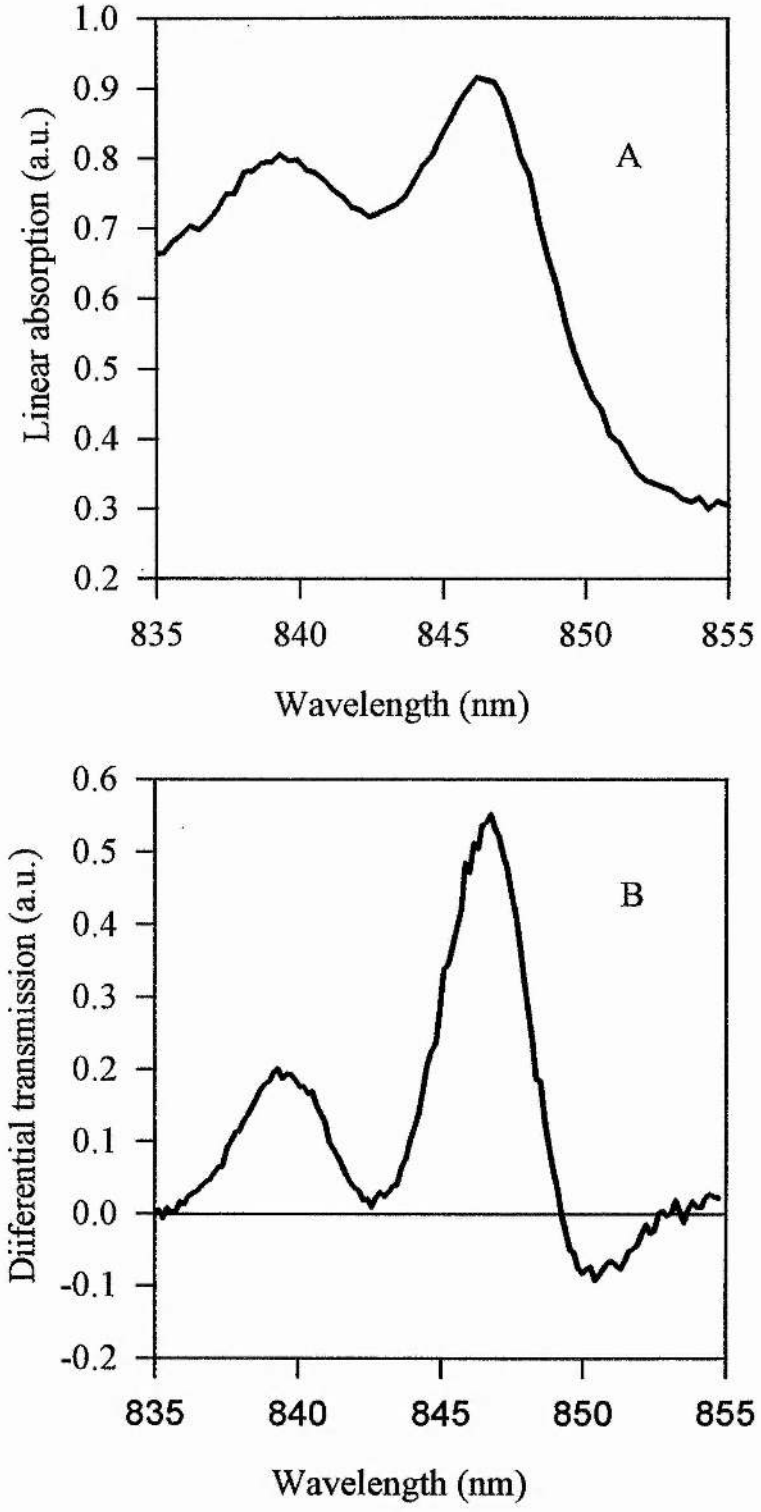

Figure 6.1 *Linear absorption (A) and differential transmission (B) as a function of wavelength for sample FK141.*

6.4 Sample G1273

Sample G1273 was grown by molecular beam epitaxy by P. Cook at the US Army Research Laboratory in New Jersey. The sample consists of 38 periods of 80Å GaAs wells surrounded by 80Å $Al_{0.3}Ga_{0.7}As$ barrier. The sample was unintentionally doped p-type, with doping levels less than $2x10^{14}cm^{-3}$. The sample was anti-reflection coated.

The linear absorption curve for G1273 is shown in Figure 6.2(a). The positions of the heavy hole and light hole exciton resonances are clearly resolved at 837 nm and 828 nm. The differential transmission spectrum is given in Figure 6.2(b).

The energy levels in the quantum wells of G1273 were calculated. The first two levels for the electron, E_e, the heavy hole, E_{hh}, and the light hole, E_{lh}, are given in the table below. The calculated position of the band edge is approximately 839 nm and the heavy hole exciton resonance at 843 nm (assuming an exciton binding energy of ~ 8 meV). These are in reasonable agreement with the features of the linear absorption spectrum and can be seen as confirmation of the stated well width.

Table 6.2 *Energy levels in sample G1273.*

	E_e (eV)	E_{hh} (eV)	E_{lh} (eV)
1st	0.0444	0.0088	0.0324
2nd	0.1426	0.0349	0.1164

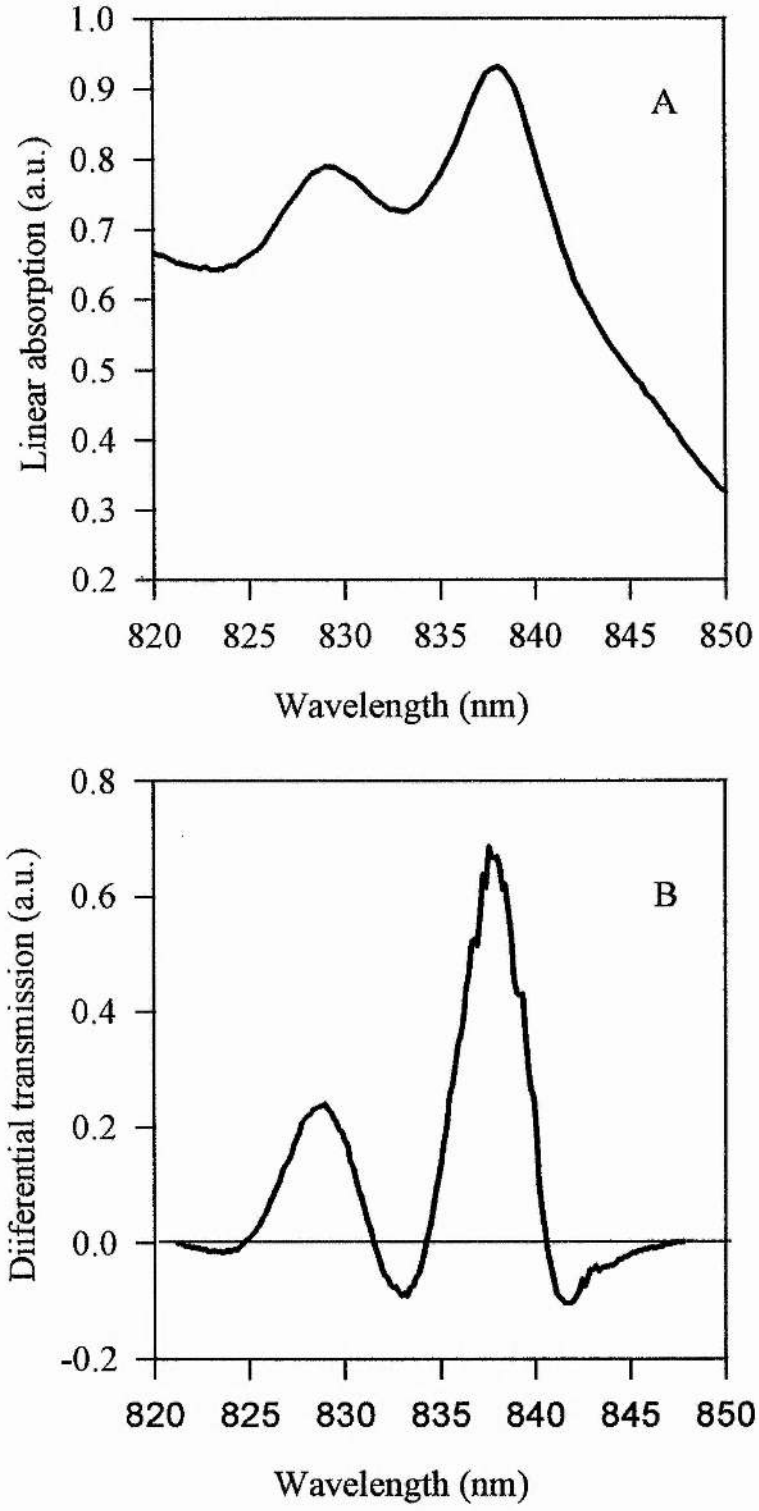

Figure 6.2 *Linear absorption (A) and differential transmission (B) as a function of wavelength for sample G1273.*

6.5 Sample KLB

Sample KLB (269) consists of 120 periods of 65Å GaAs quantum wells surrounded by 21.2nm $Al_{0.4}Ga_{0.6}As$ barriers. The background doping is $10^{16}cm^{-3}$ p-type. The sample is anti-reflection coated on both sides and mounted on a sapphire base for mechanical stability and heat sinking.

The linear absorption curve for KLB is shown in Figure 6.3(a).The positions of the heavy and light hole exciton resonances are clearly visible at 830 nm and 820 nm. The differential transmission spectra is given in Figure 6.3(b).

The energy levels in the quantum wells of KLB were calculated. The first two levels for the electron, E_e, the heavy hole, E_{hh}, and the light hole, E_{lh}, are given in the table below. These give the position of the band edge to be at approximately 824 nm and the heavy hole exciton resonance at 828 (assuming an exciton binding energy of ~ 8 meV). These are in reasonable agreement with the features of the linear absorption spectrum and can be seen as confirmation of the stated well width of 6.5 nm.

Table 6.3 *Energy levels in sample KLB.*

	E_e (eV)	E_{hh} (eV)	E_{lh} (eV)
1st	0.0632	0.0174	0.0446
2nd	0.2260	0.0685	0.1592

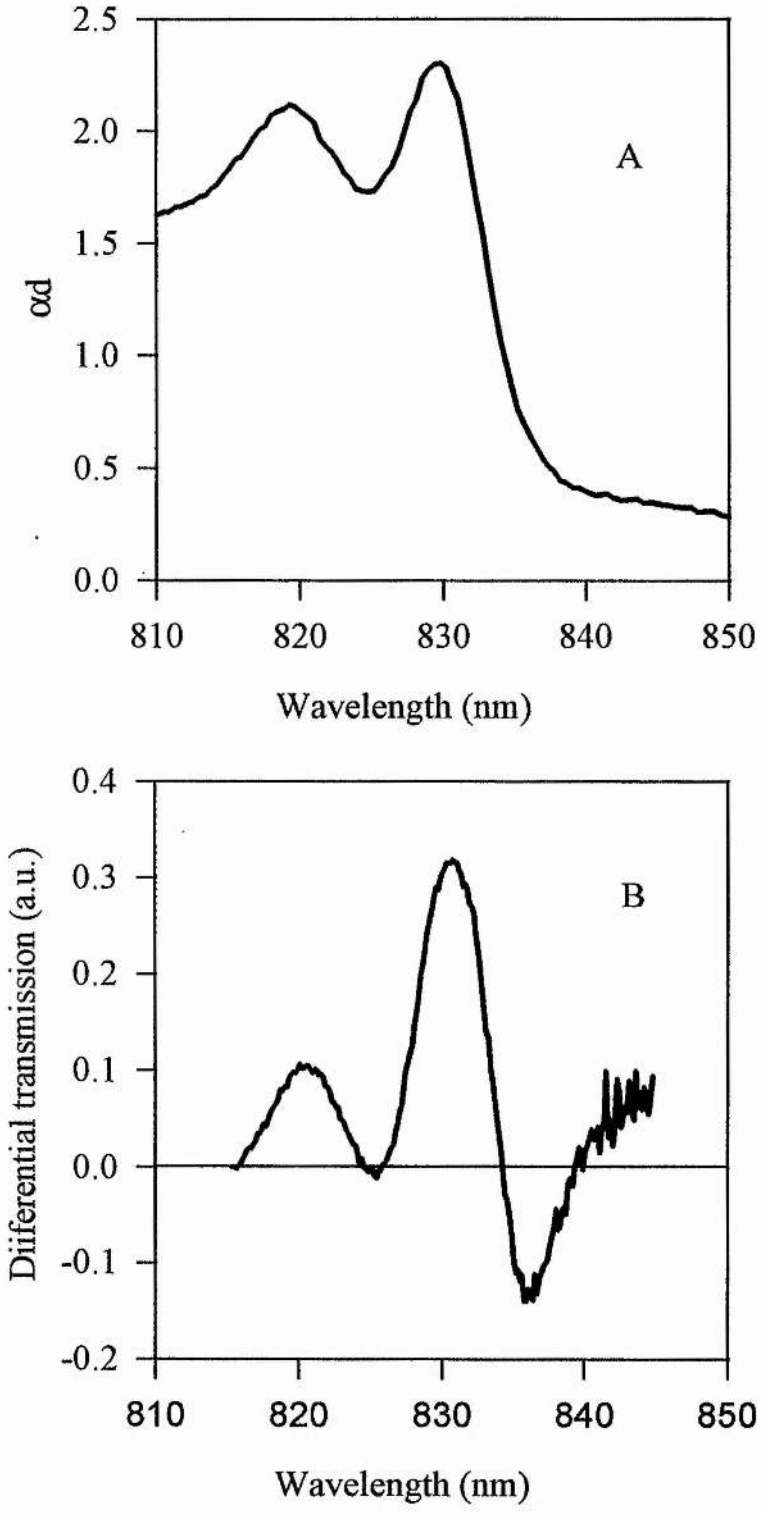

Figure 6.3 *Linear absorption (A) and differential transmission (B) as a function of wavelength for sample KLB.*

6.6 Sample S51

S51 was grown by molecular epitaxy at Sharp Laboratories in Oxford. The sample consists of 60 periods of 44Å wells surrounded by 175Å $Al_{0.33}Ga_{0.67}As$ barriers. The sample has an unintentional background p-type doping less than $2x10^{-14}$ cm^{-3}.

The linear absorption curve for S51 is shown in Figure 6.4(a).The positions of the heavy hole exciton resonance are clearly resolved around 811 nm and 798 nm. The differential transmission spectrum is given in Figure 6.4(b).

The energy levels in the quantum wells of S51 were calculated. The levels for the electron, E_e, the heavy hole, E_{hh}, and the light hole, E_{lh}, are given in the table below. These give the band edge to be at approximately 801 nm and the heavy hole exciton resonance at 805 (assuming an exciton binding energy of ~ 8 meV). These are in reasonable agreement with the features of the linear absorption spectrum and so can assume the 4.4 nm well width to be correct.

***Table 6.4** Energy levels in sample S51.*

	E_e (eV)	E_{hh} (eV)	E_{lh} (eV)
1st	0.0934	0.0303	0.0658
2nd	-	0.1134	-

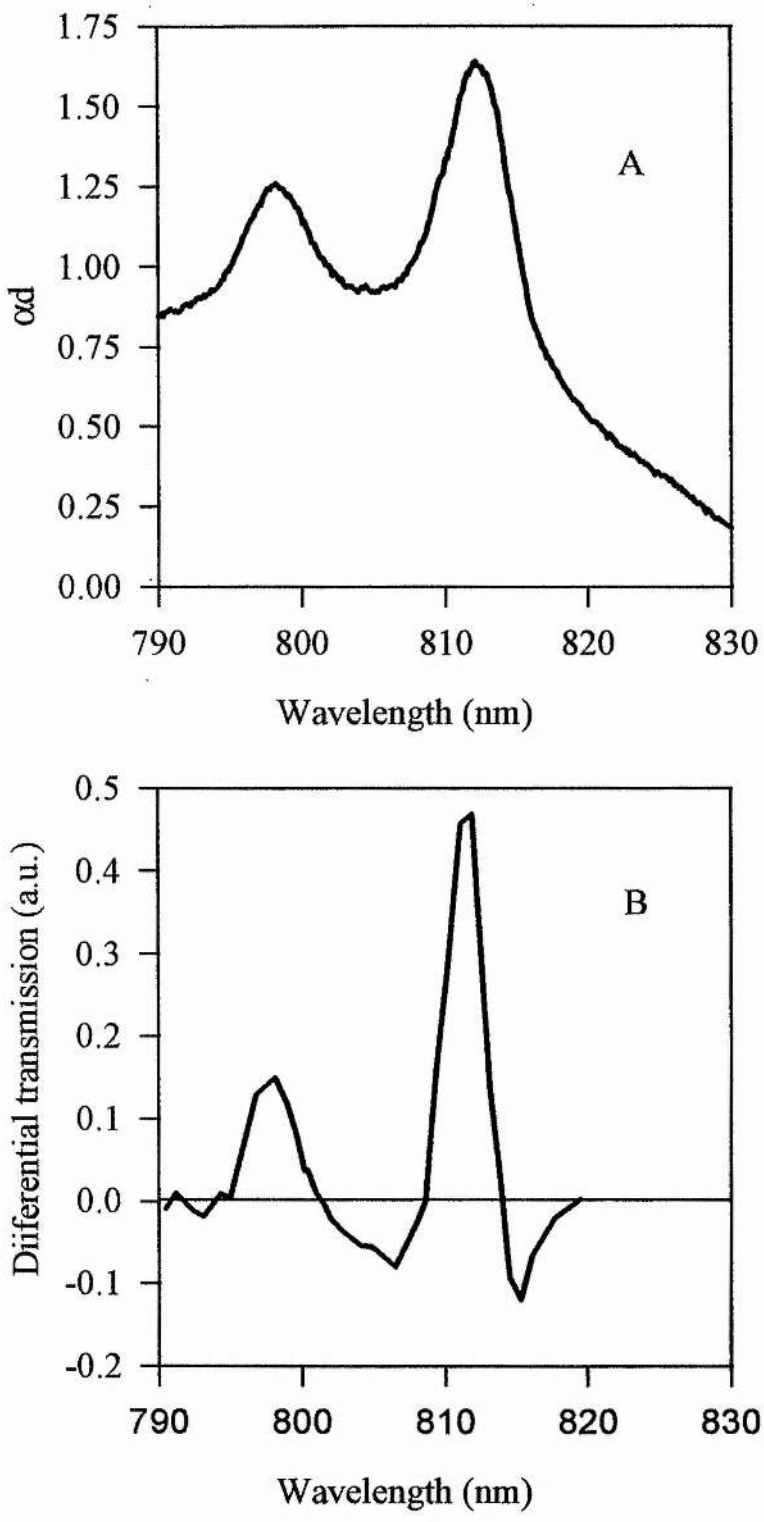

Figure 6.4 *Linear absorption (A) and differential transmission (B) as a function of wavelength for sample S51.*

6.7 Single beam saturation measurements

Single beam saturation measurements were carried out on samples KLB and S51. The laser was tuned to the heavy hole exciton resonance and the transmission of the beam was measured as a function of the laser intensity. The results obtained are shown in Figure 6.5 for KLB and Figure 6.6 for S51. From these results it is possible to measure the maximum change in the transmission of the samples as the excitonic resonance is saturated. Using the linear absorption measurements it is possible to make an estimate of the excited carrier densities necessary to induce saturation.

6.7.1 Estimation of the carrier excited carrier densities

The first thing to do in estimating the excited carrier density is to work out the energy in the exciting laser beam.

The Tsunami laser has a repetition rate of 82 MHz and assuming an average power of 1mW produces pulses with an energy of ~10pJ. The power in the pulse can be calculated if the pulse width is known. In the case of a 1psec pulse the power per pulse is ~10W. The spot size after the focusing lens was measured using a travelling razor blade to be of radius 30μm. Using this the peak intensity of the pulses is found to be ~$4x10^5$ Wcm^{-2}.

Assuming the anti-reflection coating on the samples induces no losses in the pulse intensity incident on the sample then the energy of the light absorbed is given by

$$I_{abs} = I_0\left(1 - e^{-\alpha d}\right) \qquad 6.1$$

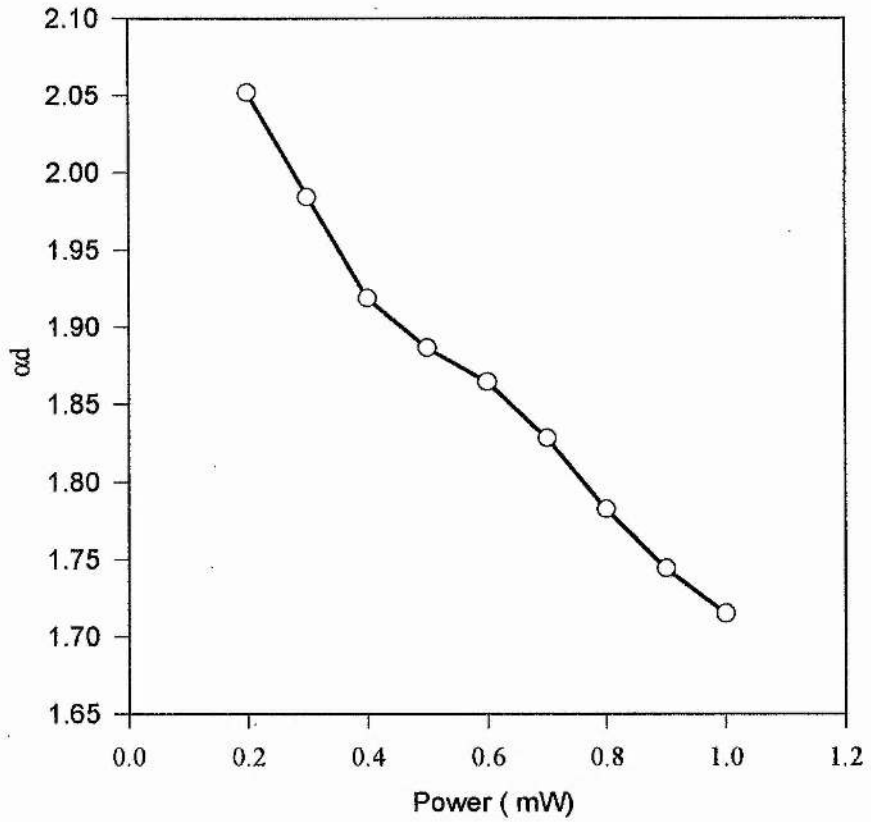

Figure 6.5 *Change in transmission of a single beam for sample KLB at the heavy hole exciton resonance (830 nm) with a spot size of 30 μm.*

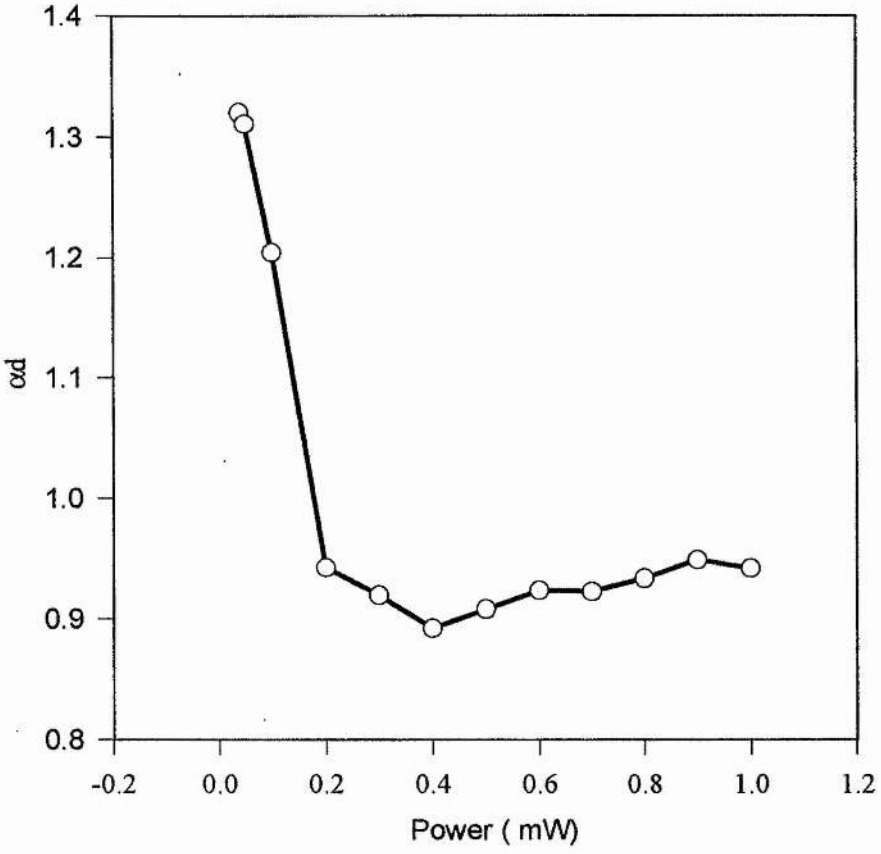

Figure 6.6 *Change in transmission of a single beam for sample S51 at the heavy hole exciton resonance (811 nm) with a spot size of 30 μm.*

The number of photons absorbed is given by

$$N_{photons} = \frac{E_{pulse}\left(1 - e^{-\alpha d}\right)}{\hbar\omega} \qquad 6.2$$

where E_{pulse} is the pulse energy and $\hbar\omega$ is the photon energy. If the internal quantum efficiency is assumed to be 100% then for every absorbed photon a free electron and hole are generated.

For sample KLB the value of αd is obtained from the linear absorption curve (see Figure 6.3(a)) to be 2.4 at the heavy hole resonance. For 1mW of average laser power this value is reduced to 1.7 due to saturation and so leads to the excitation of $\sim 1 \times 10^{10}$ electron-hole pairs cm^{-2}.

For sample S51 the number of electron-hole pairs excited by a laser tuned to be resonant with the heavy hole resonance and of average power of 1mW is also $\sim 1 \times 10^{10}$ cm^{-2}.

7

Broadening, screening and phase space filling

7.1 Summary

The contributions of screening, broadening and phase space filling to exciton saturation in multiple quantum wells are investigated. The effects arising from phase space filling are distinguished from those due to screening and broadening using the spin dependent contribution that phase space filling makes to exciton saturation. The contributions of broadening and screening are separated through their differing carrier density dependences. The results obtained for three quantum well samples of varying well width are presented and discussed.

7.2 Introduction

The effects of screening, broadening and phase space filling on exciton saturation in semiconductor quantum wells are important parameters in the measurement of optical nonlinearities and monitoring carrier dynamics. These features also limit the performance of a number of devices at high optical power levels where large densities of optically excited carriers are created. This chapter describes an experiment that has been carried out to investigate the relative importance of screening, broadening and phase space filling in multiple quantum wells

of varying widths. At room temperature, excitons are ionised by collisions with LO-phonons within a few hundred femtoseconds [7.1]. Therefore on timescales longer than the exciton ionisation time we must consider exciton saturation in terms of free carrier induced effects.

Saturation of the exciton absorption by free carriers can occur as a result of exclusion effects and Coulombic effects (such as screening and/or broadening). These effects have already been described in detail in Chapter 3 and so will only be described briefly. The effects due to the exclusion principle can be described by means of phase space filling. This arises as the carrier densities increase so that the low lying k-states become occupied thus block transitions involving them. These are the states from which the exciton is derived and so their filling rules out the possibility of creating the excitons associated with them.

The screening properties of large densities of free carriers also produce exciton saturation. The presence of free carriers will modify the dielectric constant and in so doing, change the size of the exciton orbit, usually increasing it. This leads to a reduction in the absorption strength. A simple Coulomb calculation of the screening effect is not sufficient at high carrier populations. Here the screened Coulomb potential is further modified by exchange effects for particles with equal spins and Coulomb associated effects for all particles. The exchange effects arise due to Pauli exclusion and prevents Fermions with equal quantum numbers (i.e. spin states) from occupying the same point in space. This further separates the electrons, again increasing the size of the exciton and reducing the absorption. This modification to the simple Coulomb screening is known as exchange-screening (sometimes called Fermion-exchange). Equally charged Fermions with differing quantum numbers will also avoid each other due to coulomb repulsion. This effect is termed Coulomb-hole and will also reduce the overall energy of the system. These effects are very short-ranged when compared to the long-range Coulomb correlations that give rise to classical screening. Indeed in an electron-hole plasma, the long-range many-body effects can be associated with the electrostatic screening in the classical sense. In 2D, long-range electrostatic screening is known to be less important than in 3D [7.2] . This reduction in screening can simply be explained by considering the reduced number of dimensions the carriers are free to move in.

Broadening of the exciton resonance in a quantum well will lead to reduced absorption at the peak of the exciton. This contribution is induced by collisions with free carriers and will result in an increase of the exciton linewidth while the overall oscillator strength is maintained.

There has been some misunderstanding concerning the concept of screening and its contribution to exciton saturation, most of which can be traced to Schmitt-Rink et al [7.3].

Schmitt-Rink considered exciton saturation, in multiple quantum wells, by a free carrier plasma as a result of phase space filling and Coulombic effects (neglecting broadening). The Coulombic effect on the exciton resonance was divided into two distinct terms; a long-range classical screening term (independent of the energy distribution of the plasma) and a short-range term called the exchange contribution (dependent on the energy distribution of the plasma). The classical screening term was considered to be unimportant in quantum well semiconductors and so only the exchange term was considered. The remaining terms due to phase space filling and exchange were then shown to be of equal importance. The reduced importance of classical screening in two dimensions was confirmed experimentally using a non-thermal electron-hole plasma excited well above the band edge [7.2]. The popular misconception has therefore arisen that all Coulombic effects in quantum wells are negligible. This has been shown experimentally to be incorrect [7.4] and demands that care be taken when neglecting screening effects. The term screening will be used from now on to describe processes which reduce the Coulomb interaction.

To separate the contributions of screening and broadening from those of phase space filling it is necessary to employ non-equilibrium carrier distributions. The long-range screening effects can be examined by excitation into the continuum states as described above, although the distinction of the remaining effects is not so straightforward.

Snelling et al [7.4] used circularly polarised light in pump-probe experiments to distinguish the contributions to exciton saturation. They demonstrated experimentally and theoretically that the contributions from phase space filling and Coulomb screening and broadening are of similar magnitudes at room temperature in GaAs multiple quantum wells. The monitoring of exciton saturation on the long

wavelength side of the exciton resonance using circularly polarised light allowed Snelling to observed the effects of density dependent broadening. In this chapter the broadening contribution to exciton saturation is investigated for a number of different quantum well widths. The effects due to broadening at the heavy hole exciton resonance are isolated by their density dependence from those of Coulomb screening and phase space filling.

In the following experiment the spin dependent nature of the phase space filling nonlinearity is used. The effects due to phase space filling are sensitive to carrier spin unlike those due to broadening and screening (within the Boltzmann approximation). It is therefore possible to separate their relative contributions using the spin sensitive selection rules present in quantum wells. The use of circularly polarised light allows the generation of 100% spin polarised carriers. This process is illustrated in Figure 7.1.

When a linearly polarised excite pulse is made resonant with the heavy hole exciton transition in a quantum well equal population of spin up and spin down carriers are created. This process is shown in Figure 7.1(a). Here the conduction band of the semiconductor is drawn consisting of two quadrants (labelled $\uparrow$ and $\downarrow$). These correspond to the two spin states that exist for electrons in the conduction band. A weak probe pulse of orthogonal linear polarisation, arriving after the excite pulse will then see an increase in the transmission of the sample due to the effects of screening and phase space filling.

If the excite pulse consists of circularly polarised photons then only one spin state of the conduction band is populated (as shown in Figure 7.1(b) and (c)). A delayed probe pulse of the same circular polarisation (Figure 7.1(b)) will then examine the population of this spin state and see an enhanced contribution due to phase space filling when compared with the case described for Figure 7.1(a). For the case of a probe pulse with opposite circular polarisation (as shown in Figure 7.1(c)) the probe pulse examines the empty spin state and so in this case there is no contribution from phase space filling to the exciton saturation. The probe therefore experiences a reduced transmission when compared to the case of opposite linear polarised pulses. The populations of the two spin bands equalise over time due to

spin relaxation. The temporal nature of the spin relaxation process will be discussed in the following chapter.

The remaining effects due to screening and broadening that contribute to exciton saturation can be distinguished using their dependencies on the excited carrier density.

After an initial description of the experimental set-up the results obtained are presented and discussed.

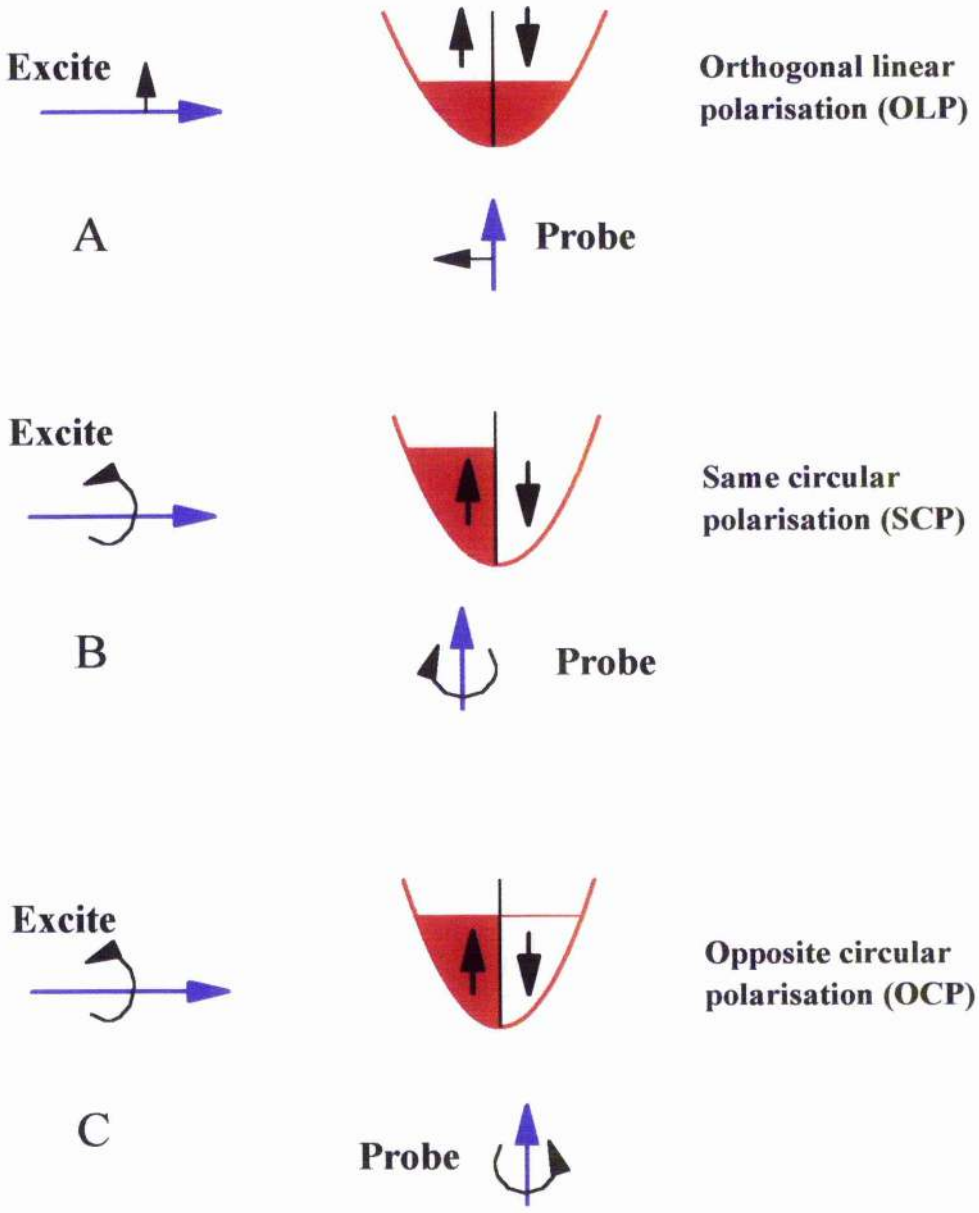

Figure 7.1 *Illustration of the spin state populations under examination. a) Opposite linear polarisation, b) Same circular polarisation, c) opposite circular polarisation.*

7.3 Experimental details

Exciton saturation in GaAs-AlGaAs multiple quantum wells, at room temperature, was investigated using the degenerate pump-probe technique described in Figure 5.7.

7.4 Results

The experiment was carried out in three quantum well samples of varying well width in order to contrast the effects. The samples used were FK141 (9.0 nm well widths), KLB (6.5 nm well widths) and S51 (4.4 nm well widths). Excitation resonant with the heavy hole exciton for each sample was carried out and the time evolution of the saturation recovery was monitored with a time delayed probe pulse. The initial change in transmission was measured for pump and probe pulses with opposite linear polarisation, opposite circular polarisation and same circular polarisation. The production of the various circular polarisation was achieved using a $\lambda/4$ plate in the pump and probe arms.

A typical result obtained is shown in Figure 7.2. The experiment was repeated for varying pump powers (corresponding to varying excited carrier densities). This allowed the power dependence of the initial transmission change to be measured. Figures 7.3, 7.4 and 7.5 show the initial change in transmission as a function of power for each of the samples. The curve labelled Coulomb is the measure of the initial transmission change present when the pump and probe pulses are opposite circular polarisation (no phase space filling contribution present). The phase space filling curve is a plot of the initial difference between the opposite linear polarisation and either same circular polarisation or opposite circular polarisation curves.

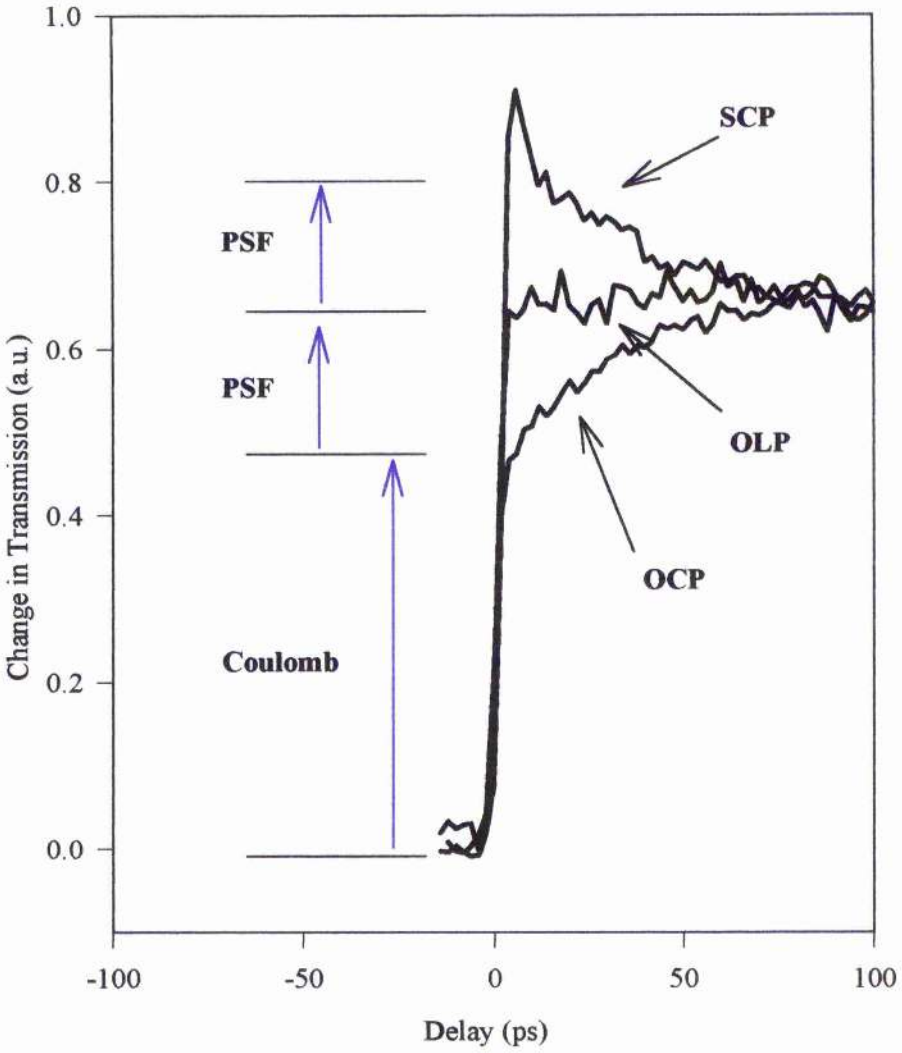

Figure 7.2 *Initial change in transmission as a function of probe delay for sample S51.*

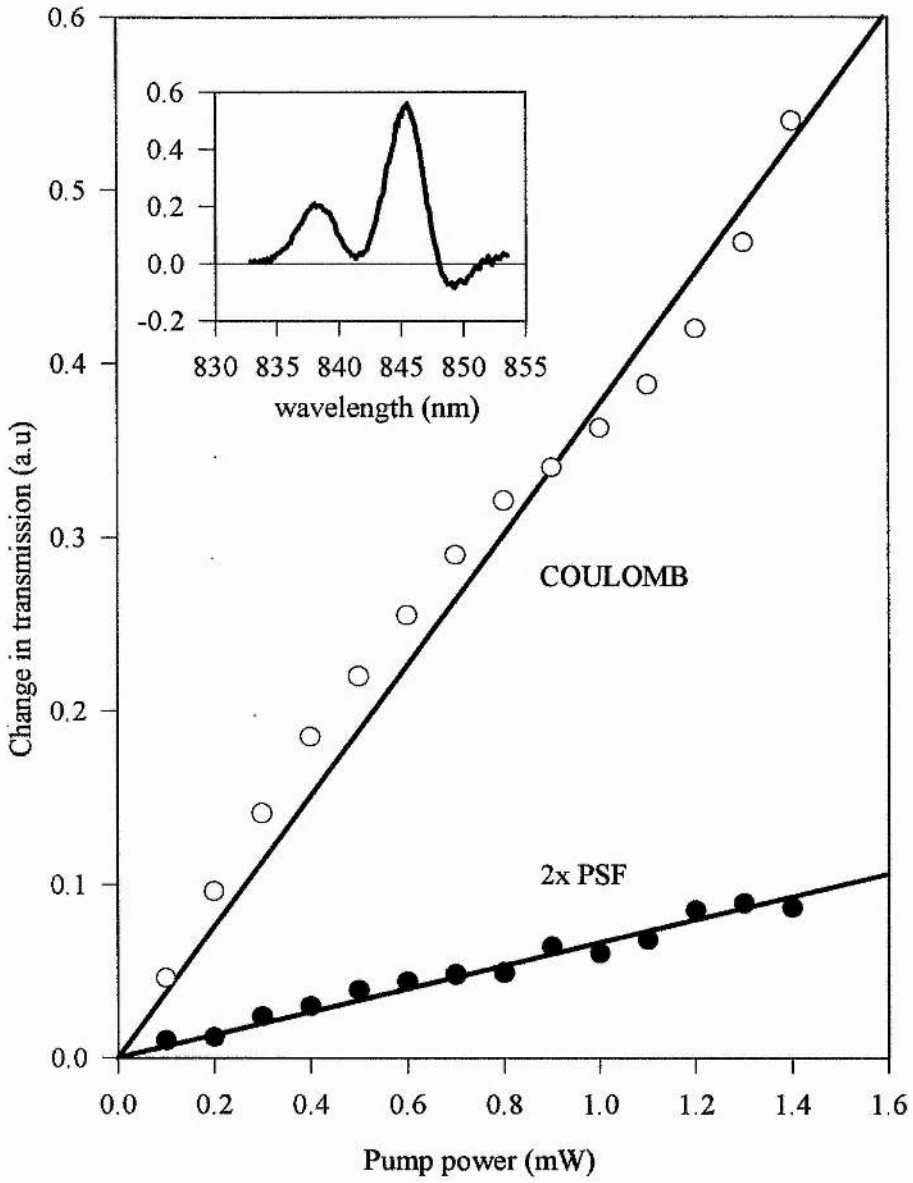

Figure 7.3 *Initial change in transmission at the 1S exciton resonance (845 nm) as a function of pump power for sample FK141. Insert shows the differential transmission as a function of wavelength.*

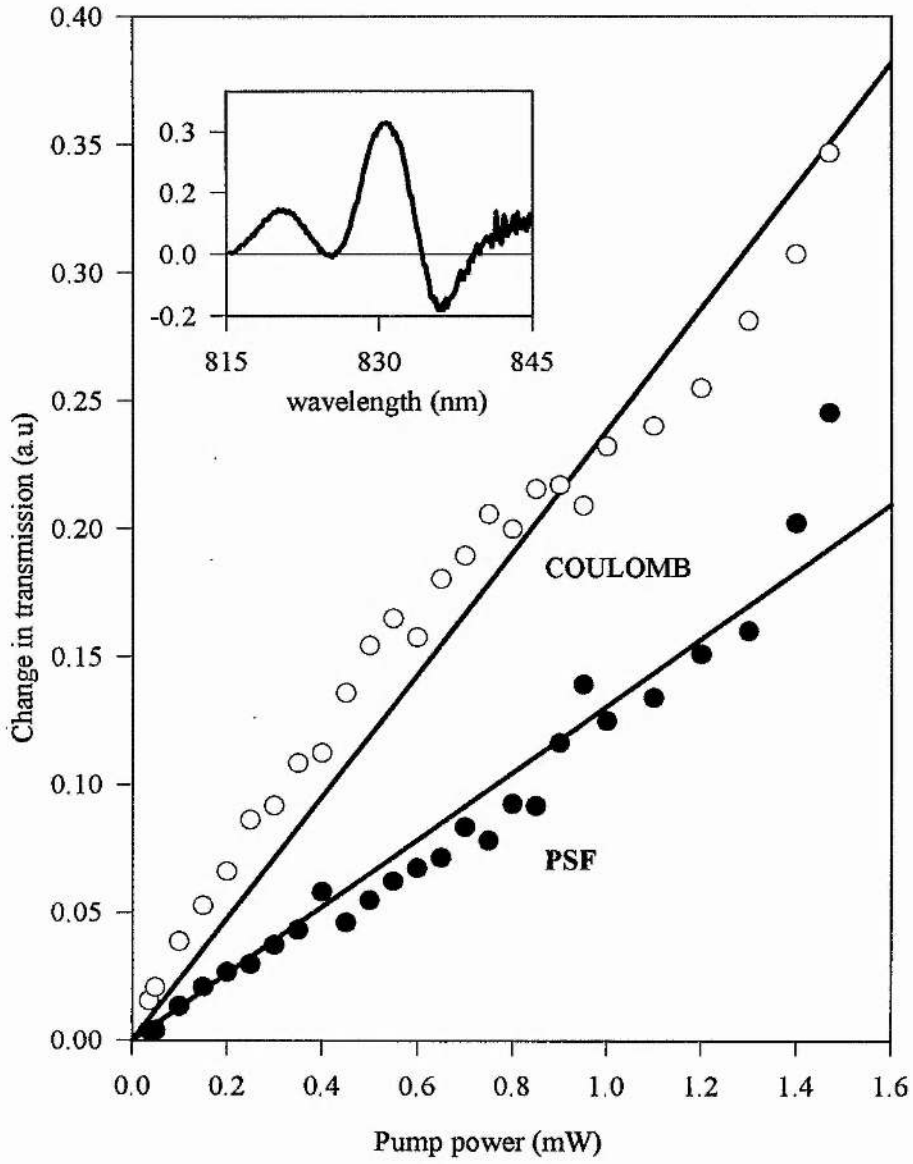

Figure 7.4 *Initial change in transmission at the 1S exciton resonance (830 nm) as a function of pump power for sample KLB. Insert shows the differential transmission as a function of wavelength.*

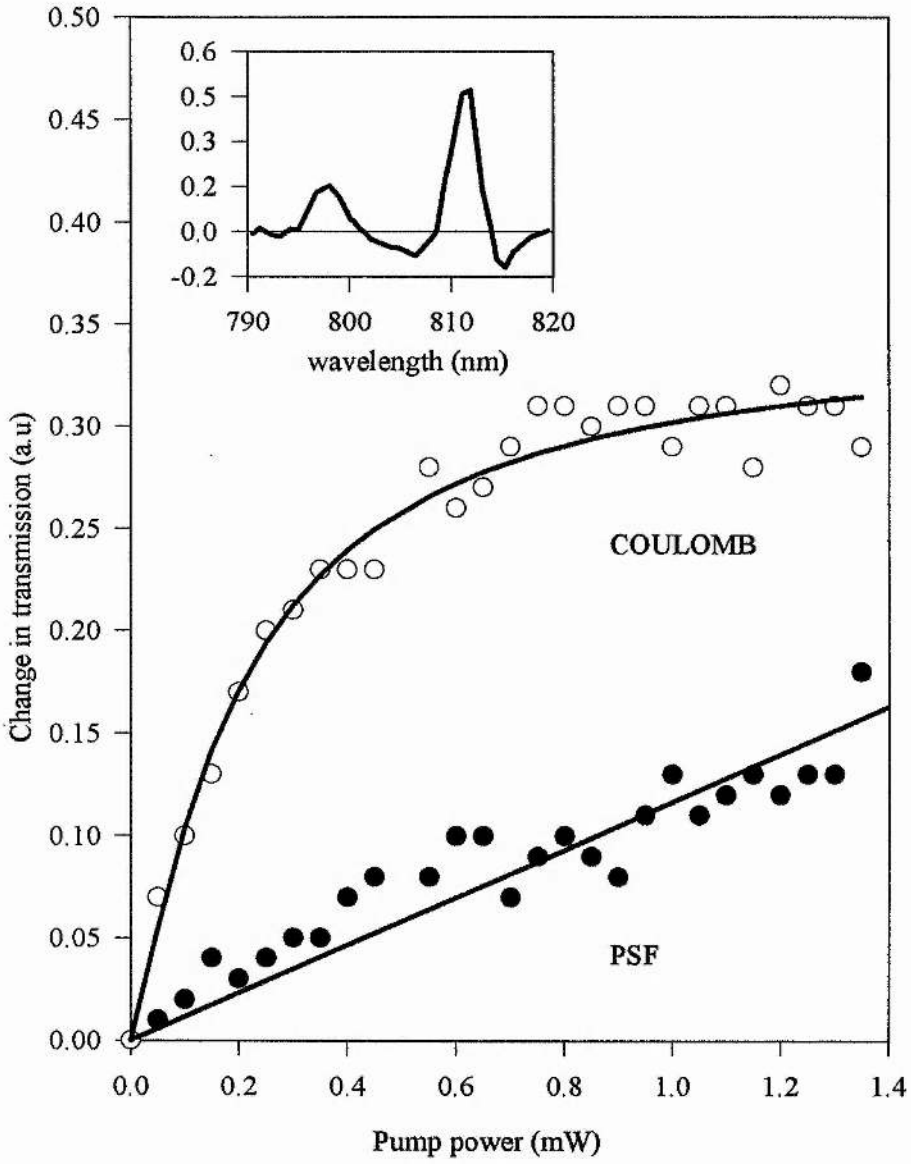

Figure 7.5 *Initial change in transmission at the 1S exciton resonance (812 nm) as a function of pump power for sample S51. Insert shows the differential transmission as a function of wavelength.*

7.5 Discussion

The first thing that is apparent from Figure 7.2 is that there is a substantial absorption change in the absence of phase space filling. In the opposite circular polarisation configuration the decrease in the exciton absorption occurs solely due to Coulombic effects (screening and lineshape broadening). This behaviour is mirrored for the other two samples and shows that screening is important in 2D systems as previously reported [7.4]. When the light polarisations are set to the other two configurations, namely opposite linear polarisation and same circular polarisation the effect of phase space filling is revealed. There is seen to be a further reduction in the exciton absorption with the effect being most pronounced for same circular polarisation. Further discussion on the time evolution and the mechanisms involved in the decay of the same circular polarisation and opposite circular polarisation traces to the opposite linear polarisation case will be discussed in the following chapter.

As is shown schematically in Figure 7.2 the change in transmission curve can be split into two distinct parts. The initial change in transmission in the opposite circular polarisation case which is attributed to Coulomb effects and the added effect of phase space filling which becomes apparent when the other polarisation configurations are used. For the purpose of this experiment the initial change in transmission was measured as a function of pump pulse power. For the opposite circular polarisation case the initial change is solely due to Coulomb effects and this is shown in Figures 7.3, 7.4 and 7.5 for the three samples and marked as Coulomb. The contribution due to phase space filling is measured as the initial difference between the change in transmission for the opposite circular polarisation case and the opposite linear polarisation case. When this becomes difficult to resolve the difference between the same circular polarisation and the opposite circular polarisation cases is used and divided by two. This is plotted as a function of pump power for the three samples in Figures 7.3, 7.4 and 7.5, and denoted as phase space filling.

The carrier densities are estimated to be $\sim 10^{16}$ cm^{-3} (for 1 mW of average pump power). These values were deduced from the spot size of the pump pulses incident on the samples and the absorption coefficients (described in Chapter 6).

Inspection of Figure 7.3 shows that the curves for the Coulomb and phase space filling contributions to the exciton saturation exhibit a linear dependence on the pump power and therefore the excited carrier density. The Coulomb term can be seen to be significantly larger than the phase space filling term. Figure 7.4 which shows the results for the slightly narrower, 6.5 nm wells, of KLB exhibits similar features. Again the Coulombic effects are larger than those due to phase space filling. We associate the linear dependence of the Coulomb term to be as a result of screening.

Figure 7.5 shows the curves obtained for the 4.4 nm well, sample S51. The phase space filling term is once more seen to have a linear dependence on the carrier density but this time the curve associated with the Coulomb term shows a more complicated structure. This is attributed to broadening of the exciton lineshape as the carrier density is increased. It is not apparent whether the curve can be described by considering broadening as the only effect present. In reality broadening and screening should both be present. One argument for considering this curve as only due to broadening is that the effect is only seen in the narrowest wells. If the simple description of screening that was given previously is considered, then, as the well width is decreased, the efficiency with which the free carrier plasma screens the Coulomb potential will be reduced. It should also be noted that the effects attributed to broadening only occur in the highest quality sample. The linear absorption of S51 (see Chapter 6) shows very clear excitonic resonances when compared to the corresponding curves of KLB and FK141. These occur due to the superior quality and the increased exciton binding energy for this well width. Further evidence to support this statement can be obtained if we examine the differential transmission spectra.

The processes that contribute to exciton saturation should have different spectral signatures. Phase space filling and screening reduce the oscillator strength and hence the optical absorption across the whole of the excitonic resonance (Figure 7.6). Lineshape broadening increases the width of the exciton resonance while maintaining the overall oscillator strength. This effect appears as a reduction in the optical absorption at the line centre with a corresponding increase in the absorption in the wings (Figure 7.7).

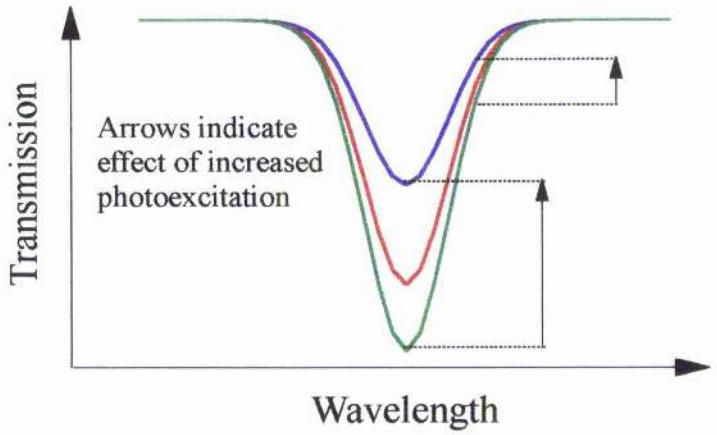

Figure 7.6 *The effect of phase space filling and screening on a simple resonance.*

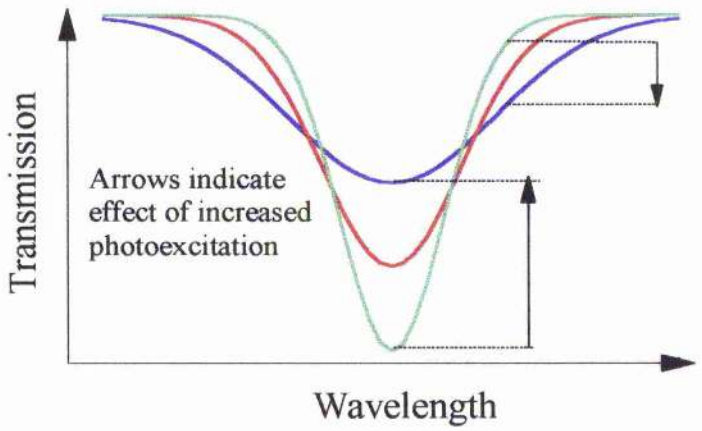

Figure 7.7 *The effect of broadening on a simple resonance.*

It is therefore apparent that the only mechanism for producing an increase in the absorption in the wings of the exciton resonance is lineshape broadening.

The differential transmission spectra for FK141 and KLB are very similar in appearance (see inserts in Figure 7.3 and 7.4). They both show large effects due to heavy hole exciton saturation. The effects from broadening which appear in the wings are small. For the case of S51 (see insert in Figure 7.5) the effects due to broadening appear more important.

The importance of broadening to exciton saturation has been addressed previously by a number of authors [7.5,7.6,7.7]. Hunsche et al [7.5] separated the effect of broadening from those of screening and phase space filling in a 10.0 nm quantum well sample. By monitoring the integrated area under the heavy hole exciton resonance it was possible to remove any contribution from broadening. The carrier density dependence was then investigated and shown to have an approximately linear dependence in agreement with the results above. The contribution from broadening was monitored by observing the reduction in the peak of the heavy hole exciton resonance. This measurement also contains the effects due to phase space filling and screening which will also contribute to a reduction in the exciton resonance. The carrier density dependence curve obtained has the same profile as the results obtained with the 4.4 nm well width sample shown above in Figure 7.5. Although the carrier density dependence of the broadening deduced in this work is similar to that of Hunsche, there is a difference in the well widths at which the broadening effects are observed. Hunsche observed a strong contribution attributed to broadening in a 10.0 nm well, whereas little broadening is evident for the case of FK141 (8.0 nm wells). This could be explained by considering the quality of the samples used. Hunsche's 10.0 nm well sample has very clearly resolved exciton peaks whereas the FK141 sample used in the above experiments does not match this.

It is expected that the three samples used should all exhibit some degree of broadening. In all but the narrowest well width this seems to be masked by the effects of screening. The results presented above allow the direct comparison of the magnitudes of phase space filling to those of Coulomb screening and broadening. This was not possible using Hunsche's method due to the difficulty in comparing an integrated transmission change with a peak transmission change.

7.6 Conclusion

The experiments of this chapter demonstrate that it is not possible to neglect the effects of screening on exciton saturation in multiple quantum wells. Indeed in the experiments described it is apparent that the screening contribution is of a similar magnitude.

The spin dependent nature of the phase space filling nonlinearity has enabled its separation from the effects due to Coulombic interactions. The Coulombic terms of screening and lineshape broadening have been shown to have differing dependencies on the free carrier density. For the samples under investigation it appears that the importance of broadening increases as the well width decreases. In the case of the narrowest well width it appears that broadening is the dominant contribution to the exciton saturation at low carrier densities.

7.7 References

7.1 W.H. Knox, R.L. Fork, M.C. Downer, D.A.B. Miller, D.S. Chemla, C.V. Shank, A.C. Gossard and W. Wiegmann, "Femtosecond dynamics of resonantly excited excitons in room-temperature GaAs quantum wells", Phys. Rev. Letts., **54**, 12, 1306-1309, (1985).

7.2 W.H. Knox, C. Hirlimann, D.A.B. Miller, J. Shah, D.S. Chemla and C.V. Shank, "Femtosecond excitation of nonthermal carrier populations in GaAs quantum wells", Phys. Rev. Letts., **56**, 11, 1191-1193, (1986).

7.3 S. Schmitt-Rink, D.S. Chemla and D.A.B. Miller, "Theory of transient excitonic optical nonlinearities in semiconductor quantum-well structures", Phys. Rev. B., **32**, 10, 6601-6609, (1985).

7.4 M.J. Snelling, P. Perozzo, D.C. Hutchings, I. Galbraith and A. Miller, "Investigation of excitonic saturation by time resolved circular dichroism in GaAs-AlGaAs multiple quantum wells", Phys. Rev. B, **49**, 24, 17160-171, (1994).

7.5 S. Hunsche, K. Leo, H. Kurz and K. Kohler, "Exciton absorption saturation by phase-space filling: influence of carrier temperature and density", Phys. Rev. B., **49**, 23, 16565-165, (1994).

7.6 D.R. Wake, H.W. Yoon, J.P. Wolfe and H. Morkoc, "Response of excitonic absorption spectra to photoexcited carriers in GaAs quantum wells", Phys. Rev. B, **46**, 20, 13452-134, (1992).

7.7 D.S. Chemla, D.A.B. Miller, P.W. Smith, A.C. Gossard and W. Wiegmann, "Room temperature excitonic nonlinear absorption and refraction in GaAs/AlGaAs multiple quantum well structures", IEEE J. Quant. Electron., **20**, 3, 265-275, (1984).

8

Spin relaxation

8.1 Summary

In this chapter the process of electron spin relaxation in multiple quantum wells is investigated. The electron spin relaxation time is measured in a number of multiple quantum well samples of varying well width. These results are then compared with those previously reported and indications for the determination of the dominant mechanism at room temperature are discussed.

8.2 Introduction

In the previous chapter the spin dependent nature of phase space filling was discussed from the point of view of exciton saturation. In this chapter the temporal dependence of the phase space filling term that relates to the time for the electron spins to randomise is discussed. The hole spins are known to relax on sub-picosecond timescales as was discussed in chapter 3. Since the dynamics of the hole spins are outside the temporal window accessible, their contribution to the phase space filling is taken as constant.

Although the topic of spin relaxation has received a great deal of attention over the last three decades, the mechanisms are still not well understood. The main cause of this seems to be the sensitivity of the spins to external perturbation that are difficult to control. A great deal of work has been carried out at low temperatures

using photoluminescence and the pump-probe technique that will be described here. For the experiments contained within this chapter the results were all obtained at room temperature. The temporal behaviour of the electron spin can easily be described using simple rate equations.

8.3 Dynamical description of spin relaxation

When circularly polarised light is used to excite a quantum well resonantly with the heavy hole exciton, 100% spin polarisation of the excited electrons occurs within the conduction band. The excited electrons either occupy the spin up or spin down states depending on whether the circular light used is left or right circularly polarised. Once excited, the electron spins relax to the equilibrium state where the conduction band is populated by equal numbers of spin up and spin down electrons. Assuming that the spins are allowed to relax exponentially until equilibrium is reached, the processes involved are described by the following rate equations.

$$\frac{dN^+}{dt} = -\frac{N^+}{r} - \frac{N^+}{s} + \frac{N^-}{s} = -\frac{N^+}{r} - \frac{N^+ - N^-}{s} \qquad 8.1$$

$$\frac{dN^-}{dt} = -\frac{N^-}{r} + \frac{N^+}{s} - \frac{N^-}{s} = -\frac{N^-}{r} + \frac{N^+ - N^-}{s} \qquad 8.2$$

where N^+ and N^- are the populations of spin up and spin down electrons. The carrier relaxation time which relates to the recombination of the electrons with holes is given by r, and the spin relaxation time is described by s.

If Eqn 8.1 and Eqn 8.2 are added, the result given by

$$\frac{d\left(N^{+}+N^{-}\right)}{dt}=-\frac{N^{+}+N^{-}}{r} \qquad 8.3$$

describes the total carrier population recombination rate characterised by r. This is observed experimentally when orthogonal linear polarisations are used.

Subtraction of the same two equations gives

$$\frac{d\left(N^{+}-N^{-}\right)}{dt}=-\left(\frac{1}{r}+\frac{2}{s}\right)\left(N^{+}-N^{-}\right) \qquad 8.4$$

The expressions for $(N^{+}+N^{-})$ and $(N^{+}-N^{-})$ can then be obtained from Eqn 8.3 and Eqn 8.4. Addition of the resulting equations will yield an expression for N^{+} which is what is observed when excite and probe pulses have the same circular polarisation. The expression for N^{+} is given by

$$N^{+}(t)=\frac{N_0}{2}e^{-t/r}\left(1+e^{-2t/s}\right) \qquad 8.5$$

where N_0 is the initial excited electron population. If the carrier relaxation time, r, is long compared with the electron spin relaxation time s, then the time for the electron spins to randomise can be measured readily by the technique described below.

The well width dependence of the spin relaxation time has been studied by Roussignol et al at low temperatures [8.1]. The relaxation rates measured refer to exciton spin relaxation and are shown in Figure 8.1.

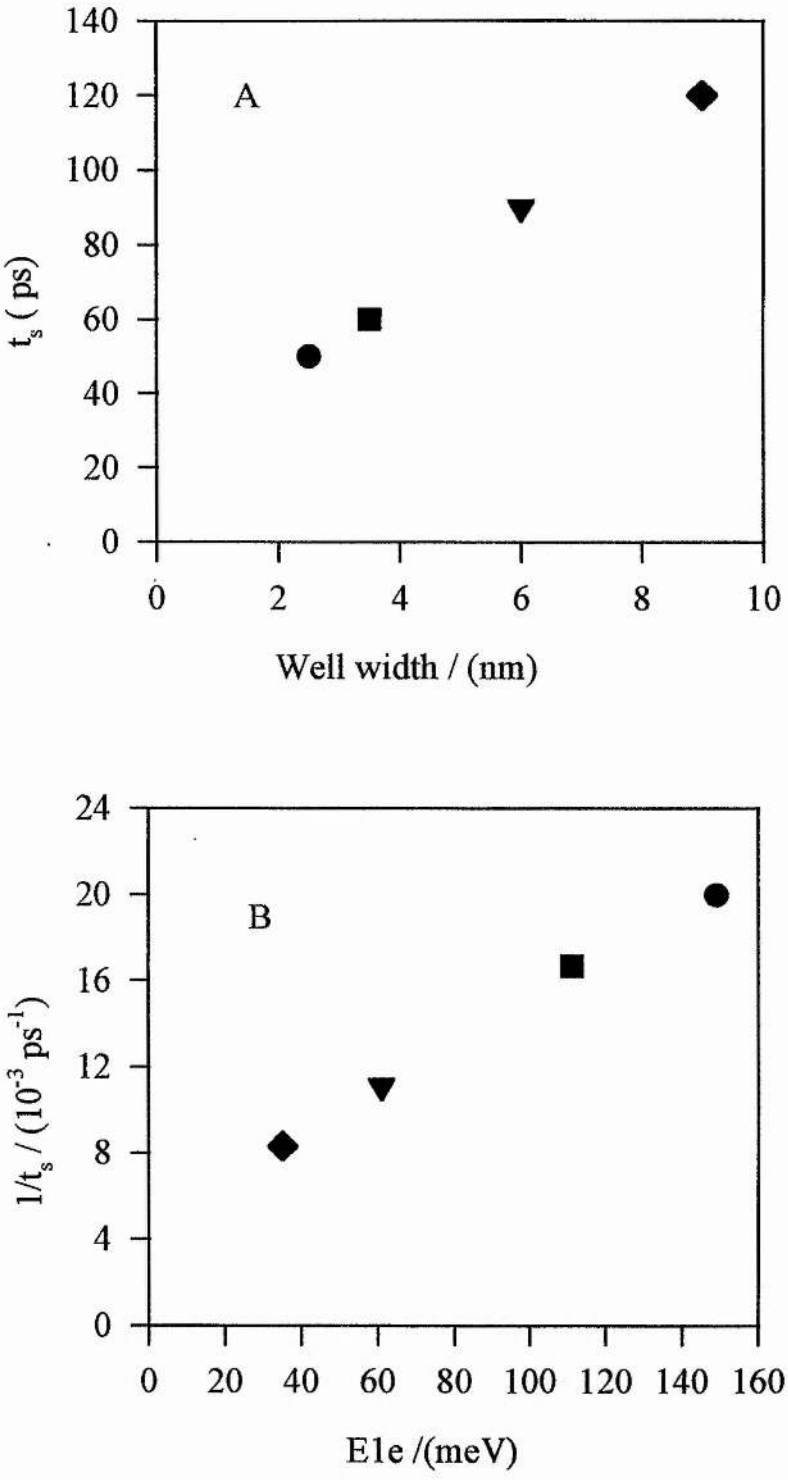

Figure 8.1 *(a) Spin relaxation time as a function of well width and (b) spin relaxation rate as a function of the first electron confinement energy, after Roussignol et al [8.1].*

The exciton spin relaxation time will be influenced by the underlying electron and hole spin flip times but has the added complication that the relaxation process involves the emission or absorption of the exchange energy as a phonon into the lattice. This tends to increase the exciton spin relaxation time compared to the free particle spin flip times [8.2].

The quantum wells used were all grown on one sample separated by wide barriers. In using this type of structure the effects due to impurities and defects should be reduced. This should allow the well width dependence of the spin relaxation rate to be measured under the same extrinsic conditions. The results show an increase in the relaxation rate with increasing electron confinement energy but slower than predicted for the DP mechanism.

Since their first measurement of the electron spin relaxation time at room temperature in a quantum well using the pump probe technique, Tackeuchi et al [8.3] have investigated the well width dependence of the electron spin relaxation rate [8.4]. They have used two samples with different well widths across each. The results show a $1/E_{1e}^{2.2}$ dependence for the electron spin relaxation rate and Tackeuchi takes this to be strong evidence of the DP mechanism.

8.4 Experimental setup

The experimental setup for the investigation of spin relaxation is shown in Figure 5.7. The $\lambda/4$ plates are used to provided the different polarisation configurations and the change in transmission due to the pump pulse is monitored with a time delayed probe as described in chapter 5.

8.5 Results

Experiments were carried out in four different samples of varying well width. The samples used were S51 (4.4 nm well width), KLB (6.5 nm well width), G1273 (8.0 nm well width) and FK141 (9.0 nm well width). In each case the experiment was repeated for the three possible polarisation configurations (namely OLP, OCP and SCP) firstly using wavelengths resonant with the position of the heavy hole exciton and secondly with pulses shifted in wavelength towards the long wavelength side of the heavy hole exciton. The results are shown in Figures 8.1-8.6. For samples G1273 and FK141 it was not possible to measure an increase in absorption on the long wavelength side of the heavy hole exciton since the broadening was minimal in these samples. The measured spin relaxation times measured, t_s, are summarised in the table below.

Table 8.1 *Spin relaxation times*

Sample	*Well-width (nm)*	t_s *(ps)*
S51	4.4	32
KLB	6.5	54
G1273	8.0	60
FK141	9.0	75

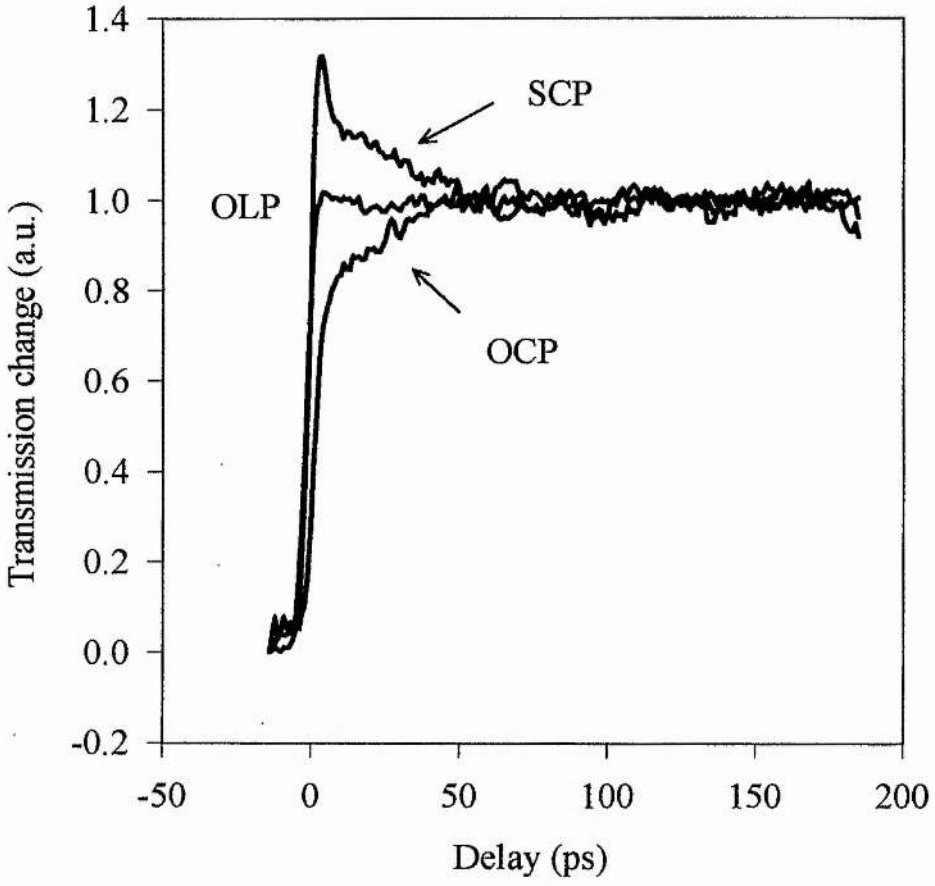

Figure 8.2 *Change in transmission for sample S51 at the heavy hole exciton (811 nm) as a function of probe pulse delay time. The three traces correspond to the three polarisation configurations used.*

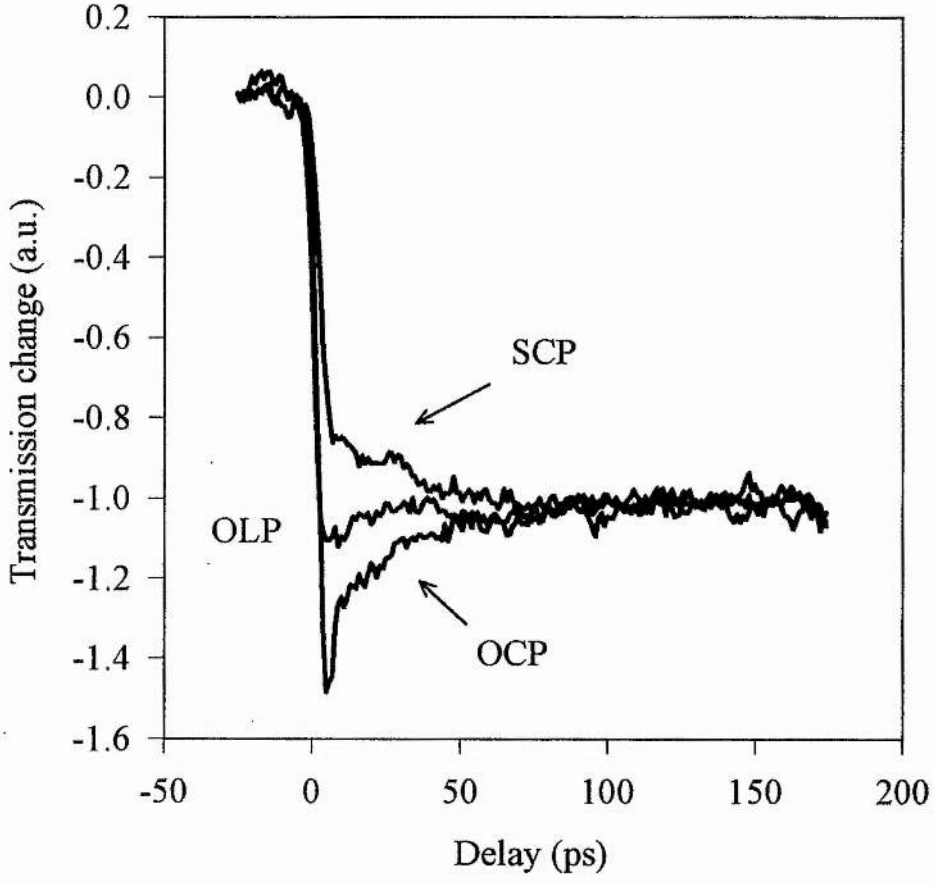

Figure 8.3 *Change in transmission for sample S51 on the long wavelength side of the heavy hole exciton (813 nm) as a function of probe pulse delay time. The three traces correspond to the three polarisation configurations used.*

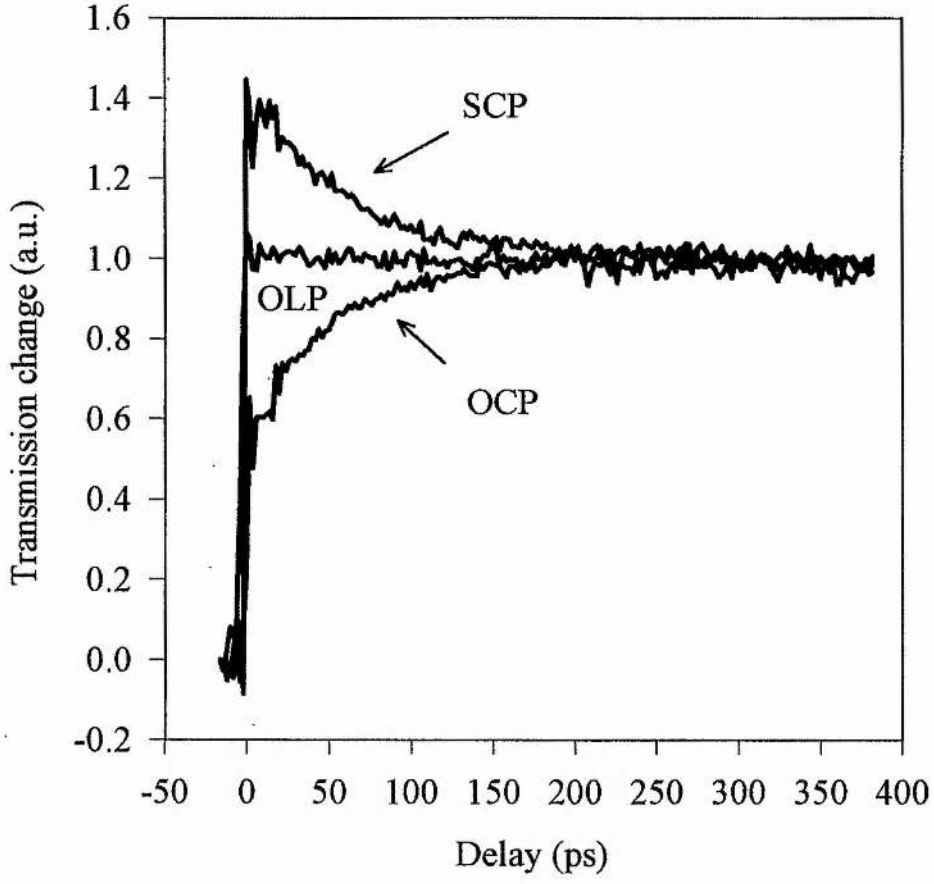

Figure 8.4 *Change in transmission for sample KLB at the heavy hole exciton (830 nm) as a function of probe pulse delay time. The three traces correspond to the three polarisation configurations used.*

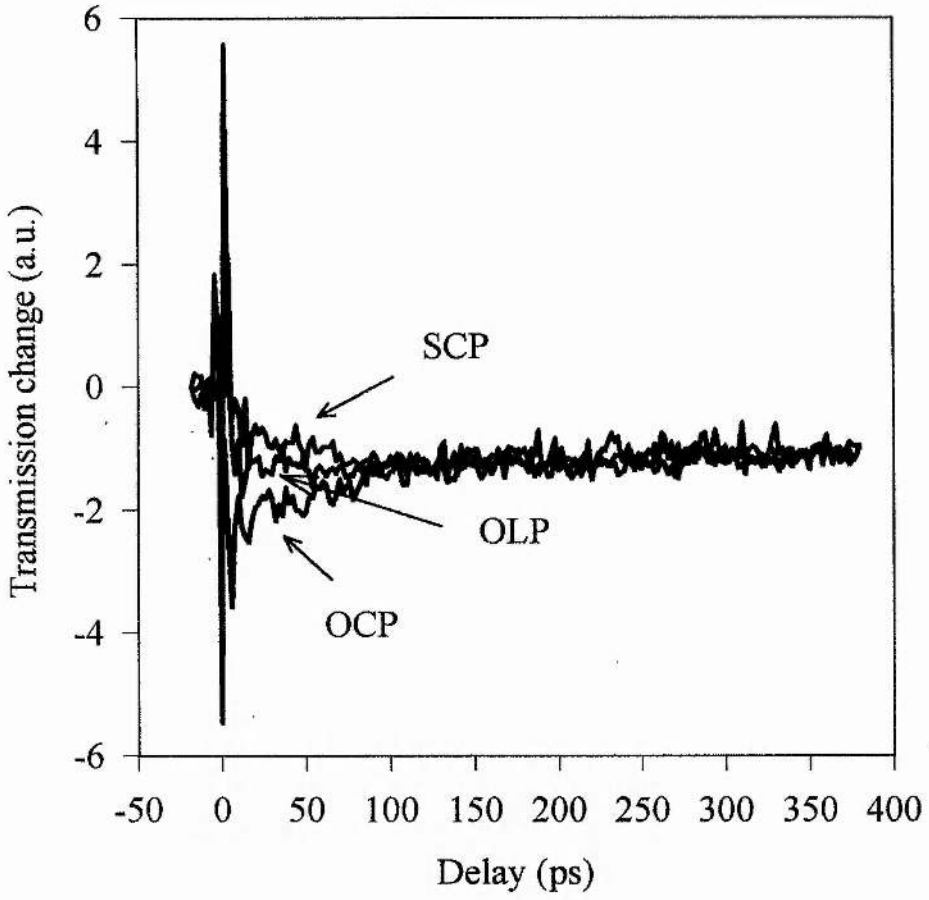

Figure 8.5 *Change in transmission for sample KLB on the long wavelength side of the heavy hole exciton (835 nm) as a function of probe pulse delay time. The three traces correspond to the three polarisation configurations used.*

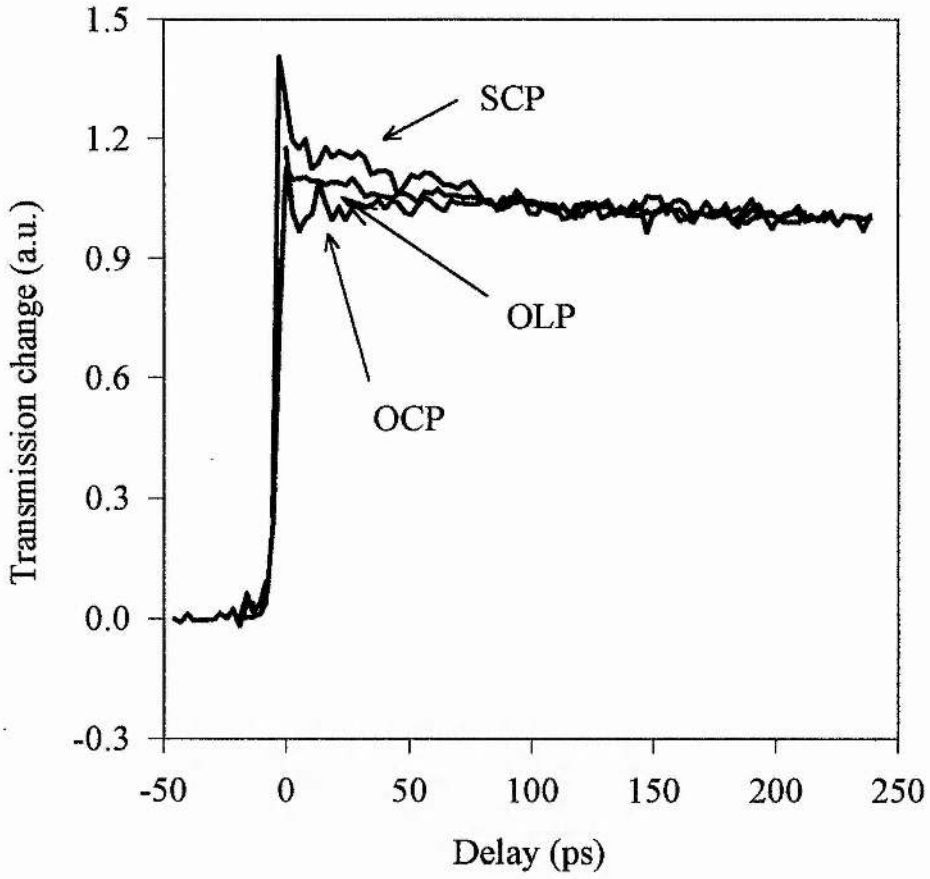

Figure 8.6 *Change in transmission for sample G1273 at the heavy hole exciton (837 nm) as a function of probe pulse delay time. The three traces correspond to the three polarisation configurations used.*

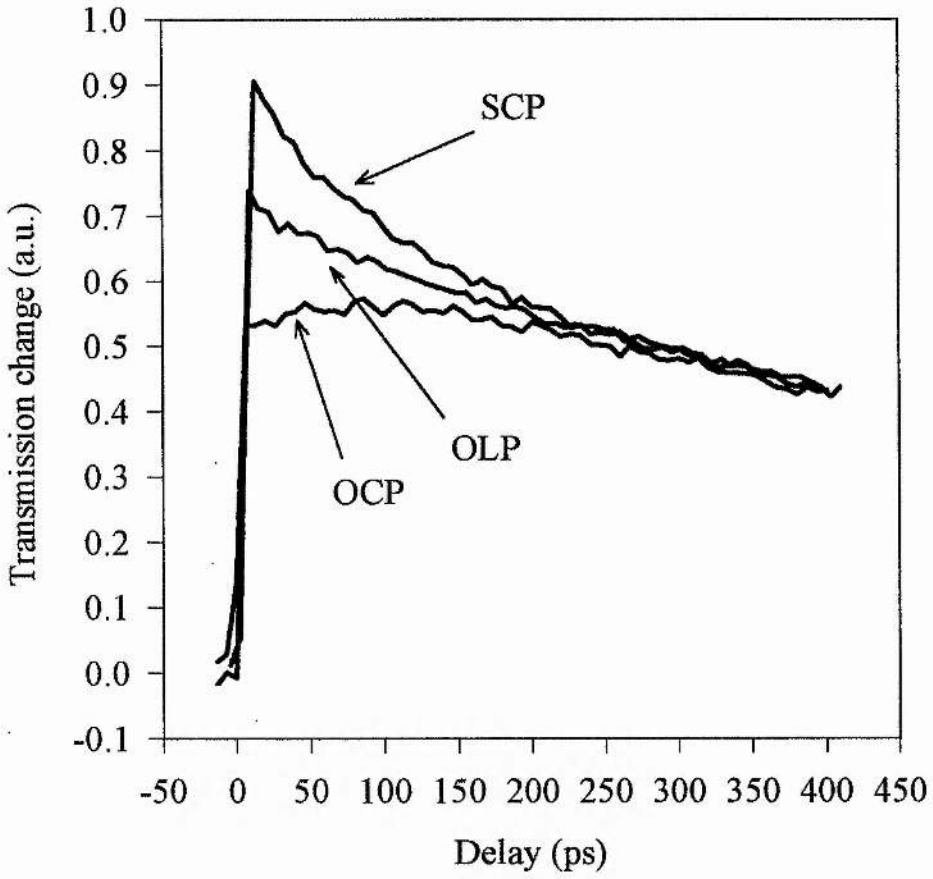

Figure 8.7 *Change in transmission for sample FK141 at the heavy hole exciton (845 nm) as a function of probe pulse delay time. The three traces correspond to the three polarisation configurations used.*

8.6 Data Analysis

The results shown in figures 8.2, 8.4, 8.6 and 8.7 show the effects of phase space filling at the peak of the heavy hole exciton. For the opposite linear polarisation (OLP) case, the pump excited equal populations of spin up and spin down electrons. The probe, which is composed of equal parts left and right circular then interrogates both spin states and sees a reduced absorption due to the presence of electrons in the low lying states. The electrons are therefore already in equilibrium in the two spin states and therefore do not expect to observe spin relaxation. Any decay of the curve will result solely from carrier recombination.

When the same circular polarisations (SCP) are used the pump pulse selectively populates only one spin state. The time delayed probe sees a larger reduction in absorption compared to the opposite linear polarisation (OLP) case. As discussed in chapter 7, this occurs because, where as before all the excited electrons were evenly spread between the two spin states, now they all initially occupy the same spin state. The absorption then recovers over time to the opposite linear polarisation level as the electron spins become mixed between the two spin states. It is this time for the electron spin to randomise that is termed the spin relaxation time, t_s.

When opposite circular polarisations (OCP) are used, 100% spin polarised electrons are again excited into the conduction band, but the probe examines the opposite spin state. The probe therefore sees an initial decrease in the absorption which is less than that observed for the opposite linear polarisation (OLP)case. This recovers over time to the same level as the opposite linear polarisation case as the spin relax.

On the long wavelength side of the excitonic resonance the effects are subtlety modified. As described in the previous chapter, the phase space filling contribution to exciton saturation, which is spin dependent, causes a decrease of the oscillator strength across the entire resonance. This by itself would lead to results very similar to those obtained at the resonance which is clearly not what is observed. The results shown in figures 8.3 and 8.5 include the effect of density dependent

broadening which leads to an overall increase in the absorption on the long wavelength side of the exciton. However the effect of phase space filling at this wavelength will counter-act the effects of broadening (see figure 7.7 and 7.8). Phase space filling will always reduced the absorption on the wings of the resonance whereas broadening will increase the absorption, which is confirmed by the results shown. The opposite circular polarisation (OCP) case, where the phase space filling contribution is smallest, gives the largest increase in absorption, whereas the same circular polarisation (SCP) case gives the smallest increase in absorption.

The initial increase in absorption at zero delay occurs solely due to density dependent broadening. This broadening is strongly evident for S51 (see figure 8.3) and slightly less so for KLB (see figure 8.5). This justifies the conclusions of the previous chapter where S51 was seen to exhibit a strong broadening signature. The broadening effect was seen to be less important for KLB and FK141.

The fact that no long wavelength increase in the absorption could be measured for FK141 or G1273 supports the idea that broadening in these samples is of reduced importance.

8.6.1 Well width dependence

The two main mechanisms thought to be responsible for electron spin relaxation in quantum wells are those proposed by DP and BAP. These have been discussed in detail in chapter 3.

Damen et al [8.5] calculated the enhancement of the BAP mechanism for the spin relaxation rate in a quantum wells when compared to bulk to be

$$\frac{1}{\tau_{s_{2D}}} = \frac{3\pi}{2k_f L}\frac{1}{\tau_{s_{3D}}} \qquad 8.6$$

where k_f is the Fermi wavevector for the 3D density and L is the well width.

A similar expression for the enhancement of the DP mechanism is given as

$$\frac{1}{\tau_{s_{2D}}} = \frac{4}{\left(k_f L\right)^4} \frac{1}{\tau_{s_{3D}}} \qquad 8.7$$

Both of these predict a decrease in the electron spin relaxation time with decreasing well width which is consistent with the experimental results given in Table 8.1. Physically, the spin relaxation time decreases with well width due to the increased localisation of the wavefunction.

Bastard et al [8.2] gives a more complete expression for the enhancement of the DP mechanisms in a quantum well as

$$\frac{1}{\tau_s} = \frac{2\left(\alpha E_{1e}/\hbar\right)^2}{E_g k_B T} \int_0^\infty \varepsilon \, \tau_\nu(\varepsilon) \exp\left(\frac{-\varepsilon}{k_B T}\right) d\varepsilon \qquad 8.8$$

where α is a numerical coefficient governing the spin splitting of the conduction band. E_{1e} is the first electron confined state in the quantum well and E_g is the band gap. τ_ν is the electron momentum relaxation time and is inversely proportional to the number of scattering events per unit time.

The equation shows that spin flip is more efficient for narrower quantum wells (as long as E_{1e} increases as the well width decreases). For infinite wells E_{1e} is proportional to $1/L^2$ and so ignoring any energy dependence of τ_ν, this approximation gives

$$\frac{1}{\tau_s} \propto \frac{1}{L^4} \qquad 8.9$$

which is consistent with Eqn 8.7. In Figure 8.8 the dependence of the first electron confinement energy on the quantum well width is plotted for the case of infinite and finite wells. This shows that the L^4 dependence is only true for wide wells where the confinement is small.

Since E_{1e} depends on other factors (such as alloy concentration) as well as well width the variation of τ_s with E_{1e} is therefore the preferred measure. However, in

nominally undoped samples, the concentration of scattering centres randomly fluctuates from sample to sample, so that the variation of τ_s with E_{1e} may be sample dependent.

The results for S51, KLB, G1273 and FK141 were all obtained at room temperature and relate solely to electron spin relaxation. The results are shown graphically in figure 8.9. Each of these samples was grown separately at different sites and contains only one quantum well width (see chapter 6). This is in contrast to the samples used by Roussignol and Tackeuchi which were grown with varying quantum well widths across the same sample. At room temperature the main scattering mechanism is due to optical phonon interactions and so the measured spin times should be less sample dependent.

A similar study has been carried out by Grevatt [8.6]. Through monitoring the change in the reflectivity of the left and right hand circular components of the reflected probe beam they have measured the electron spin relaxation time at room temperature in various quantum wells. The samples used were each of differing well width although the majority of the samples were obtained from the same source. It should be noted that this source was not the same as that for either FK141, G1273, KLB or S51. The results are shown in figure 8.10.

The Gravett and Tackeuchi results along with those for S51, KLB, G1273 and FK141 are shown in figure 8.11. Fitting to all the data points using the generic equation $Y=aX^b+c$, a value of 2.16 is obtained for b. This is in good agreement with Tackeuchi's estimate and is further evidence that the DP mechanism is dominant in undoped quantum wells at room temperature.

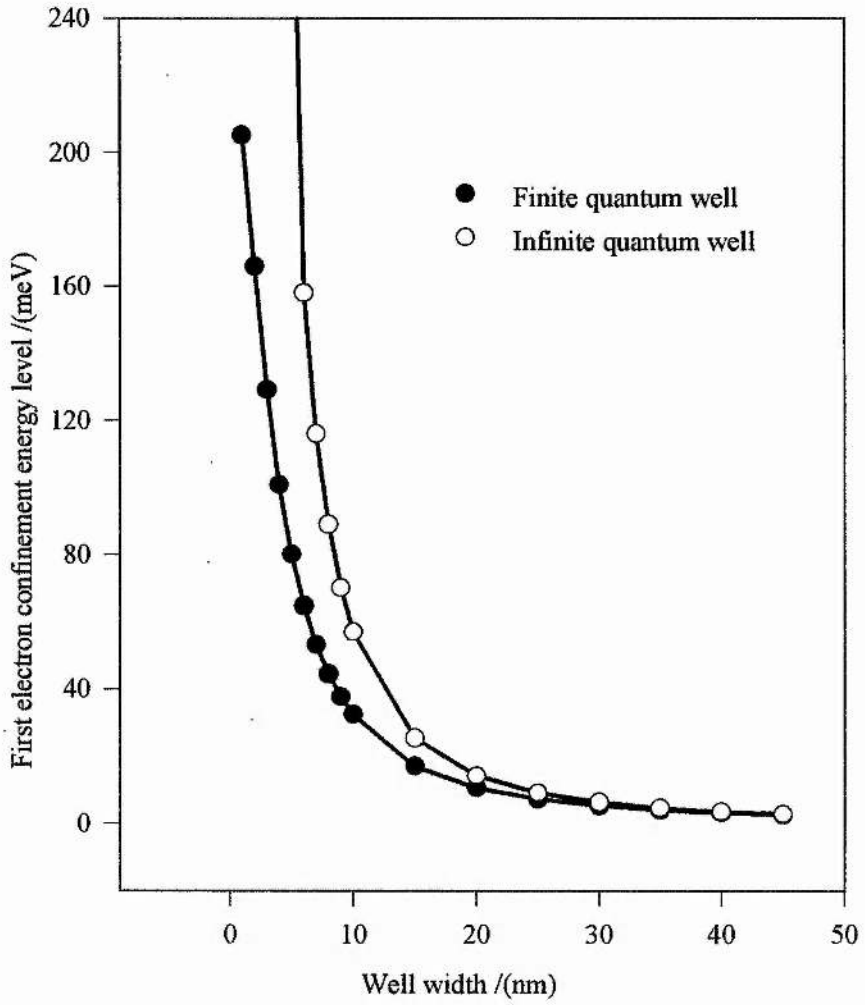

Figure 8.8 *Dependence of the first electron confinement energy on well width for infinite (○) and finite quantum well (●) cases.*

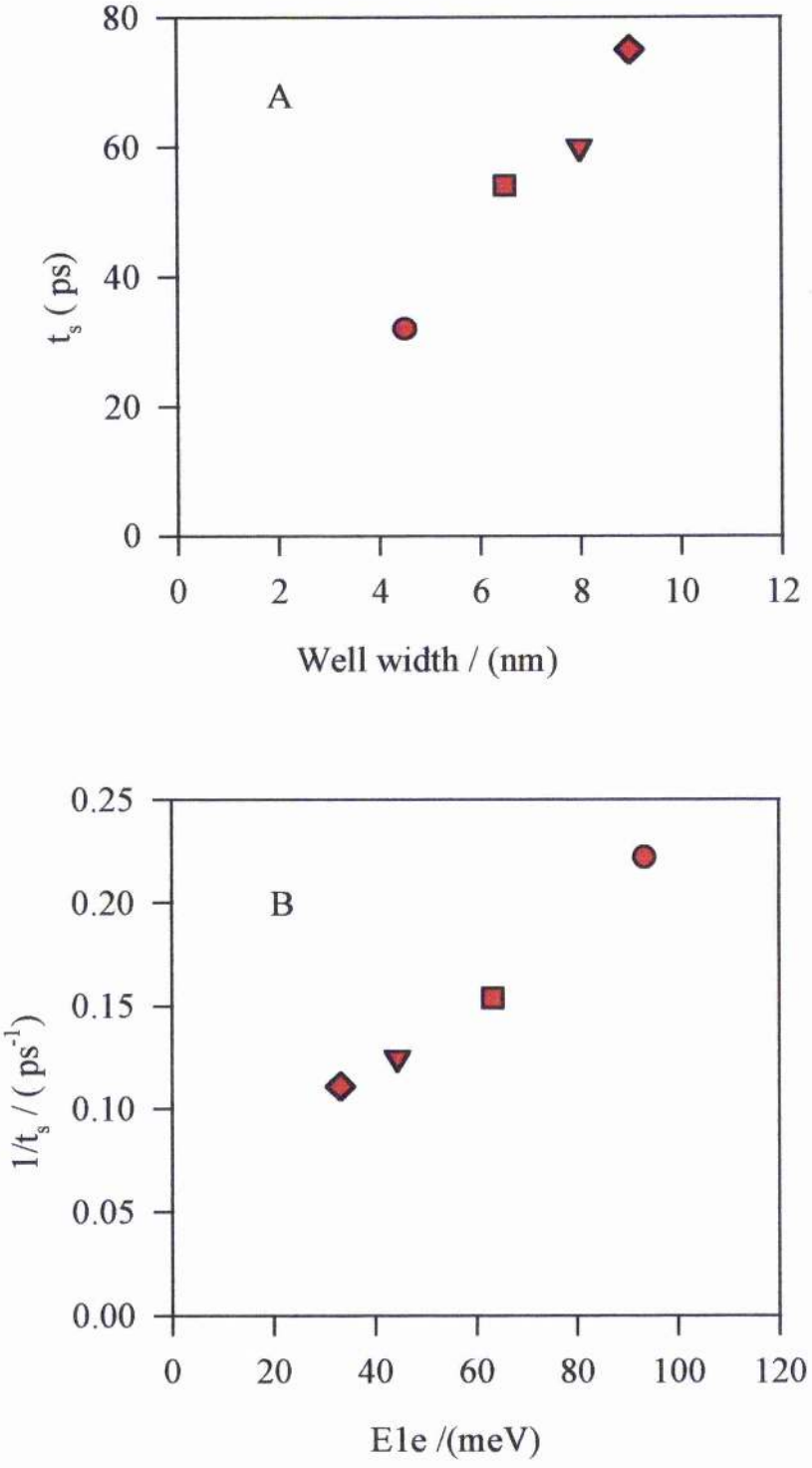

Figure 8.9 *(a) Spin relaxation time as a function of well width and (b) spin relaxation rate as a function of the first electron confinement energy, for samples S51 (●), KLB (■), FK141 (▼) and G1273(◆).*

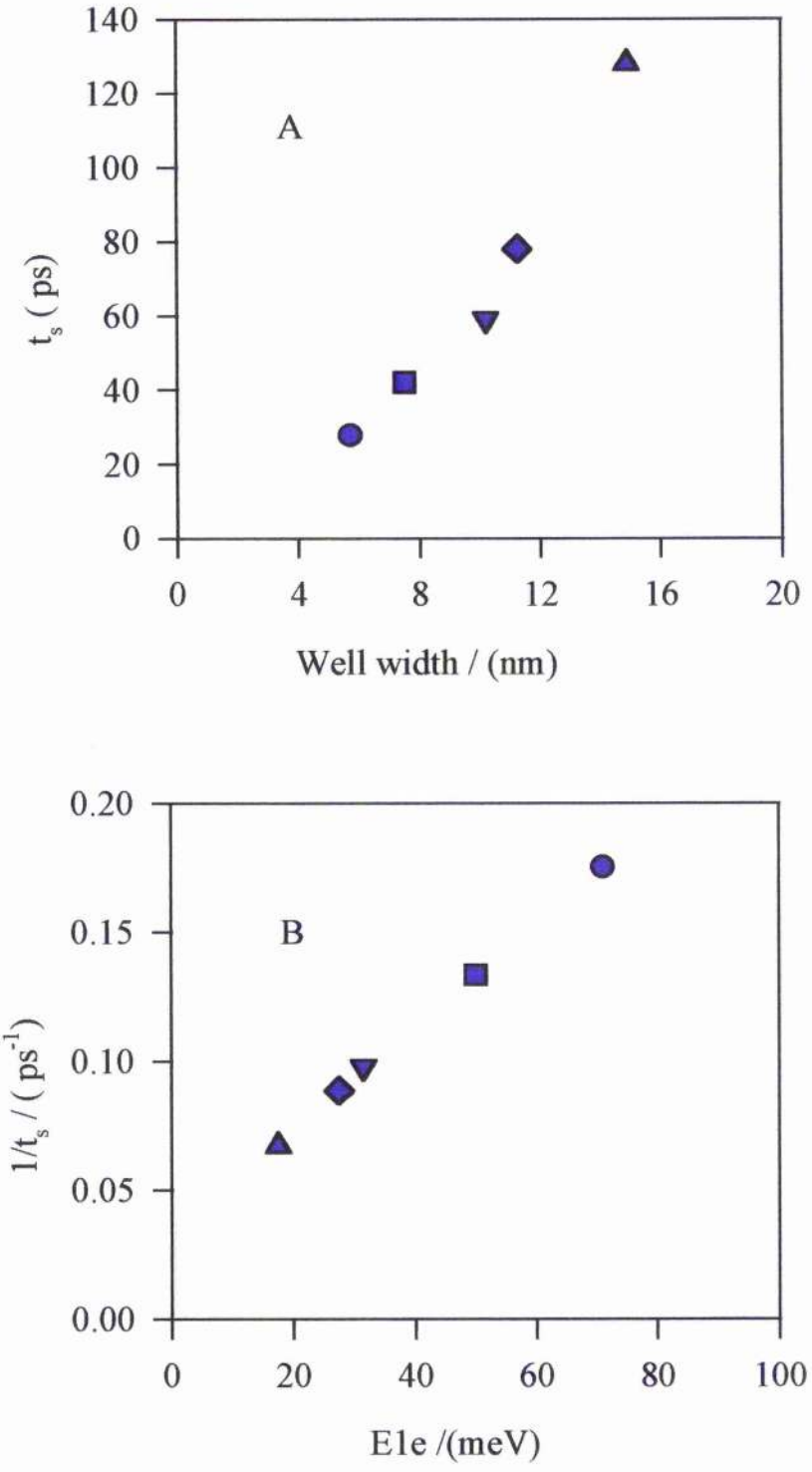

Figure 8.10 *(a) Spin relaxation time as a function of well width and (b) spin relaxation rate as a function of the first electron confinement energy, after Gravett [8.6].*

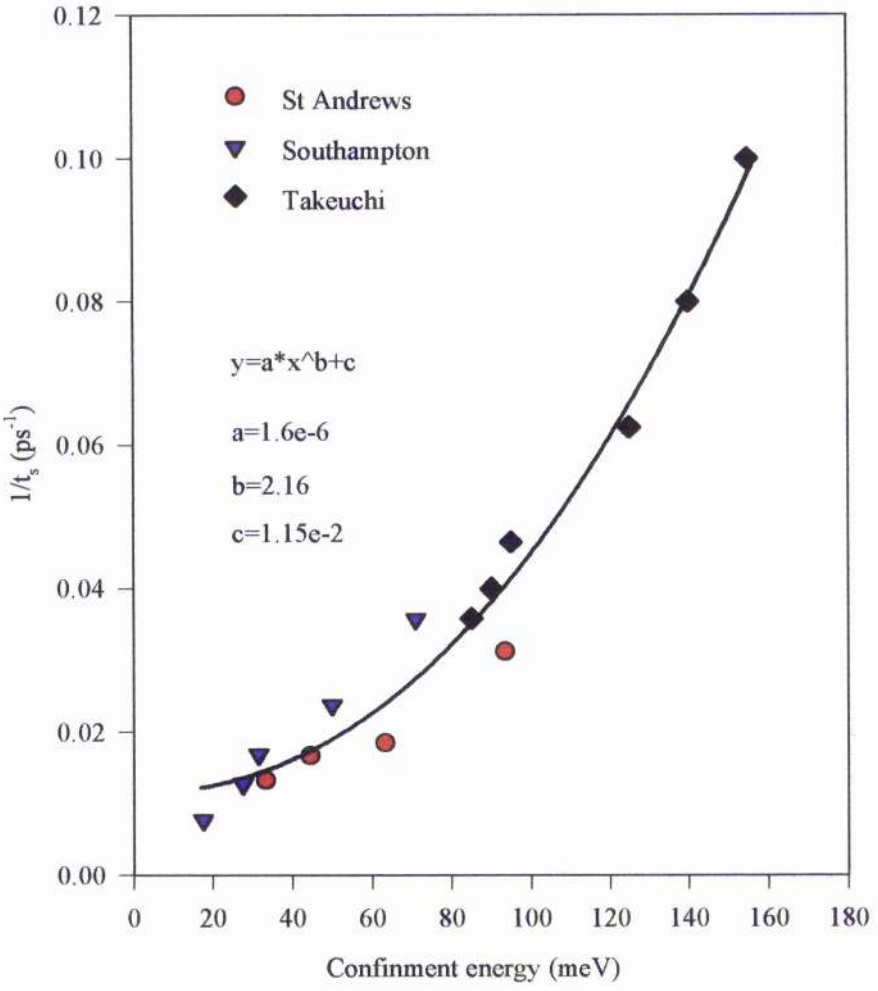

Figure 8.11 *Spin relaxation rate as a function of the first electron confinement energy for the results obtained by Tackeuchi (◆), Gravett (▼) and those for S51, KLB, FK141 and G1273(●) are all plotted together. The fitted curve* $Y=aX^b+c$ *has* $b=2.16$.

8.7 Conclusion

The spin relaxation rate has been shown to agree well with the predictions of the DP mechanism for varying well width.

The results obtained for S51, KLB, G1273 and FK141 show a decrease in the electron spin relaxation time as the well width is reduced. The results are in good agreement with those obtained by Tackeuchi using two samples with varying quantum well widths on each and those of Grevatt for a number of individual samples. The agreement is surprising since the spin relaxation time is thought to be very sample dependent as previously stated and each of the samples used was obtained from a different source. The fact that this investigation has been carried out a room temperature may influence any sample dependency as the main scattering mechanism will be due to LO-phonon collisions and not impurity or interface interactions. All the combined data give a 2.16 power dependence of the spin relaxation rate on the electron confinement energy. This strongly suggests that the DP mechanism causes the spin relaxation of electrons at room temperature in quantum wells. The accuracy of the fitted curve would benefit from more data at higher electron confinement energies.

The dependence of the spin relaxation time on well width at room temperature is important for device applications. If the dependence on well width is known then well with specific spin relaxation times can be fabricated. A number of all-optical switches based on spin relaxation in quantum wells have been demonstrated [8.8,8.9]. electron spin relaxation will give response times of 10s of picoseconds and the hole around 1 picosecond.

Kawazoe et al utilised the fast hole spin relaxation in type II quantum wells [8.7] to demonstrate a switch with switching energy density of 3 nJ/cm^2 and a repetition rate of 80 GHz. Nishikawa et al [8.9] demonstrated a 7 picosecond switch using a quantum well etalon. The switching time was achieved by utilising tunnelling in type II structures and spin relaxation. The switching energy density for this switch was 48 $fJ/\mu m^2$.

8.8 References

8.1 P. Roussignol, P. Rolland, R. Ferreira, C. Delalande, G. Bastard, A. Vinattieri, L. Carraresi and M. Colocci, "Time-resolved spin-polarisation spectroscopy in GaAs/AlGaAs quantum wells", Surface Science, **267**, 360-364, (1992).

8.2 G. Bastard, and R. Ferreira, "Spin-flip scattering times in semiconductor quantum wells", Surface Science, **267**, 335-341, (1992).

8.3 A. Tackeuchi, S. Muto, T. Inata and T. Fujii, "Direct observation of picosecond spin relaxation of excitons in GaAs/AlGaAs quantum wells using spin-dependent optical nonlinearity", Appl. Phys. Letts., **56**, 22, 2213-2215, (1990).

8.4 A. Tackeuchi, Y. Nishikawa and O. Wada, "Room-temperature electron spin dynamics in GaAs/AlGaAs quantum wells", Appl. Phys. Letts., **68**, 6, 797, (1996).

8.5 T.C. Damen, L. Vina, J.E. Cunningham and J. Shah, "Subpicosecond spin relaxation dynamics of excitons and free carriers in GaAs quantum wells", Phys. Rev. Letts., **67**, 24, 3432-3435, (1991).

8.6 T. Grevatt, *University of Southampton*, Private communication.

8.7 T. Kawazoe, Y. Masumoto and T. Mishina, "Spin-relaxation process of holes in type-II Al(0.34)Ga(0.66)As/AlAs multiple quantum wells", Phys. Rev. B., **47**, 16, 10452-104, (1993).

8.8 T. Kawazoe, T. Mishina and Y. Masumoto, "Highly repetitive picosecond polarisation switching in type-II AlGaAs/AlAs multiple quantum wells", Jpn. J. Appl. Phys., **32**, L1756-175, (1993).

8.9 Y. Nishikawa, A. Tackeuchi, S. Nakamura, S. Muto and N. Yokoyama, "All-optical picosecond switching of a quantum well etalon using spin-polarisation relaxation", Appl. Phys. Letts., **66**, 7, 839-841, (1995).

9

Amplitude grating studies

9.1 Summary

This section describes three-beam degenerate four wave mixing (DFWM) experiments. The ambipolar diffusion coefficients for two GaAs/AlGaAs multiple quantum well samples are measured and the respective hole mobility's are deduced.

9.2 Introduction

DFWM provides a very sensitive measure of nonlinear changes in refraction. This has been studied to great length in a number of semiconductors [9.1]. DFWM in multiple quantum wells was first reported by Hegarty et al [9.2] at low temperatures, and at room temperature in a GaAs/AlGaAs multiple quantum well by Miller et al [9.3]. A number of previous studies have also used two-beam self-diffraction to examine the nonlinearities [9.4-9.7], the incorporation of a third probe beam allows the spatial dynamics of the optically excited carriers to be monitored [9.8].

There are primarily two types of three-beam DFWM configurations: the standard forward propagating geometry, Figure 9.1, and the counter propagating or phase conjugate geometry, Figure 9.2.

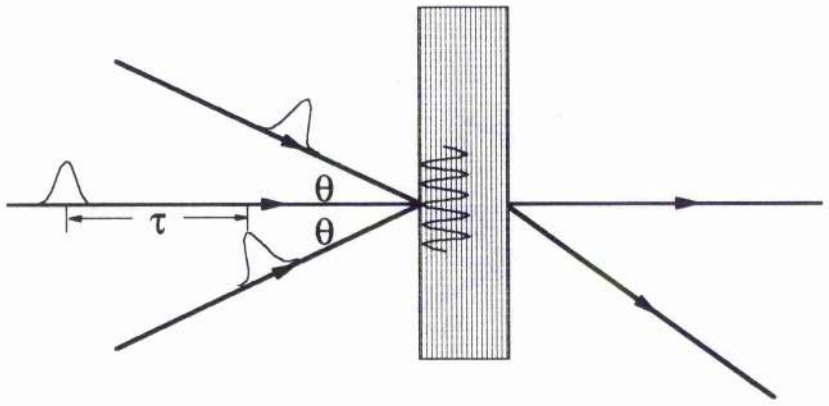

Figure 9.1 *The forward travelling geometry for three-beam DFWM.*

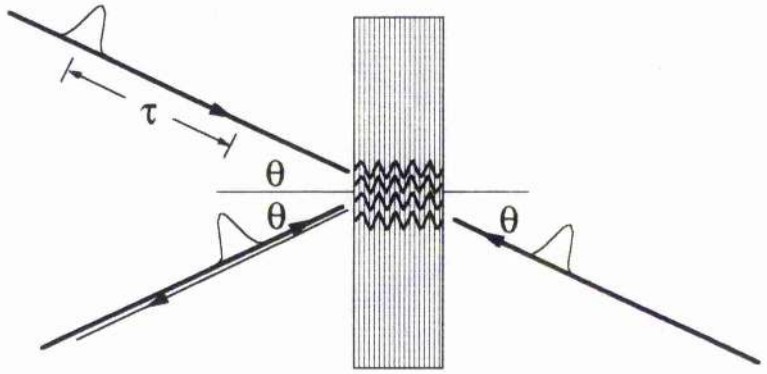

Figure 9.2 *The counter propagating or phase conjugate geometry for three-beam DFWM.*

The diffusion of carriers in multiple quantum wells can be described in terms of in-well (parallel to the quantum well layers) and cross-well (perpendicular to the quantum well layers) motion. The barriers of the quantum well severely restrict cross-well transport and lead to a highly anisotropic diffusion.

The counter propagating geometry allows the monitoring of the cross-well transport. This is important in a number of multiple quantum well optical devices such as symmetric self-electro-optic effect devices (SEEDs), field-effect-transistor (FET) SEEDs, hetreo n-i-p-i devices and vertical cavity lasers which for their operation depend on the generation or injection of electrons and holes into a multiple quantum well region. Ultimately high speed operation of theses devices is dependent on the removal of the generated/injected electron hole pairs by transport perpendicular to the quantum well layers. If the barrier regions are thin it has been shown that cross-well transport is dominated by tunnelling [9.9]. For quantum wells with thick barriers, where tunnelling can be neglected, the transport is determined by the need to thermally activate a small number of the carriers above the barrier and their subsequent motion above the barrier, whether it be drift or diffusion [9.10].

The highly anisotropic nature of the diffusion in multiple quantum wells was highlighted by Manning et al [9.11]. The measured grating decay obtained using the counter-propagating geometry were observed to be dependent on the orientation of the sample. This was attributed to the possibility of intra-well motion in addition to the expected cross-well motion when the grating was not exactly perpendicular to the quantum well layers.

The measurement of the intra-well motion of optically excited electrons and holes can be achieved using the forward-travelling DFWM configuration. This has been reported by a number of authors [9.8, 9.12, 9.13], and allows the determination of the intra-well ambipolar diffusion coefficient which governs the combined motion of electrons and holes.

The principles of DFWM concerning grating formation and decay are considered with reference to the forward-travelling geometry. The experimental technique involved in the creation of the gratings is described and the results obtained for two samples are presented. The calculated diffusion coefficients are then discussed with reference to quantum wells.

9.3 Grating formation

If two beams, of the same linear polarisation, are incident on a sample (as shown in Figure 9.1) at an angle of θ degrees either side of the normal, then they will interfere to give an intensity grating (as shown in Figure 9.3). This grating will take the form of a squared sinusoidal pattern (see Figure 9.4).

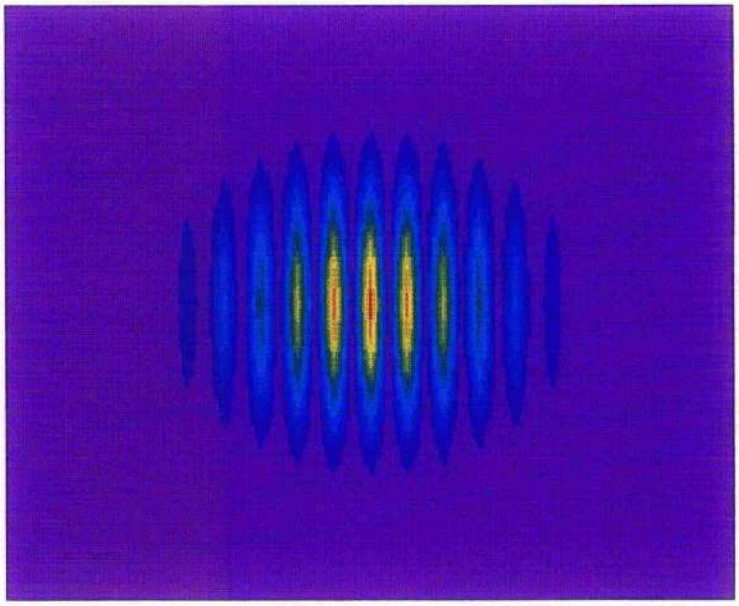

A

Figure 9.3 *Intensity distribution for the interference of two linear polarised beams with gaussian beam profiles.*

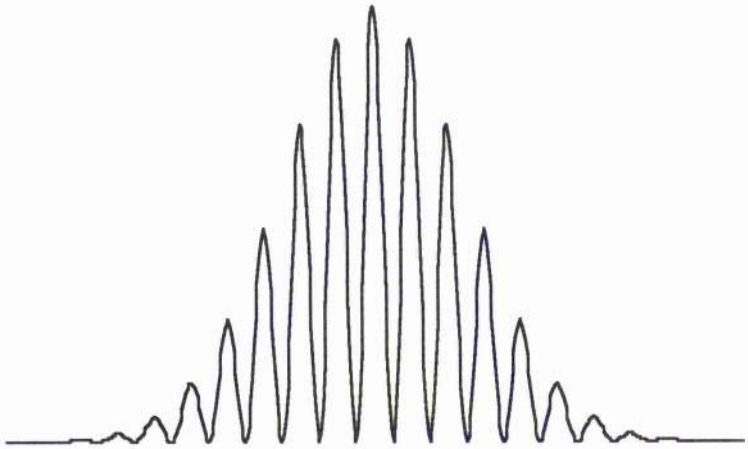

Figure 9.4 *Cross section of the intensity profile shown in Figure 9.3. The intensity grating can be clearly seen.*

The grating period can be calculated simply by considering two plane waves incident at an angle of θ degree with respect to the normal (as shown in Figure 9.5).

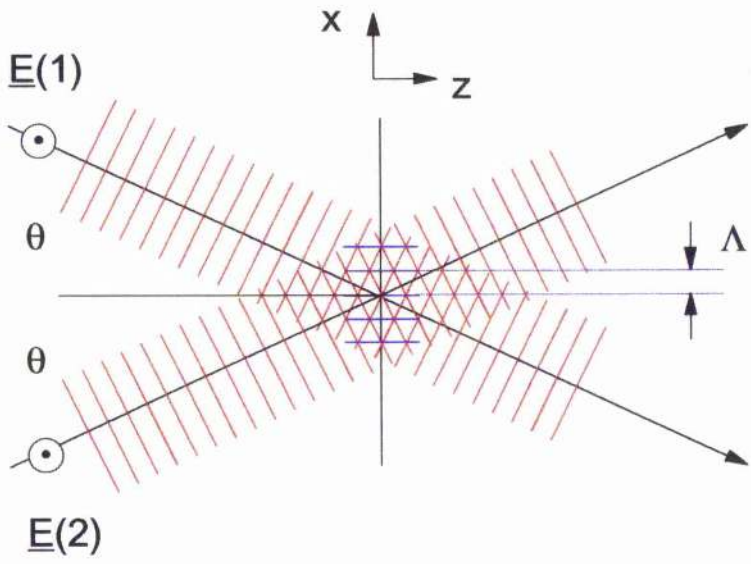

Figure 9.5 *Interference of two plane waves.*

If the waves are assumed to be polarised in the y direction and we neglect the time dependent terms the electric field amplitudes can be written as

$$\underline{E}(1) = A_{y1} \exp i\left(k_z z - k_x x\right) \tag{9.1}$$

$$\underline{E}(2) = A_{y2} \exp i\left(k_z z + k_x x\right) \tag{9.2}$$

where A_y is the electric field amplitude (polarised in the y direction) and k is the wave number in the various directions. If the electric field amplitudes for $\underline{E}(1)$ and $\underline{E}(2)$ are assumed to be equal then the resultant intensity distribution, I(x) is given by

$$I(x) = 2I_0\left(1+\cos\left(2k_k x\right)\right) \tag{9.3}$$

where I_0 is the intensity of a single beam and $2k_x$ is the wave number of the grating (Figure 9.6).

The grating period, Λ, can be obtained simply using

$$\Lambda = \frac{2\pi}{2k_x} \tag{9.4}$$

and

$$k_x = \frac{2\pi \sin(\theta)}{\lambda} \tag{9.5}$$

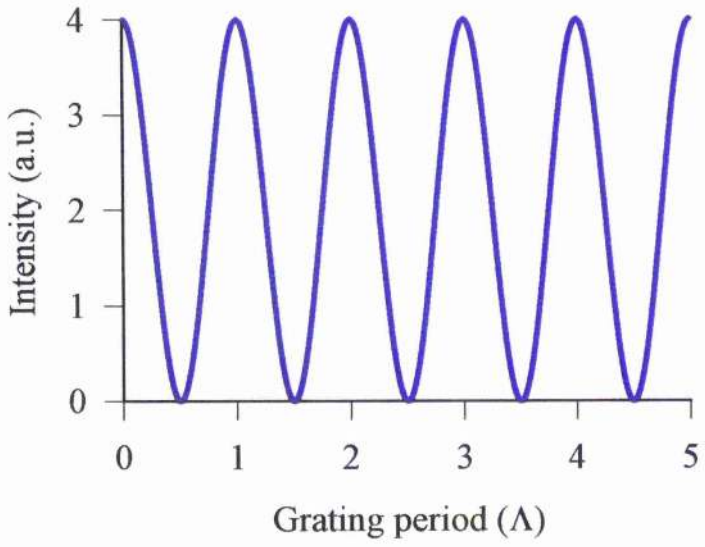

Figure 9.6 *Intensity distribution in units of I_0 as a function of grating period.*

where λ is the wavelength of the waves. Substitution of Eqn 9.5 into Eqn 9.4 then gives the grating period in terms of the wavelength and the angle to the normal as

$$\Lambda = \frac{\lambda}{2\sin(\theta)} \qquad 9.6$$

If a third beam is then made incident on the grating it will be diffracted with an angle, ϕ, from the normal given by

$$\sin\phi = \frac{\lambda}{\Lambda} = 2\sin(\theta) \qquad 9.7$$

The above theory is equally applicable to ultrashort pulses incident on a semiconductor multiple quantum well sample. In this case if the wavelength of the pulses correspond to an absorption feature a transient population grating is formed. If excitation results in exciton formation then their subsequent rapid ionisation will result in a population grating of electrons and holes. A probe pulse incident on the grating will then be diffracted from it. The diffraction efficiency, η, of the concentration grating that is formed is given by, [9.14],

$$\eta = \left| J_1\left(\frac{2\pi n_{eh}}{\lambda} + \frac{i\sigma_{eh}}{2} \right) N l_\alpha \right|^2 \exp(-\alpha l) \qquad 9.8$$

where J_1 is the first-order Bessel function, α is the absorption coefficient, l_α is the effective sample thickness given by

$$l_\alpha = \frac{1 - \exp(-l\alpha)}{\alpha} \qquad 9.9$$

n_{eh} is the nonlinear refractive index per carrier pair and σ_{eh} is the nonlinear absorption per carrier pair.

9.4 Grating decay

When ultra-short pulses are used to produce gratings in multiple quantum wells their behaviour becomes time-dependent. The intensity modulation at the sample surface only exists for the length of time that the pulses are overlapped and is therefore a coherent process. The concentration grating that is produced will "wash out" as a result of diffusion and recombination. In a semiconductor optical excitation produces equal numbers of electrons and holes so diffusion is ambipolar from regions of high to low population density within the wells.

From Eqn 9.8 it can be seen that the diffraction efficiency is proportional to the square of the modulation in the refractive index. If the grating decay is characterised by a time constant Γ, then the diffraction efficiency will decay with a rate equal to twice this i.e. 2Γ.

$$\eta(t) \propto \exp(-2\Gamma t) \tag{9.10}$$

With pulses shorter than the time scales encountered, the continuity equation for the excess carrier density at a position, x, along the wells and at any time, t, after excitation can be written as

$$\frac{\partial N(x,t)}{\partial t} = D_a \nabla^2 N(x,t) - \frac{N(x,t)}{\tau_R} \tag{9.11}$$

where N(x,t) is the excess carrier concentration, D_a is the ambipolar diffusion coefficient and τ_R is the electron-hole recombination time. The excess carrier density is given by [9.14]

$$N(x,t) = N(0,0)\left[\frac{1}{2} + \frac{1}{2}\cos\left(\frac{2\pi x}{\Lambda}\right)\exp\left(-\frac{t}{\tau_D}\right)\right]\exp\left(-\frac{t}{\tau_R}\right) \tag{9.12}$$

The evolution of the excess carrier density is graphed in Figure 9.7 where time increases from red→blue→green.

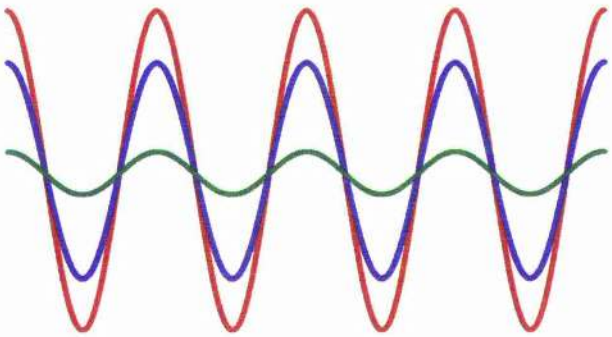

Figure 9.7 *Time evolution of the excess carrier concentration grating produced by an amplitude grating.*

Substitution of Eqn 9.12 into Eqn 9.11 gives the grating decay rate in terms of a diffusion rate and a recombination rate i.e.

$$\Gamma = \frac{1}{\tau_D} + \frac{1}{\tau_R} \qquad 9.13$$

as

$$\Gamma = \frac{4\pi^2 D_a}{\Lambda^2} + \frac{1}{\tau_R} \qquad 9.14$$

9.5 Experimental set-up

The production of transient gratings using the forward travelling DFWM geometry and the monitoring of their subsequent decay was carried out using the method described in section 5.5.

The experiment was carried out in the multiple quantum well samples of S51 and KLB. The results obtained and their interpretation is now presented.

9.6 Results

9.6.1 Time independent

The peak of the diffraction efficiency, for sample KLB, has previously been shown to lie on the long-wavelength side of the heavy hole exciton resonance [9.15]. This is expected for nonlinear refraction associated with the absorption saturation of a resonant feature. The power dependence of the diffraction efficiency should be quadratic at low powers (Eqn 9.8). KLB follows this behaviour at low powers and then appears to saturate for higher powers where the dependence approaches linear scaling [9.15].

The change in the transmission at the exciton resonance for sample S51 is measured as a function of the excite beam power and shown in Figure 9.8.The power dependence does not appear to follow that of KLB even at low powers. This measurement was carried out previously for KLB by Manning et al [9.15].

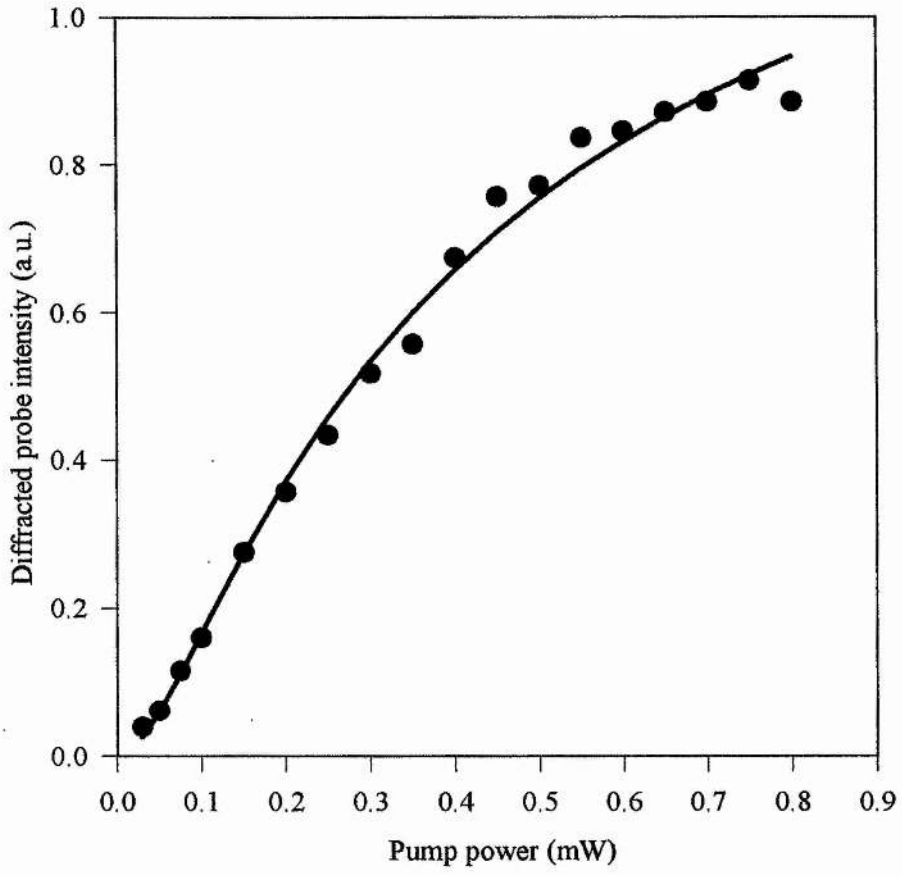

Figure 9.8 *Diffracted probe intensity as a function of the power in each of the pump arms for sample S51 at 811 nm.*

9.6.2 Time dependent results

The diffraction efficiency was monitored as a function of probe delay. The curves obtained for both samples are all characterised by exponential decays, with time constants much shorter than the electron-hole recombination time. Their decay is therefore solely attributed to the diffusion of the carriers in the plane of the quantum wells. In general the results were taken at powers where the diffraction efficiency had begun to saturate. The comparison of high and low power results revealed no difference in the decay times measured.

Figure 9.9 and Figure 9.10 show the decay curves obtained for samples KLB and S51 for a single grating period. The grating period was varied and the results for three different spacing are shown in Figure 9.11 for KLB and Figure 9.12 for S51.

Since the decay of the diffraction efficiency is given by Eqn 9.10 and the grating decay rate is given by Eqn 9.14, plotting the diffraction efficiency decay rate, 2Γ, against $8\pi^2/\Lambda^2$ will give a straight line graph with a gradient equal to the ambipolar diffusion coefficient. These graphs for KLB and S51 are shown in Figure 9.13 and Figure 9.14 respectively. It should be noted that the y-axis intercept of this line will give a measure of the electron-hole recombination rate, although in both the curves presented this intercept is indistinguishable from zero.

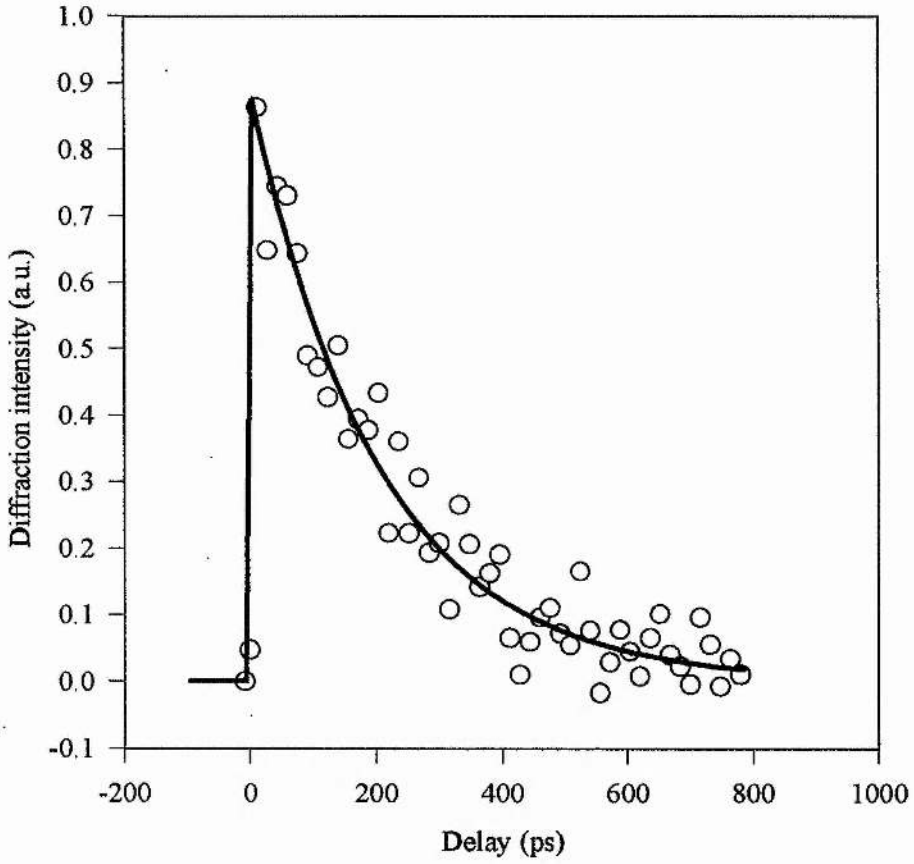

Figure 9.9 *Decay of the diffracted intensity for a 5 μm grating period in sample KLB. The fitted decay curve has a time constant of 200 ps.*

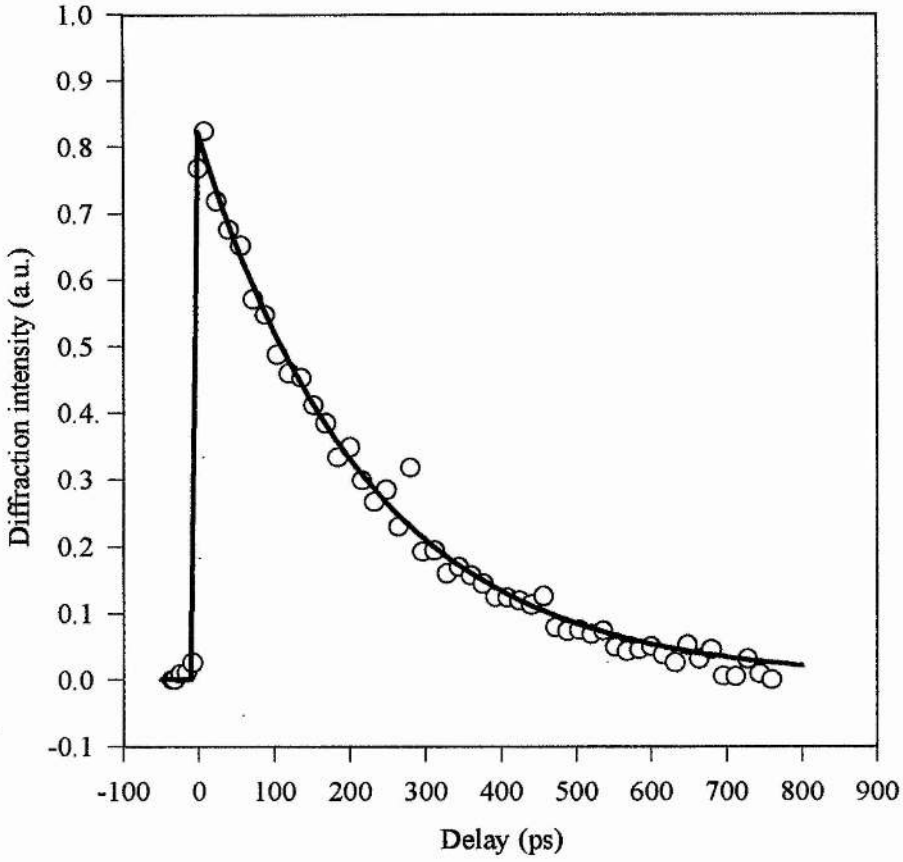

Figure 9.10 *Decay of the diffracted intensity for a 4.5 μm grating period in sample S51. The fitted decay curve has a time constant of 250 ps.*

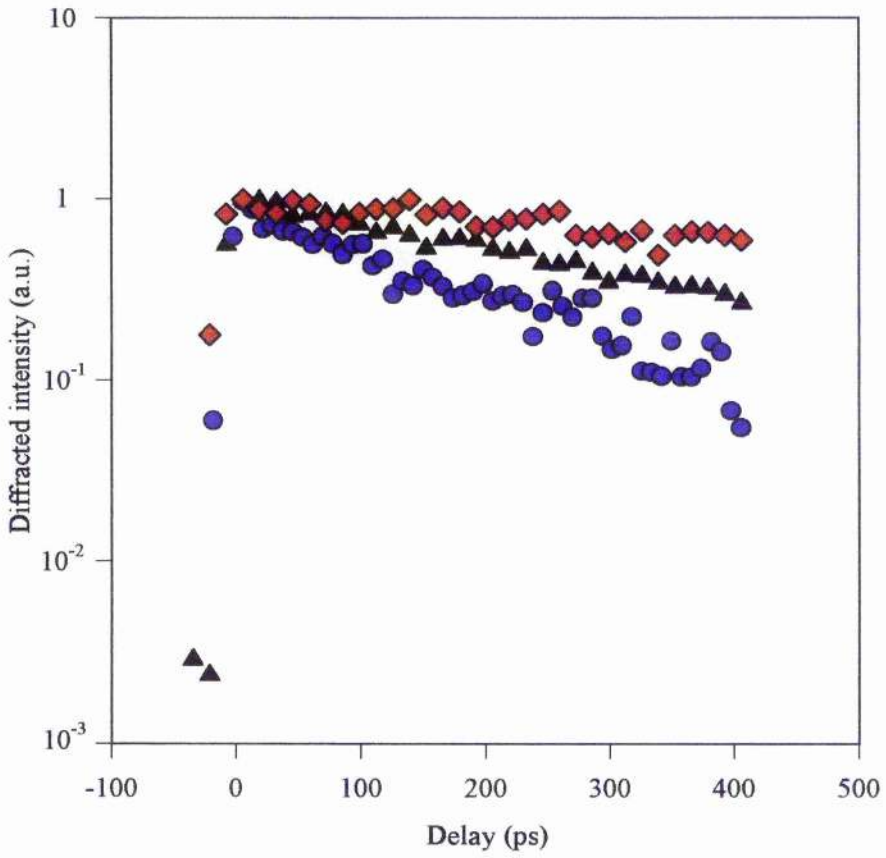

Figure 9.11 *Diffraction efficiency decay for three different grating periods. ◆ (10 μm grating period), ▲ (7 μm grating period), ● (5 μm grating period) in sample KLB.*

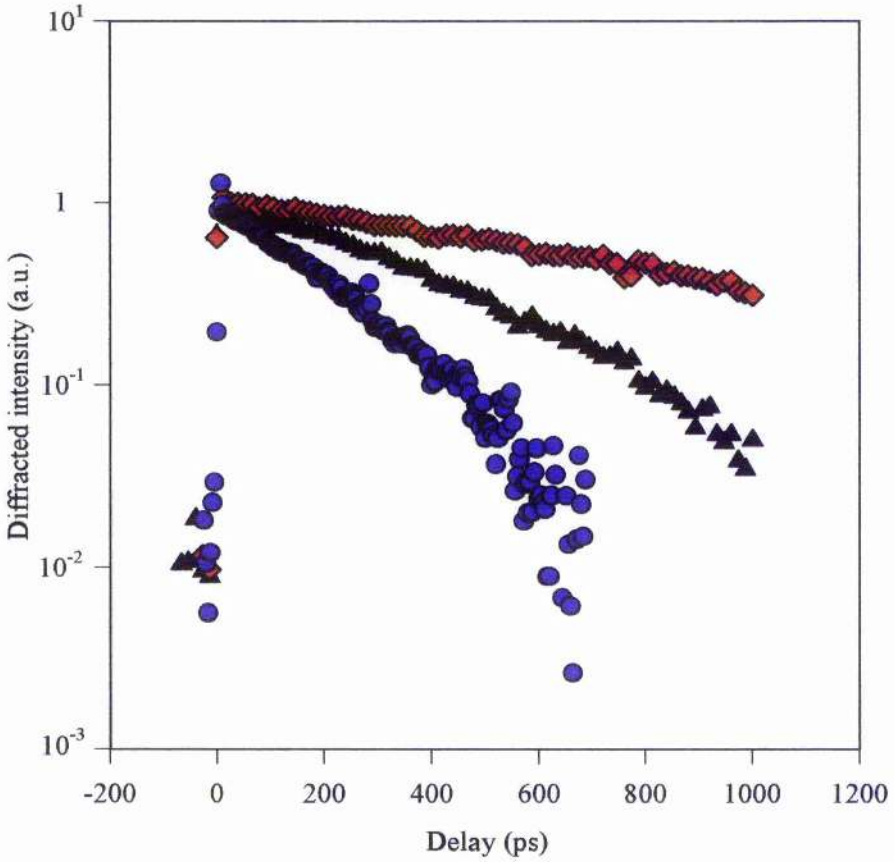

Figure 9.12 *Diffraction efficiency decay for three different grating periods.* ◆ *(10 μm grating period),* ▲ *(6 μm grating period),* ● *(4.5 μm grating period) in sample S51.*

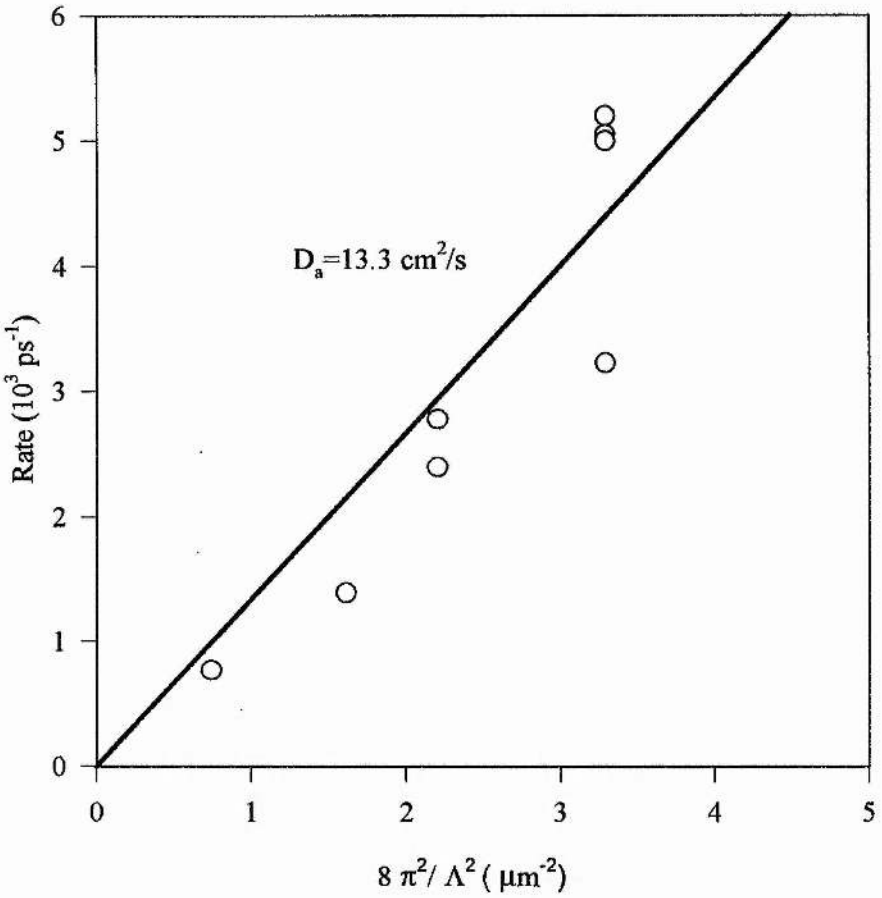

Figure 9.13 *Measured decay rates of the diffracted signal against $8\pi^2/\Lambda^2$ for sample KLB. Gradient gives an ambipolar diffusion coefficient of 13.3 cm^2/s.*

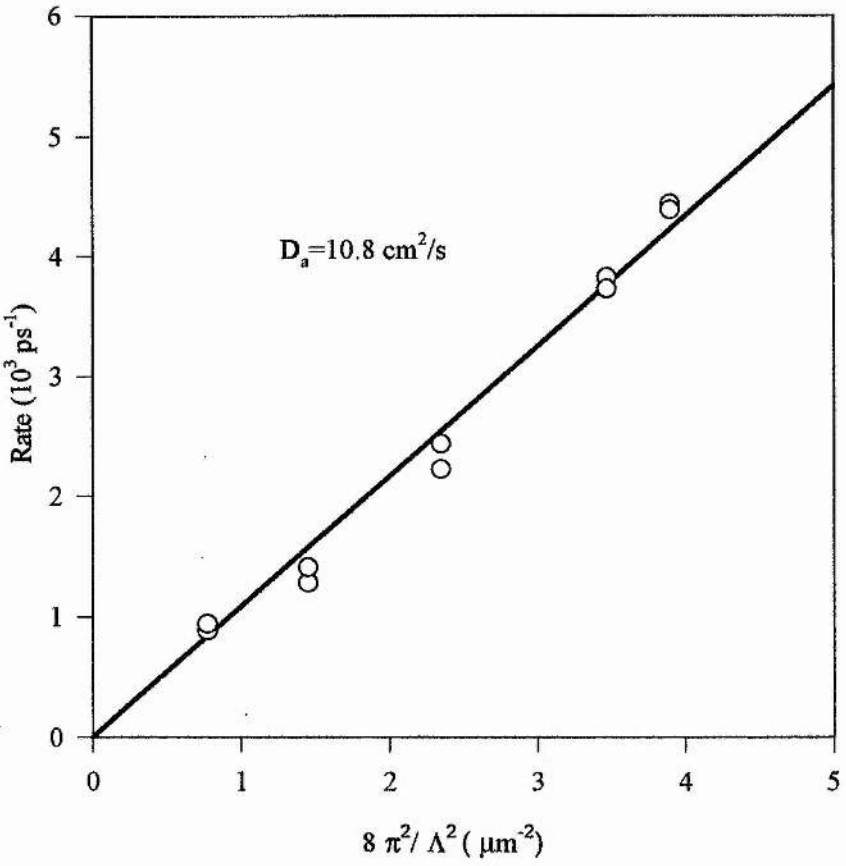

Figure 9.14 *Measured decay rates of the diffracted signal against $8\pi^2/\Lambda^2$ for sample S51. Gradient gives an ambipolar diffusion coefficient of 10.8 cm^2/s.*

9.7 Analysis

The ambipolar diffusion coefficient obtained for sample KLB from Figure 9.13 is found to be 13.3 cm^2/sec. The value calculated for sample S51 using Figure 9.14 is 10.8 cm^2/sec. This is surprising since in many respects sample S51 is of superior quality compared to KLB and so is expected to have a larger ambipolar diffusion coefficient.

As described in Chapter 7, S51 is known to exhibit pronounced saturation due to broadening. Figure 9.8 shows that the measured diffracted intensity (which is proportional to the diffraction efficiency) does not obey the quadratic behaviour that KLB has previously been shown to have [9.15]. This indicates that in order to accurately interpret the diffusion curves and obtain the correct ambipolar diffusion coefficient for S51 the saturation must be taken into account.

9.7.1 The effect of saturation on the measurement of grating decay times

A simple description of the creation of a grating and the subsequent diffraction of a probe beam is sufficient to highlight the problem that is experienced with sample S51.

The excitation of a concentration grating within a semiconductor occurs due to an intensity modulation on the sample surface which in turn produces a modulation of optically excited carriers ΔN_0. In the low density regime this modulation will decay with a characteristic time constant t_g , i.e.

$$\Delta N = \Delta N_0 e^{-\frac{t}{t_g}} \qquad 9.15$$

This modulation of the carrier concentration induces a corresponding modulation of the complex refractive index (absorption and refraction). For sample KLB it has been shown that the diffraction efficiency (which is proportional to the square of the

change in the complex refractive index) varies with the square of the carrier density. For sample S51 the measured change in transmission of the diffracted beam with power is seen to have a linear variation for low power levels (see Figure 9.8). This variation is attributed to broadening of the exciton resonance which was highlighted in the power dependence experiments described in Chapter 7. Since the measured change in the transmission for the diffracted beam is proportional to the square of the change in the complex refractive index this implies that the diffraction efficiency for sample S51 is not proportional to the square of the carrier density but to the carrier density alone. This has important implication in the measurement of the ambipolar diffusion coefficient.

In previous studies the change in the complex refractive index has been seen to vary quadratically with the carrier density. This is what leads to the measurement of a decay for the diffracted signal which is actually twice the grating decay rate. In S51 since the diffraction efficiency shows a linear dependence on the carrier density, the diffraction efficiency that we measure is directly proportional to the decay of the grating and so Eqn 9.10 is replaced with the following

$$\eta(t) \propto \exp(-\Gamma t) \qquad 9.16$$

where Γ is the same rate defined in Eqn 9.14. This means that the calculated diffusion coefficient for S51 of 10.8 cm^2/sec is incorrect by a factor of two. Therefore the correct ambipolar diffusion coefficient for S51 is 21.6 cm^2/sec.

The increased value of the diffusion coefficient for S51 when compared to KLB agrees well with S51 being of higher quality. Hole mobility's for KLB and S51 can be deduced from the ambipolar diffusion coefficients and are found to be 257 and 458 cm^2/Vs respectively. A discussion of the magnitude of the deduced mobilities is left to a future chapter.

9.8 References

9.1 A. Miller, D.A.B. Miller and S.D. Smith, "Dynamic non-linear optical processes in semiconductors", Advances in Physics, **30**, 6, 697-800, (1981).

9.2 J. Hegarty, M.D. Sturge, A.C. Gossard and W. Wiegman, "Resonant degenerate four-wave mixing in GaAs multiquantum well structures", Appl. Phys. Letts., **40**, 2, 132-134, (1982).

9.3 D.A.B. Miller, D.S. Chemla, D.J. Eilenberger, P.W. Smith, A.C. Gossard and W. Wiegmann, "Degenerate four-wave mixing in room-temperature GaAs/GaAlAs multiple quantum well structures", Appl. Phys. Letts., **42**, 11, 925-927, (1983).

9.4 D.S. Chemla, "Coherent ultrafast nonlinear optical processes in semiconductor quantum wells", Solid. State. Comms., **92**, 1, 37-43, (1994).

9.5 L. Schultheis, M.D. Sturge and J. Hegarty, "Photon echoes from two-dimensional excitons in GaAs-AlGaAs quantum wells", Appl. Phys. Letts., **47**, 9, 995-997, (1985).

9.6 L. Schultheis, J. Kuhl, A. Honold and C.W. Tu, "Picosecond phase coherence and orientational relaxation of excitons in GaAs", Phys. Rev. Letts., **57**, 14, 1797-1800, (1986).

9.7 L. Schultheis, A. Honold, J. Kuhl, K. Kohler and C.W. Tu, "Optical dephasing of homogeneously broadened two-dimensional exciton transitions in GaAs quantum wells", Phys. Rev. B, **34**, 12, 9027-9030, (1986).

9.8 A. Miller, R.J. Manning, P.K. Milsom, D.C. Hutchings, D.W. Crust and K. Woodbridge, "Transient grating studies of excitonic optical nonlinearities in GaAs/AlGaAs multiple-quantum-well structures", J. Opt. Soc. Am. B, **6**, 4, 567-578, (1989).

9.9 F. Capasso, K. Mohammed and A.Y. Cho, "Resonant tunnelling through double barriers, perpendicular quantum transport phenomena in superlattices, and their device applications", IEEE J. Quant. Electron., QE-**22**, 9, 1853-1869, (1986).

9.10 D.P. Norwood, A.L. Smirl and H.E. Swoboda, "Short-period transient grating measurements of perpendicular over-barrier diffusion in GaAs/AlGaAs multiple quantum wells", J. Appl. Phys., **77**, 3, 1113-1119, (1995).

9.11 R.J. Manning, A. Miller, D.W. Crust and K. Woodbridge, "Orientational dependence of degenerate four-wave mixing in multiple-quantum-well structures", Opt. Letts., **13**, 10, 868-870, (1988).

9.12 C.A. Hoffman, K. Jarasiunas, H.J. Gerritsen and A.V. Nurmikko, "Measurement of surface recombination velocity in semiconductors by diffraction from picosecond transient free-carrier gratings", Appl. Phys. Letts., **33**, 6, 536-538, (1978).

9.13 S.C. Moss, J.R. Lindle, H.J. Mackey and A.L. Smirl, "Measurement of the diffusion coefficient and recombination effects in germanium by diffraction from optically-induced picosecond transient gratings", Appl. Phys. Letts., **39**, 3, 227-229, (1981).

9.14 H.J. Eichler, and F. Massmann, "Diffraction efficiency and decay times of free-carrier gratings in silicon", J. Appl. Phys., **53**, 4, 3237-3242, (1982).

9.15 R.J. Manning, D.W. Crust, D.W. Craig, A. Miller and K. Woodbridge, "Transient-grating studies in GaAs/GaAlAs multiple quantum wells", J. Mod. Optics., **35**, 3, 541-551, (1988).

10

Polarisation grating studies

10.1 Summary

This section describes a new optical method for direct measurement of the electron mobility in multiple quantum well semiconductors at room temperature. The technique utilises optically induced electron spin gratings, and was applied to samples S51 and KLB to measure their in-plane electron mobility. This is the first time that electron diffusion has been determined by an optical technique

10.2 Introduction

In the previous chapter transient gratings were used to measure the ambipolar diffusion coefficients for the sample S51 and KLB. The experiment used the intensity modulation produced when two pulses of the same linear polarisation interfere to produce a concentration grating of electrons and holes within the multiple quantum well samples. The subsequent decay of the grating is then dominated by the motion of the slower carrier, in this case the hole, and the diffusion coefficient obtained describes ambipolar motion parallel to the quantum well layers. In this chapter a new type of transient grating is described which relies on the production of a polarisation modulation across the quantum well surface which in turn produces a spin grating parallel to the quantum well layers.

10.3 Polarisation gratings

When two pulses of opposite polarisation interfere a polarisation grating is produced. In this case no intensity modulation exists which precludes the formation of an amplitude grating. What does occur is a periodic modulation of the electric field polarisation. For equal excite intensities, the polarisation changes from linear to circular to orthogonal linear to circular of the opposite sense and back to linear, as shown in Figure 10.1.

Figure 10.1 *The polarisation modulation produced when two orthogonally polarised light beams interfere.*

The period of the modulation is defined by the angle between the two excite beams used and is identical to that produced for an amplitude grating (see Eqn. 9.6).

The crossed-linear configuration described above has previously been used to create orientational gratings in semiconductors via the modulation of the linear polarisation through anisotropic state filling [10.1-10.3] (state filling gives preferential excitation of the electrons and holes into specific $\underline{k}$-directions) or alignment of exciton dipoles [10.4-10.5]. Figure 10.1 also shows that the interference of orthogonally polarised excite beams gives rise to a modulation in circular polarisation. It is possible to deconvolve the grating of Figure 10.1 into that of two circular polarisation gratings [10.6-10.7] as shown in Figure 10.2.

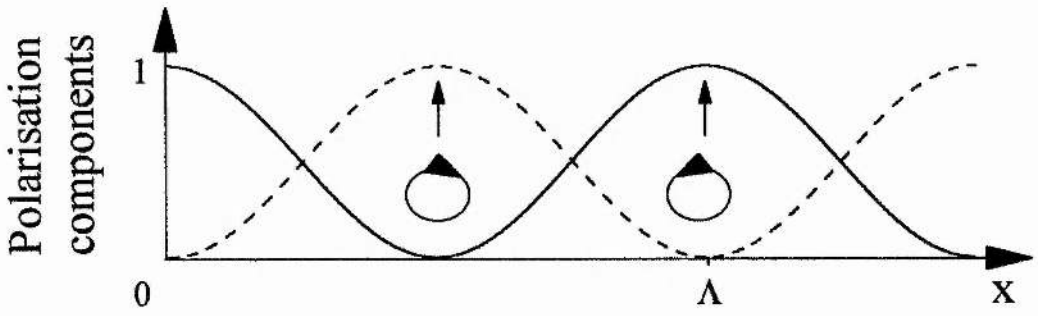

Figure 10.2 *Amplitudes for right and left circular components of the intensity as a function of distance in the plane of the grating.*

If the excite electric fields are described by the equations

$$\underline{E}_x = E_0 \underline{x}\, e^{i(\omega t - \underline{k}_1 r)} \qquad 10.1$$

and

$$\underline{E}_y = E_0 \underline{y}\, e^{i(\omega t - \underline{k}_2 r)} \qquad 10.2$$

then the resultant electric field on interference is given by

$$\underline{E} = E_0 \underline{x}\, e^{i(\omega t - \underline{k}_1 r)} + E_0 \underline{y}\, e^{i(\omega t - \underline{k}_2 r)} \qquad 10.3$$

The electric field modulation, E(x) along the grating direction, x, can be written in terms of two circular polarisation components and is given by

$$E(x) = E'_0 \left\{ \sin\left(\frac{\pi x}{\Lambda}\right) e^{-i\frac{\pi}{4}} \frac{\underline{x} + i\underline{y}}{\sqrt{2}} + \cos\left(\frac{\pi x}{\Lambda}\right) e^{i\frac{\pi}{4}} \frac{\underline{x} - i\underline{y}}{\sqrt{2}} \right\} + c.c. \qquad 10.4$$

where Λ is the grating spacing and $\underline{x}$ and $\underline{y}$ are unit vectors describing the polarisation directions of the incident beams. If a suitable nonlinearity exists, which is sensitive to circular polarisation, then a grating will be produced from the interference of two orthogonal linearly polarised beams.

In multiple quantum well semiconductors the confinement of the holes leads to the lifting of the degeneracy between the light and heavy holes (see Chapter 3). This allows access to polarisation sensitive selection rules (see figure 3.4). Excitation with circularly polarised light resonant with the heavy hole transition will generate electron-hole pairs with well defined spin. As has been previously stated, at room temperature the excitons are rapidly ionised by LO-phonons leaving free electrons and holes. As was seen in Chapter 8 the electrons retain their spin orientation for tens of picoseconds. The holes spin orientation, on the other hand may be expected to relax on sub-picosecond timescales at room temperature due to band mixing and the mixed spin character of the valence states. Thus excitation with orthogonal linearly polarised excite beams resonant with the heavy-hole exciton will produce a spatial modulation of the electron spins (Figure 10.3).

The spin dependent nature of the phase space filling contribution to exciton saturation has been discussed previously (see Chapter 7) and therefore a spatial modulation of the electron spins will produce a polarisation grating which will diffract a circularly polarised probe beam. Since we can consider a linear probe beam as consisting of equal components of left and right hand circular polarisation, diffraction will still occur with each of the circular components being diffracted by the corresponding circular grating.

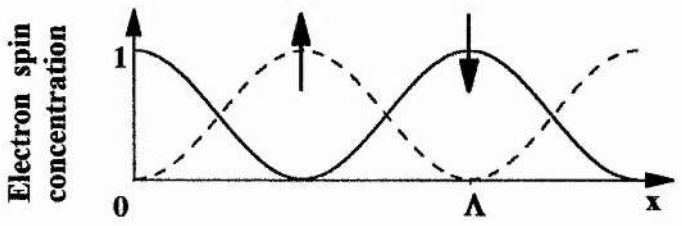

Figure 10.3 *The electron spin concentration as a function of distance in the plane of the grating.*

10.4 Grating decay

The decay of a spin-orientational grating is very similar in nature to that of the previously discussed concentration grating. The decay of the spin grating is essentially due to the electrons alone (the hole spins having relaxed on a sub-picosecond timescales) in contrast to the concentration grating case where the decay is dependent on the electron and holes. The decay time is determined by a combination of the spin relaxation rate and the diffusion of the electrons within the quantum well layers. The decay rate can be written,

$$\Gamma = \frac{4\pi^2 D_e}{\Lambda^2} + \frac{1}{\tau_s} \qquad 10.5$$

where D_e is the electron diffusion coefficient and τ_s is the electron spin relaxation time. The phase space filling nonlinearity that is used in the production of the spin grating has been shown to have a linear dependence on the carrier density and so the diffraction efficiency is expected vary quadratically with power. Since this applies equally well to sample S51 as to sample KLB it is correct to use Eqn 10.5. It must be emphasised that the previous discussion concerning concentration gratings in S51 is only applicable to gratings where effects of Coulomb screening and broadening are combined with those of phase space filling. In the case of spin gratings the only mechanism present is that due to phase space filling and so the effects of saturation in the other terms can be ignored.

10.5 Experimental set-up

Transient spin-orientational grating were produced and their subsequent decay was monitored using the set-up shown in Figure 10.4.

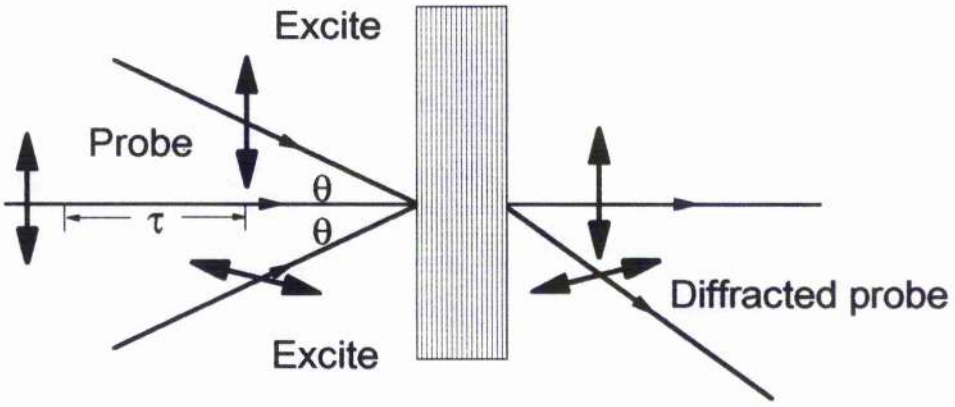

Figure 10.4 *Schematic of the experimental set-up for spin grating studies in multiple quantum wells showing the relative polarisations of the probe and excite beams as well as the diffracted probe polarisation.*

A λ/2 plate is used to rotate the polarisation of one of the pump beams relative to the other and hence allow the production of two orthogonal linearly polarised pump beams. The decay of the spin grating is monitored by a temporally delayed linearly polarised probe pulse which is coincident spatially with the interfering pump pulses. The detection method and the technique used to vary the grating period are the same as those used previously for the concentration grating studies as described in Chapter 5.

10.6 Results

Spin grating studies were carried out for samples KLB and S51. The results obtained allow the determination of the in-plane electron diffusion coefficient and hence the electron mobility.

10.6.1 Rotation of the probe polarisation

The spin grating experiments employed a linearly polarised probe beam. The use of both left and right circular polarisations (combined within a linear probe beam) increases the strength of the diffracted signal due to the addition of the diffraction signal from each of the circular gratings. An interesting consequence of this was that the polarisation of the probe beam was observed to be rotated by $\pi/2$ after diffraction from the spin grating (see Figure 10.5). This can be explained as follows.

If we consider a linear probe beam polarised in the x direction given by

$$\underline{E} = E_0 \underline{x} \qquad 10.6$$

then this can be resolved into left and right hand circular components as shown below

$$\underline{E} = \frac{E_0}{2}\left(\underline{x} + i\underline{y}\right) + \frac{E_0}{2}\left(\underline{x} - i\underline{y}\right) \qquad 10.7$$

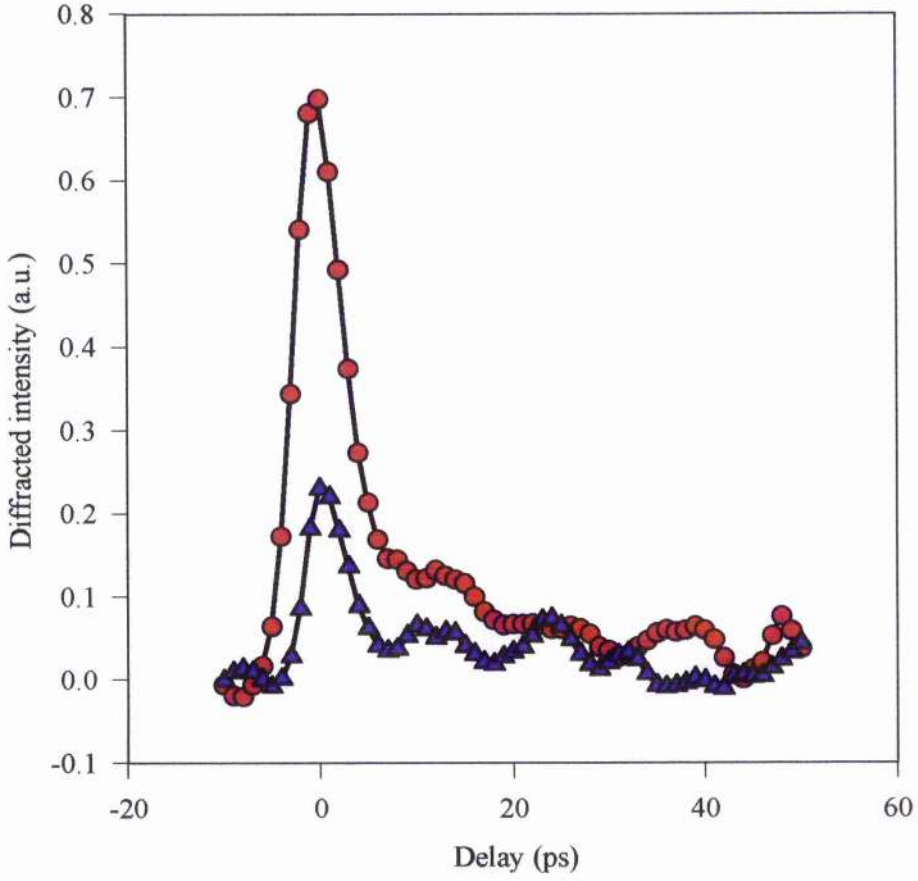

Figure 10.5 *Decay of the diffracted efficiency from a spin grating for sample S51 monitored with an analyser aligned perpendicular to the initial probe polarisation (●) and parallel to the initial probe polarisation (▲).*

The left and right hand circular polarisation components of the grating can be seen from Figure 10.2 to be π phase shifted relative to each other. So the diffracted linear probe light will have one of its constituent circular components phase shifted by π. The electric field of the diffracted probe beam can therefore be written as

$$\underline{E}_{diff} = \frac{E_0}{2}\left(\underline{x} + i\underline{y}\right) + \frac{E_0}{2}e^{i\pi}\left(\underline{x} - i\underline{y}\right) \qquad 10.8$$

which simplifies to

$$\underline{E}_{diff} = iE_0\underline{y} \qquad 10.9$$

We can see that the diffracted probe beam is rotated by $\pi/2$ and now has the polarisation vector of its electric field along the y-direction.

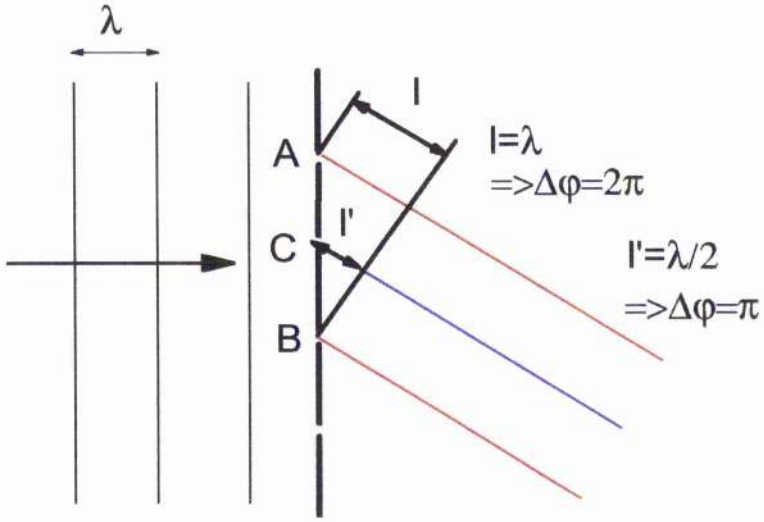

Figure 10.6 *Graphical representation of the π phase change between the diffraction from two $\lambda/2$ shifted gratings.*

This phenomenon can also be explained visually using plane waves by considering diffraction from two gratings, shifted by half a grating period relative to each other (Figure 10.6). Slits A and B are separated by one grating period, Λ, and so have a phase difference of 2π. Point C lies equidistant between points A and B and so in the diffraction direction has a phase difference of π compare to the diffracted waves emerging from either A or B. In the case of two same linearly polarised beams no diffraction would occur in the direction shown as the beams would interfere destructively with each other. In the case of circularly polarised beams diffracting from two circular polarisation gratings all that occurs is a phase shift of π in one of the circular components.

10.6.2 Time dependent results

As in the case for amplitude grating the transmission of the diffracted probe beam was monitored as a function of the probe delay. The measured decay times were all much shorter than the electron spin relaxation time for the two samples. Care was taken to check that the grating decay signals showed no dependence on carrier concentration at the power levels of interest. Figure 10.7 and Figure 10.8 show typical grating decay signals for samples S51 and KLB. Figure 10.9 shows the grating decay signals for sample KLB at a number of different grating periods. Figure 10.10 shows a similar curve for sample S51.

The diffracted signal decay rates are plotted against $8\pi^2/\Lambda^2$, where Λ is again the grating period, in Figure 10.11 for sample KLB and in Figure 10.12 for sample S51. The gradient of the best fit lines gives the in-plane electron diffusion coefficient for the two samples. The y-axis intercept on the graphs is the infinite grating period case which for spin gratings refers to the electron spin relaxation time.

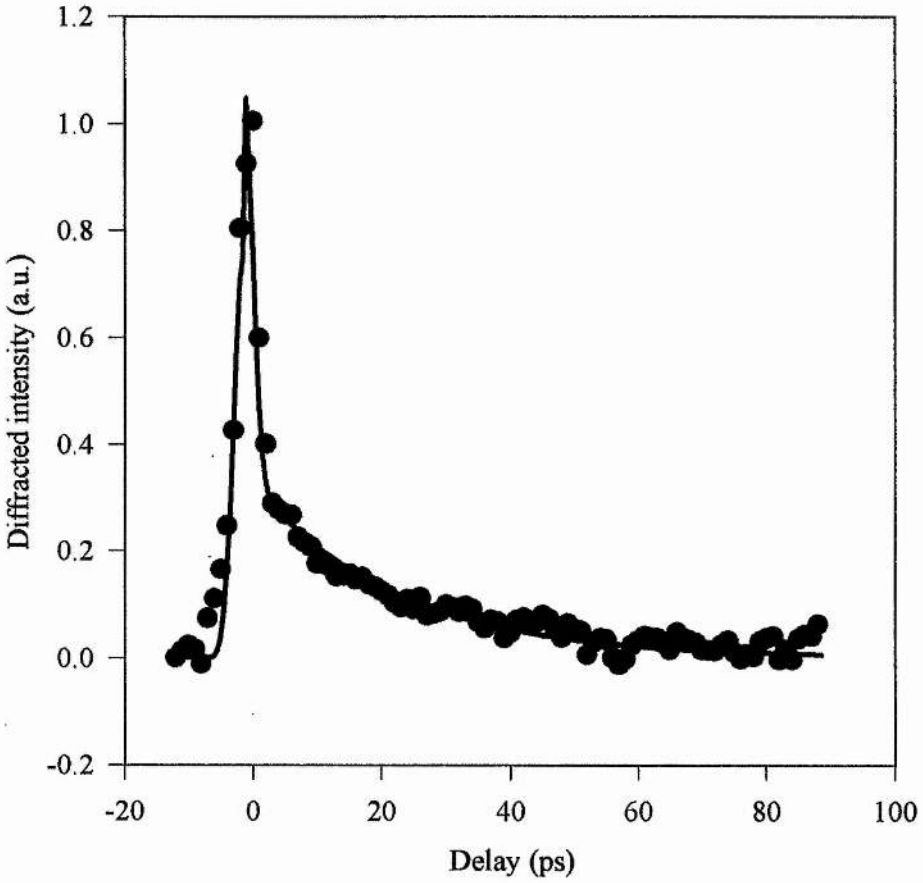

Figure 10.7 *Decay of the diffracted intensity for a 7 μm spin grating period in sample KLB. The fitted decay curve has a time constant of 22 ps.*

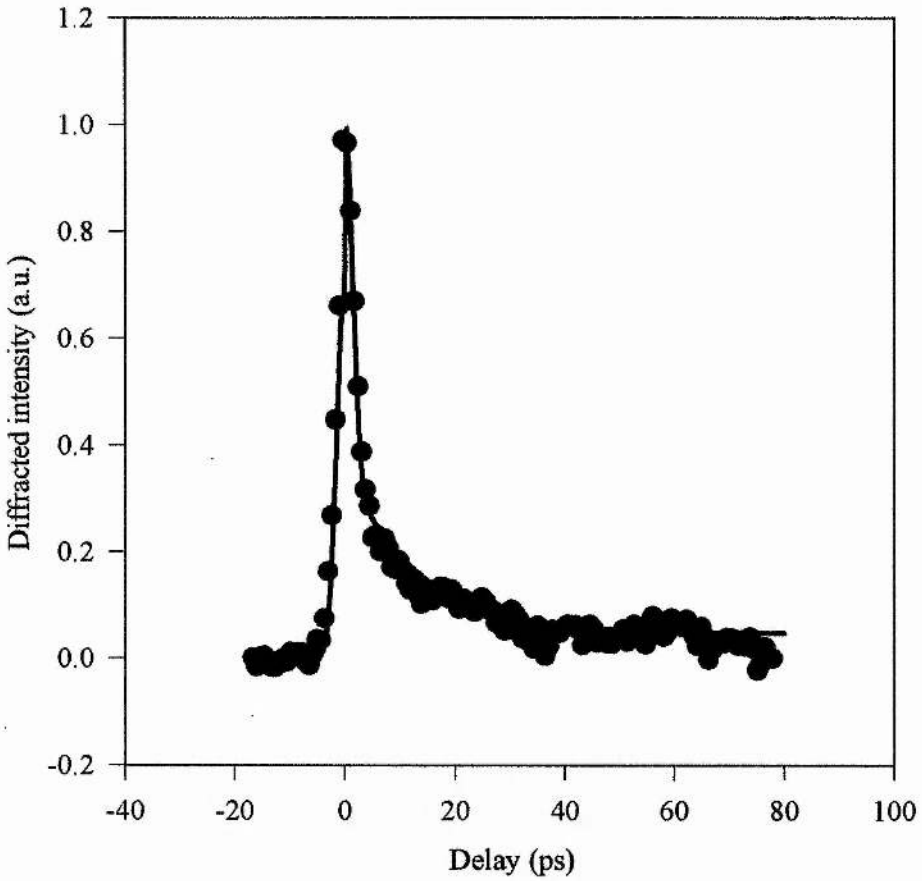

Figure 10.8 *Decay of the diffracted intensity for a 7 μm spin grating period in sample S51. The fitted decay curve has a time constant of 13 ps.*

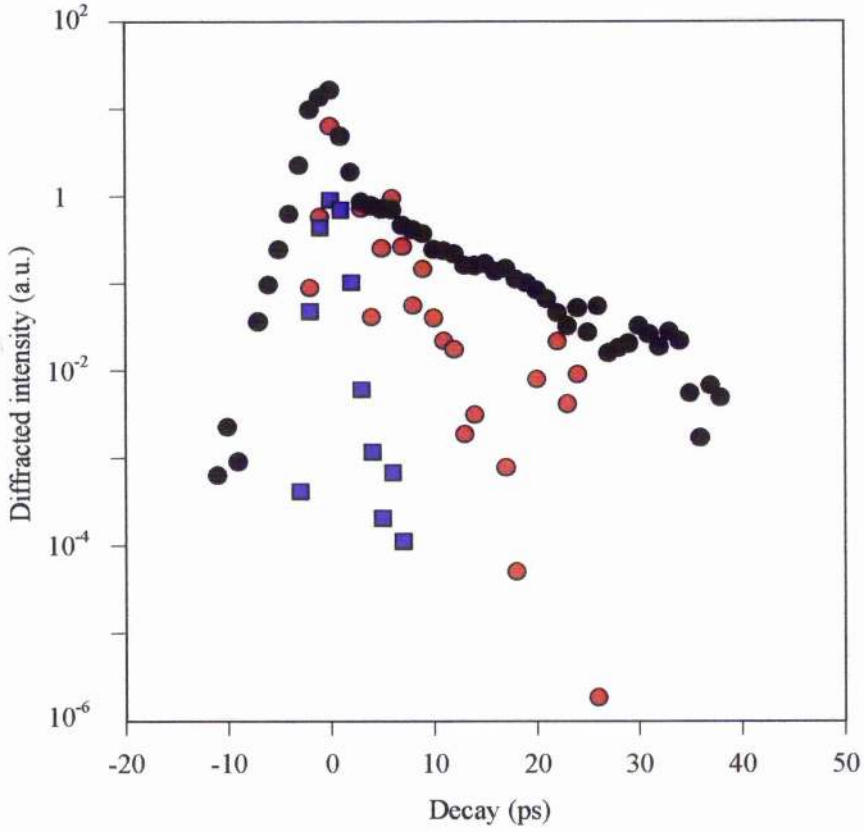

Figure 10.9 *Decay of the diffraction efficiency for three different spin grating periods in sample KLB. (● 7 μm grating period, ● 6 μm grating period and a ■ 5 μm grating period).*

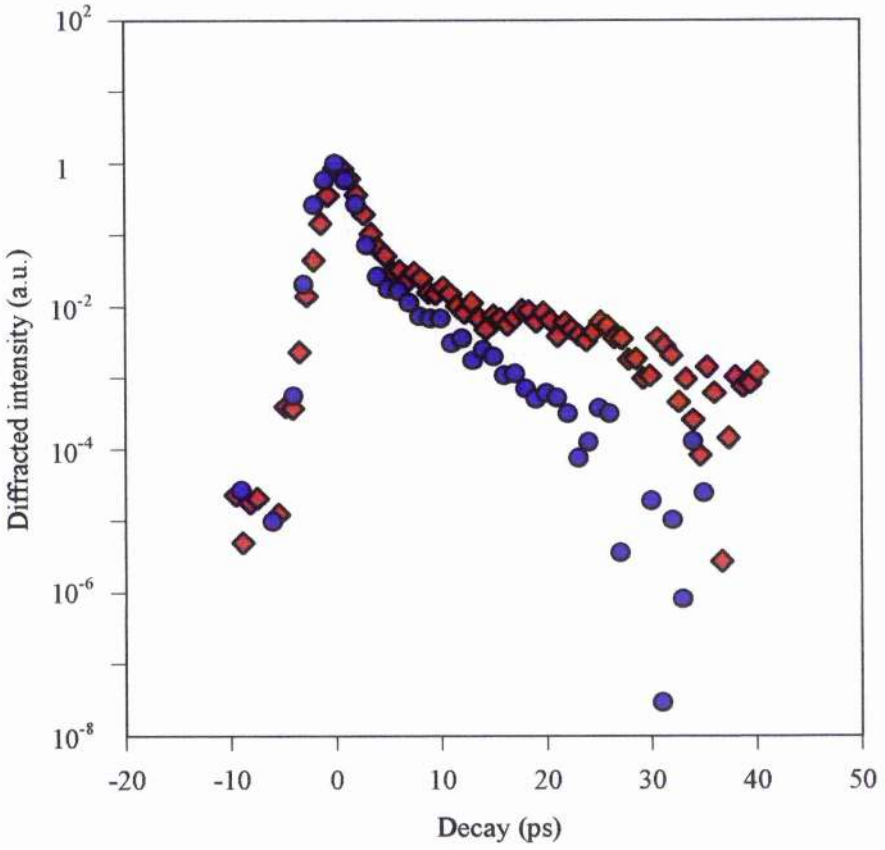

Figure 10.10 *Decay of the diffraction efficiency for three different spin grating periods in sample KLB. (◆ 7 μm grating period and a ● 6 μm grating period).*

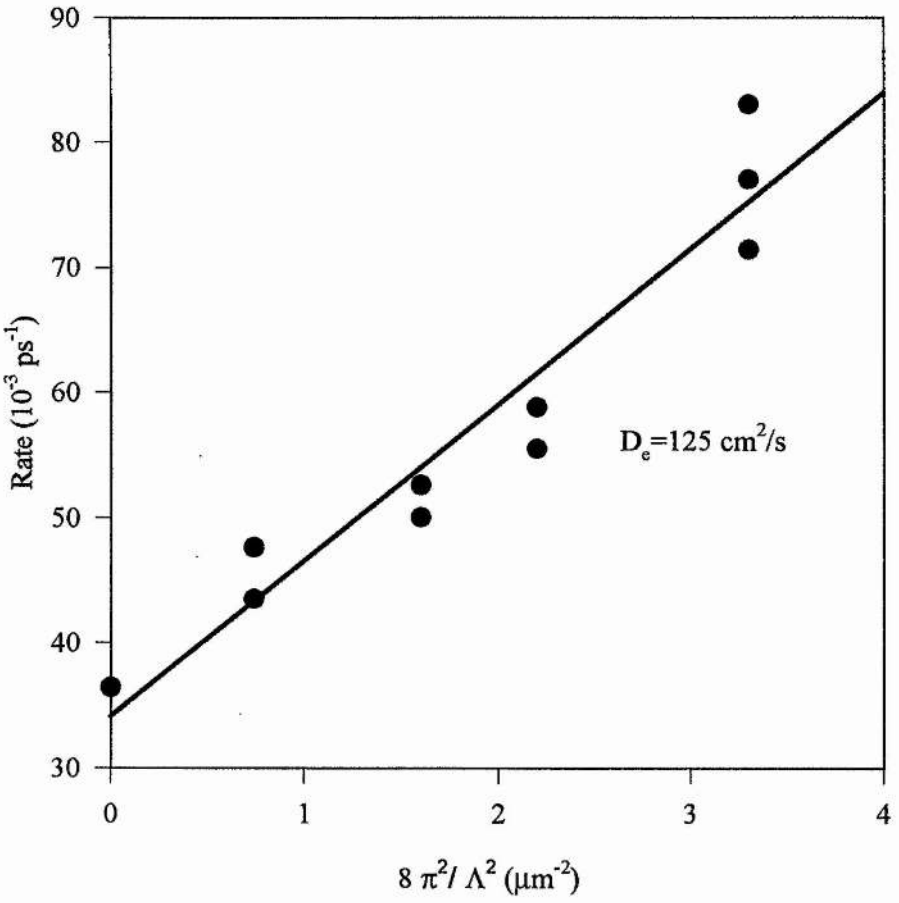

Figure 10.11 *Measured decay rates of the diffracted signal against $8\pi^2/\Lambda^2$ for sample KLB. The gradient gives an electron diffusion coefficient of 125 cm^2/s.*

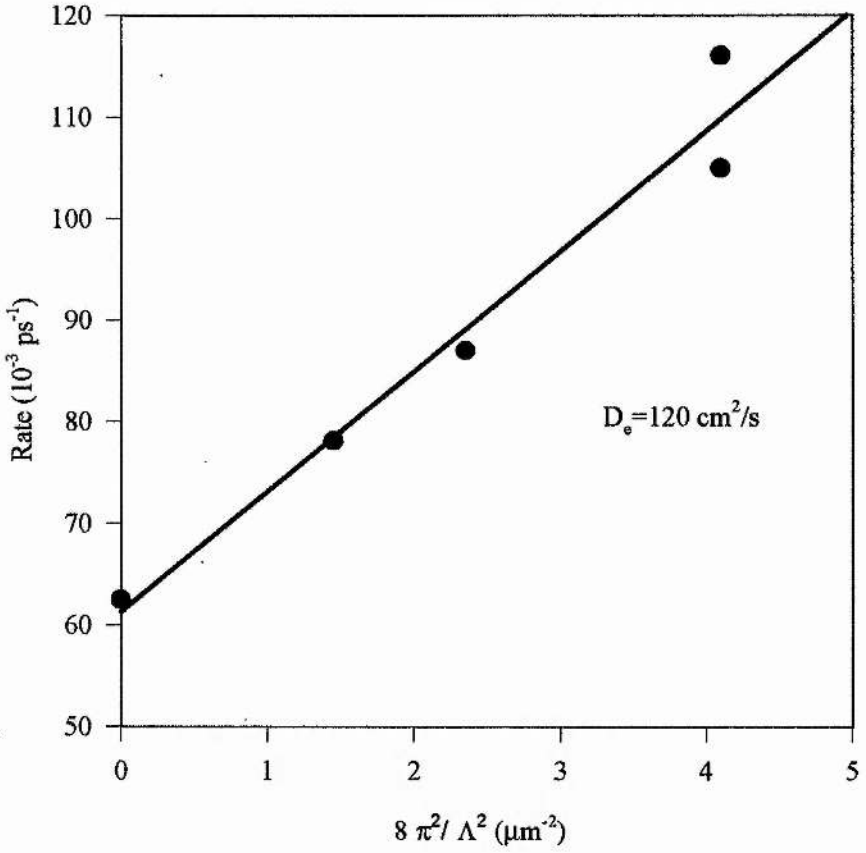

Figure 10.12 *Measured decay rates of the diffracted signal against $8\pi^2/\Lambda^2$ for sample S51. The gradient gives an electron diffusion coefficient of 120 cm^2/s.*

10.7 Discussion and conclusion

The in-plane electron diffusion coefficients, D_e, deduced from the results are D_e= 125 cm^2/sec for KLB and 120 cm^2/sec for S51. These give electron mobilities of μ_e= 4800 cm^2/ V sec for KLB and μ_e= 4600 cm^2/V sec for S51. These results are clearly much higher than those obtained in the previous chapter and confirm that the "wash-out" of the grating is purely due to electrons and not electrons and holes as is the case in concentration gratings.

Transient spin gratings have allowed the first direct optical measurement of the in-plane electron mobility in a multiple quantum well semiconductor at room temperature. This technique requires no "special" sample preparation as is the case in time of flight measurements [10.8,10.9] where contacts or special masks must be prepared.

The results from the previous chapter and those described here, are considered together in the following chapter to allow comparison with the results previously obtained for bulk and quantum well GaAs samples by other methods. The results are then examined with special reference to the effect of the variation of the in-plane mass of the heavy hole in quantum wells. The scattering mechanisms that limit the electron and hole motion in bulk and quantum wells are then described with special reference to the results obtained.

10.8 References

10.1 A.L. Smirl, T.F. Boggess, B.S. Wherrett, G.P. Perryman and A. Miller, "Picosecond optically induced anisotropic state filling in semiconductors", Phys. Rev. Letts., **49**, 13, 933-936, (1982).

10.2 T.F. Boggess, A.L. Smirl and B.S. Wherrett, "Picosecond transient grating measurement of orientational effects in semiconductors", Opts. Commun., **43**, 2, 128-133, (1982).

10.3 A.L. Smirl, T.F. Boggess, B.S. Wherrett, G.P. Perryman and A. Miller, "Picosecond transient orientational and concentration gratings in germanium", IEEE J. Quant. Electron., **19**, 4, 690-700, (1983).

10.4 D.S. Kim; J. Shah, T.C. Damen, L.N. Pfeiffer and W. Schafer, "Femtosecond time-resolved four-wave mixing from biexcitons in GaAs quantum wells: dominance of the interaction-induced signal", Phys. Rev. B., **50**, 8, 5775-5778, (1994).

10.5 L. Schultheis, J. Kuhl, A. Honold and C.W. Tu, "Picosecond phase coherence and orientational relaxation of excitons in GaAs", Phys. Rev. Letts., **57**, 14, 1797-1800, (1986).

10.6 J.T. Fourkas, R. Trebino and M.D. Fayer, "The grating decomposition method: A new approach for understanding polarization-selective transient grating experiments. I. Theory", J. Chem. Phys., **97**, 1, 69-77, (1992).

10.7 J.T. Fourkas, R. Trebino and M.D. Fayer, "The grating decomposition method: A new approach for understanding polarization-selective transient grating experiments. II. Applications", J. Chem. Phys., **97**, 1, 78-85, (1992).

10.8 R.K. Ahrenkiel, D.J. Dunlavy, D. Greenberg and J. Schlupmann, "Electron mobility in p-GaAs by time of flight", Appl. Phys. Letts., **51**, 10, 776-778, (1987).

10.9 S. Gupta, L. Davis and P.K. Bhattacharya, "Optical-time-of-flight measurement of carrier transport in GaAs/Al(x)Ga(1-x)As and In(0.53)Ga(0.47)As/In(0.52)Al(0.48)As multiquantum wells", Appl. Phys. Letts., **60**, 12, 1456-1458, (1992).

11

Interpretation of the mobility results

11.1 Summary

The transport of carriers within bulk and multiple quantum well semiconductors have important implication in a number of device applications. The mobility results for samples S51 and KLB are compared and contrasted. The various scattering mechanisms that limit the mobility of carriers within the multiple quantum wells are discussed.

11.2 Introduction

The measured ambipolar (D_a) and electron (D_e) diffusion coefficients for sample S51 and KLB are given in Table 11.1. The hole diffusion coefficients (D_h) are calculated using the ambipolar diffusion equation for equal excess electron and hole populations (see Chapter 4,Eqn 4.16).

The measured electron and hole diffusion coefficients can be represented in terms of drift mobility's through the Einstein relation (see Chapter 4, Eqn 4.14) where kT/e=25.9 mV at room temperature.

The scattering mechanisms discussed in Chapter 4 affect the samples in different ways due to their well width and their ionised impurity levels. These factors are now discussed.

Table 11.1 *The diffusion coefficients and deduced drift mobility's for sample S51 and KLB obtained from the grating experiments.*

	D_a (cm^2/s)	D_e (cm^2/s)	D_h (cm^2/s)	μ_e (cm^2/Vs)	μ_h (cm^2/Vs)
KLB	13.3	125	7	4800	270
S51	21.6	120	11.9	4600	450

11.3 Analysis of mobility results

The results obtained for the electron and hole mobilities in samples S51 and KLB show some differences. These can be explained by considering the relative importance of each scattering mechanisms when applied to each sample.

Sample S51 is a high quality sample, with few ($<10^{14}$ cm^{-3}) ionised impurities. The quantum well width is 4.4nm compared to KLB's 6.5nm. The linear absorption spectrum (see Chapter 6, Figure 6.4) clearly shows the quality of the sample, with the exciton peak well resolved even at room temperature. An interesting feature is the presence of a tail in the linear absorption just below the band edge. In Chapter 4 it was stated that the presence of interface roughness and barrier-alloy scattering would result in the appearance of these tail states. This provides an indication on the importance of these scattering mechanisms for S51.

Sample KLB contain quantum wells of 6.5nm width. The linear absorption again shows the exciton features clearly resolved at room temperature. Unlike S51 there does not appear to be any absorption tail below the band edge. This is as expected because the wider wells of KLB should be less sensitive to the scattering mechanisms associated with the interface. An additional consideration which exists for KLB and not S51 is the relatively large p-type background doping ($\sim 10^{16}$ cm^{-3}).

The reported electron and hole drift mobilities for bulk GaAs at room temperature are given in Table 11.2, the electron, heavy hole and light hole effective masses are also displayed.

Table 11.2 *The electron and hole drift mobility's and effective masses in bulk GaAs at room temperature (after [11.1]).*

Bulk (T=300K)	μ_e *(cm²/Vs)*	μ_h *(cm²/Vs)*	m_e	m_{hh}	m_{lh}
GaAs	8000	320	0.063 m_0	0.500 m_0	0.076 m_0

The results obtained are in good agreement with previous studies which have used the transient grating technique to determine the in-plane ambipolar diffusion coefficient in GaAs multiple quantum wells. Miller et al [11.2] reported ambipolar diffusion coefficients of 13.8 cm^2 /s and 16.2 cm^2 /s for two different GaAs multiple quantum well samples each having a well width of 6.0 nm. Using the data from Table 11.2 the ambipolar diffusion coefficient for bulk GaAs is 16.0 cm^2 /s which is also in good agreement with the results obtained.

The electron drift mobility for bulk GaAs at room temperature from Table 11.2, is 8000 cm^2/Vs. The results obtained for the samples used were 4800 cm^2/Vs for KLB and 4600 cm^2/Vs for S51. The measured electron mobility is clearly reduced in comparison with bulk. For KLB the high background doping is expected to the important limiting factor for the electron mobility. The reduction of the bulk electron mobility in the presence of an ionised impurity concentration of $\sim 10^{-16}$ cm^{-3} is given by Sze [11.3] to be

$$\mu_e \text{ (bulk)} \approx 6000 \text{ cm}^2/\text{Vs}.$$

A further reduction in the predicted value of the electron mobility is expected in quantum well sample due to the increased efficiency of the ionised impurity scattering and the effects of interface roughness and barrier-alloy scattering.

For sample S51 the effects due to ionised impurity scattering are expected to be reduced because of the lower background doping. The reduced well width on the other hand will increase the scattering mechanisms resulting from the interface.

The hole mobility results obtained for both samples show a closer agreement with those measured for bulk GaAs. The mobility of 270 cm^2/Vs obtained for KLB is slightly below the bulk value. This can be attributed to the ionised impurity scattering of holes which is expected to follow that of electrons. Sze [11.3] reports

$$\mu_h \text{ (bulk)} \approx 300 \text{ cm}^2/\text{Vs}$$

for the hole mobility in the presence of $\sim 10^{-16}$ cm^{-3} ionised impurities in bulk GaAs at room temperature. The effects on the hole mobility due to interface roughness and barrier-alloy scattering within the quantum wells are not expected to play such a dominant role when compared to those on the electrons.

The hole mobility for S51 was found to be slightly larger than the bulk case. Since the ionised impurity scattering is expected to be reduced compared to that of KLB and the fact that the scattering of holes by the interface has been stated to be less important than for electrons it is not possible to explain the increased mobility.

In multiple quantum wells it is known that the in-plane hole mass is dependent on the quantum well width (see Chapter 3), in order to properly explain the increased hole mobility results for S51 the concept of in-plane mass must be more closely examined.

11.3.1 The in-plane effective mass

The transport properties discussed above clearly refer to the in-plane motion of the electrons and holes within the quantum wells. It is therefore only prudent to consider the in-plane band structure and effective masses when trying to interpret the mobility.

Table 11.3 gives the effective masses for the electrons and holes within an ideal 2D quantum well.

Table 11.3 *The effective masses in an ideal 2D GaAs semiconductor for the electron, the transverse heavy and light holes and the in-plane heavy and light holes. Calculated values if the in-plane heavy hole mass for different well widths (L_z) in a quantum well surrounded by $Al_{0.33}Ga_{0.66}As$ barriers are also given [11.4].*

	m_e	$m_{hh\perp}$	$m_{lh\perp}$	$m_{hh//}$	$m_{lh//}$
Ideal QW	$0.063m_0$	$0.377\ m_0$	$0.09\ m_0$	$0.11\ m_0$	$0.21\ m_0$
L_z=4.5nm				$0.11\ m_0$	
L_z=6.5nm				$0.16\ m_0$	
L_z=10nm				$0.18\ m_0$	

The confinement of the electron within a quantum well does not strongly affect its' in-plane mass and so this discussion is only relevant to the holes.

The ideal quantum well case clearly shows that the in-plane mass of the heavy hole is much lighter than its transverse mass. Likewise for the light hole, the in-plane mass is much heavier than the transverse mass. This phenomena was described in Chapter 2. The in-plane heavy hole masses for three different quantum well widths were calculated [11.4] and are also given in Table 11.3. These show that as the quantum well width increases, and we move away from the ideal case, the in-plane heavy hole mass gradually regains its "heavy" character. These calculation give the mass at the zone centre of the band. At room temperature the non-parabolicity of the valence bands away from the zone centre must be taken into account.

Figure 11.1 gives the calculated heavy and light hole valence bands for a quantum well of width 6.5nm. The corresponding valence bands calculated for the case of a 4.5nm quantum well are given in Figure 11.2. The non-parabolic nature of the bands away from the zone centre is clearly evident, along with the mass reversal of the heavy and light hole bands.

In a quantum well, the density of states is given by [11.5]

$$g(E) = \frac{k_{//}}{\pi} \frac{dk_{//}}{dE} \qquad 11.10$$

where $k_{//}$ is the in-plane wave-vector and E is the energy. The deduced density of states for the heavy hole is shown in Figure 11.3 for the 6.5 nm quantum well and in Figure 11.4 for the 4.5 nm quantum well. The density of states for an ideal parabolic band in 2D is a constant step which is proportional to the effective mass. In real quantum wells, the motion of the holes corresponding to the heavy hole band is dependent on an average effective mass which includes the effect of non-parabolicity.

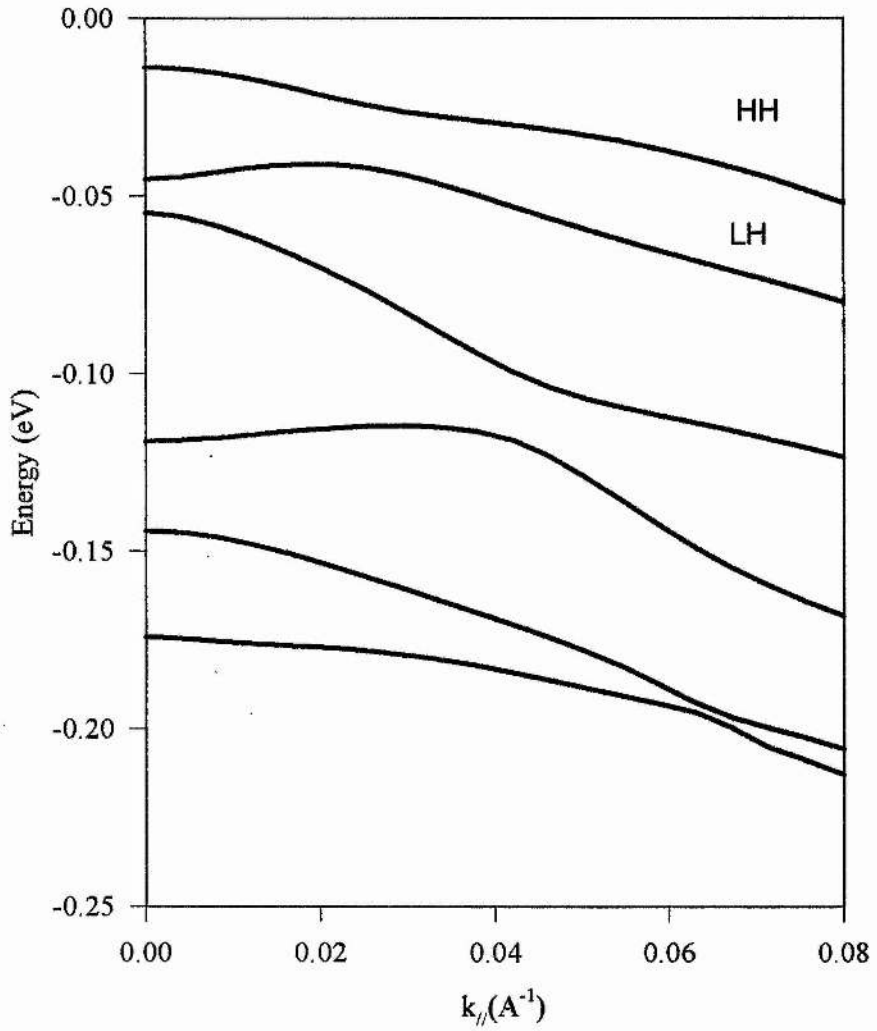

Figure 11.1 *Calculated valence band structure for a 6.5 nm GaAs/AlGaAs quantum well [11.4].*

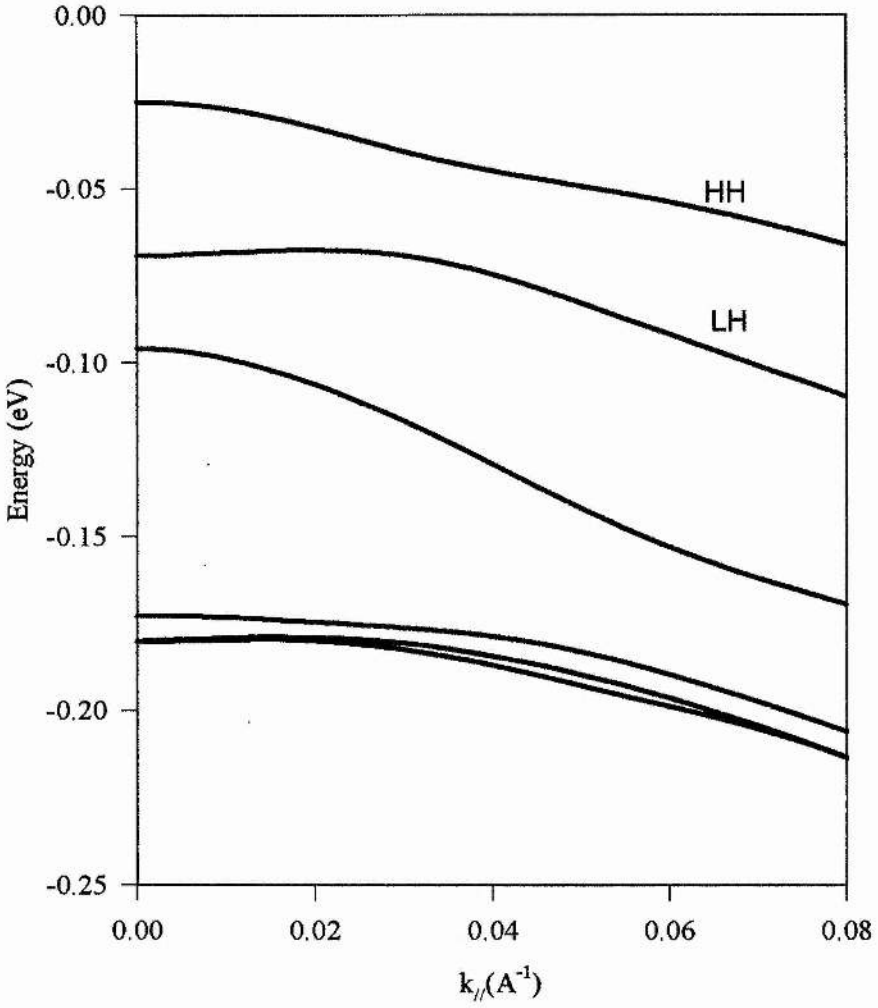

Figure 11.2 *Calculated valence band structure for a 4.5 nm GaAs/AlGaAs quantum well [11.4].*

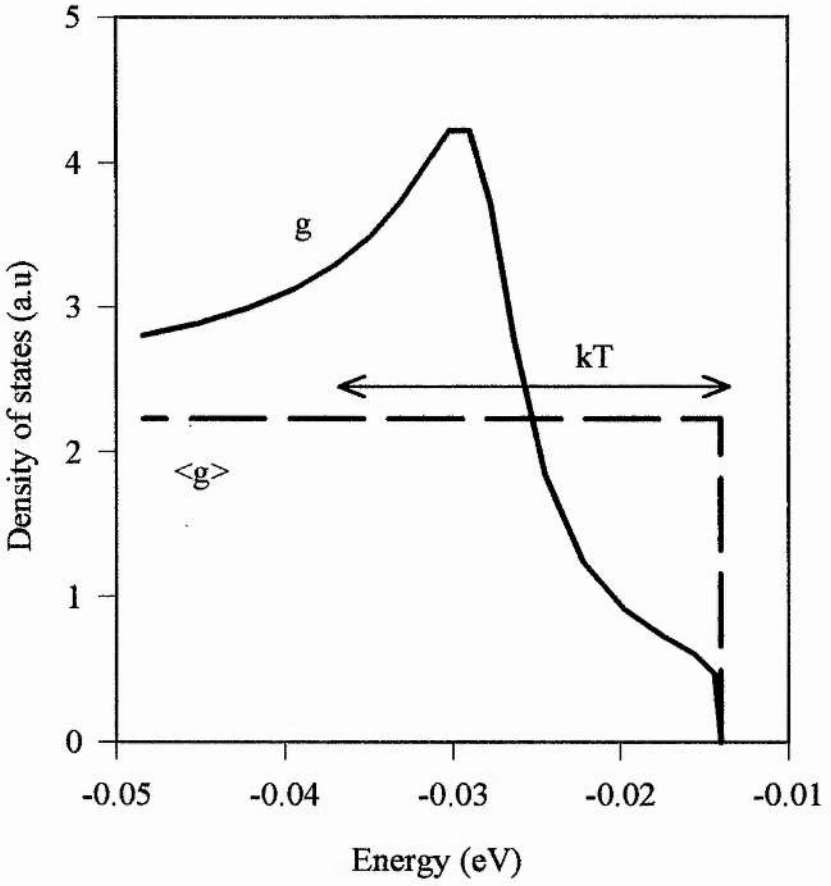

Figure 11.3 *Calculated density of states, g, for the heavy hole valence band of a 6.5 nm quantum well. An average density of states, <g>, is also calculated assuming an effective parabolic band.*

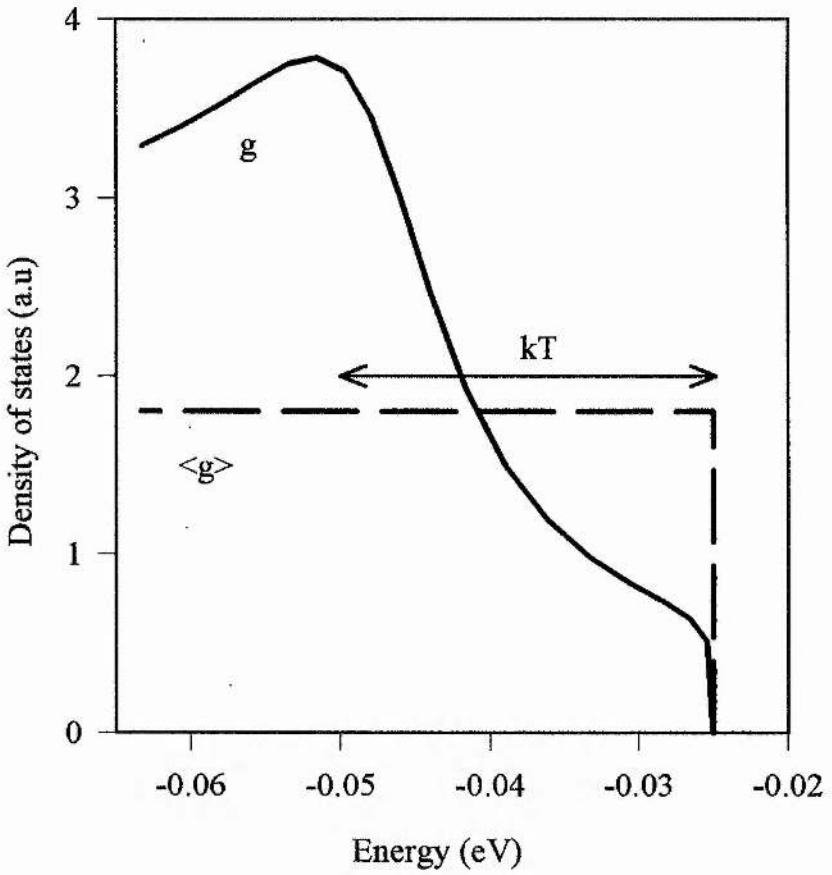

Figure 11.4 *Calculated density of states, g, for the heavy hole valence band of a 4.5 nm quantum well. An average density of states, <g>, is also calculated assuming an effective parabolic band.*

To describe its influence on the heavy hole mass the average density of states <g> is calculated using the formula

$$\langle g \rangle = \frac{\int g(E) f(E) dE}{\int f(E) dE} \qquad 11.11$$

where f(E) is the Fermi distribution which is determined for a given carrier density n by the equation

$$n = \int g(E) f(E) dE \qquad 11.12$$

Figure 11.3 and Figure 11.4 show <g> plotted for the respective well widths. These calculated average densities of states correspond to ideal parabolic bands with a mass of $0.43m_0$ for a 4.5nm quantum well width and $0.53m_0$ for a 6.5nm quantum well width. These results clearly show that the non-parabolicity of the heavy hole valence band has the effect of increasing the average in-plane mass of the heavy hole when compared to the ideal 2D parabolic band case.

The heavy hole mass for KLB is expected from the above argument to be slightly heavier than is the case for bulk GaAs. This would explain the slightly lower value of the hole mobility obtained. S51 by contrast is expected to exhibit a lighter heavy hole mass when compared to the bulk case. This provides good evidence on the increased hole mobility that was measured.

The arguments presented above show that careful consideration must be paid to the relevant scattering mechanisms when trying to interpret mobility results. In the case of the hole mobility, the effects of reduced in-plane heavy hole mass due to non-parabolicity must be evaluated. The results obtained from the transient grating experiments agree well with those expected for GaAs multiple quantum wells.

11.4 References

11.1 J.P. McKelvey, *Solid State and Semiconductor Physics*, (Harper & Row, 1975).

11.2 A. Miller, R.J. Manning, P.K. Milsom, D.C. Hutchings, D.W. Crust and K. Woodbridge, "Transient grating studies of excitonic optical nonlinearities in GaAs/AlGaAs multiple-quantum-well structures", J. Opt. Soc. Am. B, **6**, 4, 567-578, (1989).

11.3 S.M. Sze, *Physics of Semiconductor Devices* (2 nd ed., Wiley, 1981).

11.4 I. Galbriath, *Heriot-Watt University,* Private communication.

11.5 N. Peyghambarian, S.W. Koch and A. Mysyrowicz, Introduction to Semiconductor Optics, (Prentice-Hall, 1993).

12

Conclusion

An investigation into the dynamics of exciton saturation in multiple quantum well semiconductors at room temperature has been carried out using picosecond pulses from a self-mode-locked Ti:sapphire laser. The contributions to exciton saturation due to Coulomb screening and phase space filling have been discussed and the importance of exciton lineshape broadening investigated. A study of the electron spin relaxation time has been carried out and the well width dependence has been reported. Finally the first demonstration of an electron spin grating in a semiconductor quantum well is reported. This has allowed the first direct optical measurement of the in-plane electron diffusion coefficient.

The samples used in this thesis were GaAs quantum wells obtained from a number of different sources. The samples used were FK141 (9.0 nm quantum well width), G1273 (8.0 nm well width), KLB (6.5 nm well width) and S51 (4.4 nm well width). Sample S51 exhibits extremely narrow exciton resonances at room temperature and allowed the contribution of broadening in exciton saturation to be investigated.

The dominant contribution to exciton saturation at room temperature arise due to the combined effects of phase space filling, Coulomb screening and lineshape broadening. The spin dependent nature of the phase space filling nonlinearity has allowed its separation from the other two. At room temperature the exciton linewidth results predominantly from the effects of LO-phonon collisions. Further broadening may be induced under optical excitation due to carrier density dependent effects. Monitoring the initial change in transmission of a weak probe beam using the

standard pump-probe technique has allowed the contributions to exciton saturation to be investigated.

The optical selection rules in multiple quantum wells allow the creation of spin polarised carriers using circular polarised light. Altering the polarisations of the pump and probe beams allows the effects due to phase space filling to be enhanced or negated. This method has been used to separate the contributions due to Coulomb screening and broadening from those of phase space filling. The density dependence of the effects due to Coulomb screening and broadening have been investigated. The experiment was carried out in samples FK141, KLB and S51 allowing a well width dependence to be observed. The effects of broadening and screening have been shown to have differing dependencies on the excited free-carrier density. It was found that the contribution from broadening became increasingly important in the narrow wells. For S51 it has been shown that broadening is the dominant contribution to exciton saturation at low carrier densities.

The dynamics of electron spin relaxation have been studied as a function of the well width of the quantum wells. The spin relaxation time was observed to increase with the quantum well width. The measure times were 32 ps for S51, 54 ps for KLB, 60 ps for G1273 and 75 ps for FK141. The results were compared with those of a number of different authors and show good agreement. The use of samples from different sources and the agreement of the spin relaxation results with those obtained by other authors suggests that at room temperature the main scattering mechanism which leads to spin relaxation is due to LO-phonon collisions and not impurity or interface scattering. Combining the results allowed a determination of the power dependence of the spin relaxation rate on electron confinement. The data was observed to fit a 2.16 power dependence, implying that the D'Yakonov-Perel mechanism describing spin relaxation is the dominant spin flip mechanism for electrons in quantum wells at room temperature. The variation of the spin relaxation time with well width is important for any future device applications.

DFWM studies have been carried out in samples S51 and KLB. The creation of concentration gratings of electrons and holes and the monitoring of the grating decay has enabled the ambipolar diffusion coefficient to be measured for both samples. The results for S51 and KLB give ambipolar diffusion coefficients of 21.6

cm^2/s and 13.3 cm^2/s. The larger diffusion coefficient obtained for S51 is indicative of its superior quality. The hole mobilities for each of the samples were deduced from the ambipolar diffusion coefficients and shown to be 257 cm^2/Vs and 458 cm^2/Vs for KLB and S51 respectively.

The first demonstration of an electron spin grating in a semiconductor quantum well has been reported. The grating was produced using the polarisation grating produced when orthogonally polarised light beams interfere and the spin selection rules in quantum wells. These allowed the creation of a periodic modulation of electron spins within the sample. The decay of this grating is solely due to the motion of the electrons unlike the previously described concentration gratings where it occurs due to electrons and holes. This allowed the first optical measurement of the in-plane electron diffusion coefficient at room temperature in a quantum well semiconductor. The experiments were carried out in samples KLB and S51. The electron diffusion coefficients measured were 125 cm^2/s and 120 cm^2/s for KLB and S51 respectively. These allowed electron mobilities of 4800 cm^2/Vs and 4600 cm^2/Vs to be deduced for KLB and S51.

The influences of background doping, interface roughness and barrier-alloy scattering have been discussed with reference to the results obtained. The in-plane hole mass was calculated for both samples in order to explain the lower hole mobility for S51 and the heavier hole mobility for KLB when compared to bulk GaAs.

Further investigation of the broadening contribution to exciton saturation is required. At the present time the contribution due to broadening has only been observed in one high quality sample. A more thorough study of the broadening as a function of well width in high quality samples would allow a more complete picture to be formed.

The spin relaxation mechanism at room temperature needs further investigation. More data at high electron confinement energies would lead to a more accurate fit and should enable the mechanism to be confirmed. It would also be interesting to try to time resolve the hole spin relaxation as this lies outwith the temporal resolution currently available. The mechanism responsible for the hole spin flip could then be investigated.

Spin gratings would allow a future study into the scattering mechanism of electron in quantum wells. Scattering is an important factor in the operation of high mobility devices and so a fuller understanding of the mechanisms involved would lead to improved device performance.

13 Publications

Journal publication

A.R. Cameron, P. Riblet and A. Miller, "Spin gratings and the measurement of electron drift mobility in multiple quantum well semiconductors", Phys. Rev. Letts, **76**, 25, (1996).

Conference publications

A.R. Cameron, P. Riblet and A. Miller, "Electron spin gratings in multiple quantum well semiconductors, Paper QO.1.5, CMMP'95, Liverpool, UK.

A.R. Cameron, P. Riblet and A. Miller, "Determination of the electron mobility in multiple quantum wells by time-resolved optical measurements", Paper TuE39, Ultrafast Phenomena 96, San Diego, USA.

A.R. Cameron, P. Riblet and A. Miller, "Broadening, screening and phase-space filling in GaAs multiple quantum wells revisited", Paper QTuB4, CLEO/QELS'96, Anaheim, USA.

A.R. Cameron, P. Riblet and A. Miller, "Electron spin grating in multiple quantum well semiconductors", Paper QWG5, CLEO/QELS'96, Anaheim, USA.

A.R. Cameron, P. Riblet and A. Miller, "Dynamics of electron spin gratings in multiple quantum wells semiconductors", Paper ME3, IQEC'96, Sydney, Australia.

14 Acknowledgements

I would like to thank my supervisor Professor Alan Miller for his continued support, guidance and "*subtle*" explanations throughout this project. I also thank him for allowing me to learn more about life than physics during my time in his research group. I would also like to thank Professor Wilson Sibbett for acting as reserve supervisor in case Alan found St Andrews too cold.

I would like to thank all the secretaries for their faxing, phoning and constant help with my spelling and to all the other members of staff at St Andrews who made my stay so enjoyable.

To all the postgraduate students, research assistants and members of the workshop, both mechanical and electronic, I thank you all for your help, patience and friendship.

Special mentions go to:

Cameron Rae for all the games of golf, and not laughing at my putting.

George Cunningham for rebuilding my golf swing on several occasions and for agreeing to hold Mark and I's hand on our first outing on the Old Course.

I would especially like to thank the members of the Semiconductor Physics group both past, present and future.

To the RA's, Peggy for introducing me to spin relaxation and Ultimate Frisbee, Philippe for all his help and without whom none of this would have been possible and Gordon for never asking me to explain anything.

To Mark for all the weekend games of golf and for allowing me to avoid answering all his semiconductor theory questions.

Jim for his attitude to life (and physics) and the use of his flat to write chapter 8.

To Steven White, all I can say is that I warned you not to do it, so don't blame me.

Special thanks go to Steven French for starting this whole crazy thing with me, building the Lab into what it is/was and for the smell of coffee and blueberry muffins in the mornings.

I'd like to thank Peter, sorry Dr Roberts and Geoff (soon to be Dr Stockham) for putting up with my early morning showers and the appearance of Margaret every fourth weekend.

I thank Mum, Dad and Jillian for everything and the dogs, Bungy, Katie and Benji who were always willing to listen to the problems involved in doing a PhD.

Last but not least I would like to thank Margaret without whose love, laughter, understanding and sound advice this thesis would never have been written.

I leave you now with some interesting thoughts on life and PhDs

We are the music makers and we are the dreamers of dreams. Wandering by lone sea breakers and sitting by desolate streams; world-losers and world-forsakers on whom the pale moon gleams. Yet we are the movers and shakers of the world forever, it seems.

He who is certain he knows the ending of things when he is only beginning them is either extremely wise or extremely foolish; no matter which is true, he is certainly an unhappy man for he has put a knife in the heart of wonder.

The truth isn't easily pinned to the page. In the bathtub of history the truth is harder to hold than the soap and much more difficult to find.

This principle is so perfectly general that no particular application of it is possible.

But you see, I can believe a thing without understanding it. It's all a matter of training.

Various authors

Finally I am grateful to the University of St Andrews for financial support.